FIBER BRAGG GRATINGS SENSOR SYSTEM

HUANG YUHENG

Ph. D.

The Hong Kong

Polytechnic University

2014

The Hong Kong Polytechnic University

Department of Electronic and Information Engineering

FIBER BRAGG GRATINGS SENSOR SYSTEM

Huang Yuheng

A thesis submitted in partial fulfilment of the requirements for

The Degree of Doctor of Philosophy

August, 2012

CERTIFICATE OF ORIGINALITY

I hereby declare that this thesis is my own work and that, to the best of my knowledge and belief, it reproduces no material previously published or written nor material which has been accepted for the award of any other degree or diploma, except where due acknowledgement has been made in the text.

Huang Yuheng

ABSTRACT

Fiber Bragg grating (FBG) is a key component in the optical sensing field. The unique advantages of FBG sensors make them the preferences for the applications that normal electrical sensors are unworkable. However, the complexity and cost of the sensing systems have limited the applications of FBG sensors. Various multiplexing and interrogation schemes have been explored to enhance the competitiveness of FBG sensing systems in the global sensor market. This thesis presents a number of techniques that may simplify the FBG sensor detection systems.

Code division multiplexing (CDM) is one multiplexing technique for Bragg grating sensor systems. It uses the orthogonal property of codeword to resolve the reflections from the different grating sensors in a serial array. This enables the advantages of time division multiplexing (TDM) technique to be maintained and at the same time overcomes some limitations of current TDM schemes. However, many aspects related to the application of CDM in fiber sensor systems including code design, optimum system architecture and system performance were not investigated. In this thesis these problems are addressed through investigating the use of code-division multiplexing method for a proposed optical fiber sensor system. Effort has been made to study the performance of CDM technique for FBG sensor multiplexing.

Tunable laser is a useful component for optical sensor interrogation. However, the drawbacks of high cost, low tuning speed and poor tuning repeatability have limited the usefulness of tunable laser in the practical sensing systems. In this thesis,

two wavelength tuning schemes are proposed to improve the performance of tuning sources for the FBG sensor interrogation systems.

For applications that large tuning range is not required, vertical cavity surface emitting laser (VCSEL) driven in a special way can be used as a narrow band tuning laser source. The tuning properties of VCSEL as a wavelength tuning source are studied in this thesis. It is applied to a tilted FBG vibration sensing system for fast vibration detection. Experimental results show that the coupled power is about 15dB larger than the broadband ASE source and a better system performance is obtained. Vibration measurement up to 200Hz has been achieved.

Another approach to achieve wavelength tuning light source for sensing applications is using a modulated laser pulse sequence to feed into a loop with single-sideband (SSB) modulator. The wavelength of pulse will shift after every loop. A series of pulses can be generated at the output port of the 3dB coupler and can be used as a wavelength tuning source to interrogate the wavelength shifts of the FBG sensors. The advantages of this scheme are stable wavelength output, high accuracy and easy tuning range adjustment by using different optical band pass filter. Its performance in a FBG sensing system is evaluated.

ACKNOWLEDGEMENTS

I would like to express my sincere gratitude to my chief supervisor, Professor Ping-Kong Alexander Wai, and my co-supervisor, Professor Chao Lu, for introducing me to the world of fiber optic sensor research and their invaluable guidance, support and encouragement during my Ph.D. study. In addition, I would like to thank Professor Hwa-Yaw Tam for his invaluable discussion, suggestion and support.

Many thanks to my colleagues, and note especially Dr. Tuan Guo, Dr. Hongyan Fu, Dr. Xinyong Dong, Dr. Kevin Lui, and Dr. C. C. Lee for their kindly collaboration and technical support. I would like to thank Dr. Feng Li, Dr. Xinhuan Feng, Dr. Jian Zhao, Dr. K. K. Qureshi, Dr. Liyang Shao, Dr. C. Y. Li, Dr. Shaohao Wang, Dr. Qian Li, Dr. Jie Li, Mr. Liqing Gan, Mr. Yuan Mao and Mr. Qi Sui for their support and suggestions.

I also wish to thank my parents and my wife for their continuous moral support all these years.

LIST OF ABBREVIATIONS

Abbreviation	*Definition*
ADC	analog-to-digital converter
APC	angled physical contact
ASE	amplified spontaneous emission
BPF	bandpass filter
CCD	charge-coupled device
CDM	code-division multiplexing
DBR	distributed Bragg reflector
EDFA	erbium-doped fiber amplifier
EMI	electromagnetic interference
EOM	electro-optic modulator
FBG	fiber Bragg grating
FMCW	frequency-modulated continuous wave
FP	Fabry-Perot
FWHM	full width half maximum
IWDM	intensity and wavelength division multiplexing
LPG	long-period fiber grating
MZI	Mach-Zehnder interferometer
MZM	Mach-Zehnder modulator
NRZ	non-return-to-zero
OSA	optical spectrum analyzer
OTDR	optical time domain reflectrometry
PC	polarization controller
PD	photodetector
PRBS	pseudorandom bit sequence
RF	radio frequency
SDM	spatial-division multiplexing

SLED	superluminescent light-emitting diode
SSB	single-sideband
SNR	signal to noise ratio
TDM	time-division multiplexing
TFBG	tiled fiber Bragg grating
TOF	tunable optical filter
UV	ultraviolet
VCO	voltage-controlled oscillator
VCSEL	vertical cavity surface emitting laser
WDM	wavelength-division multiplexing

LIST OF FIGURES

Figure 2.1 Schematic of uniform Bragg gratings……..…..…..13

Figure 2.2 Reflection spectra of apodized Bragg gratings……..16

Figure 2.3 Structure of the refractive index change 17

Figure 2.4 Schematic diagram of a WDM sensing system ……..……...19

Figure 2.5 Schematic diagram of a TDM sensing system……...21

Figure 2.6 Example of multiple reflection interference…….…….23

Figure 2.7 Example of spectral shadowing interference…….23

Figure 2.8 Schematic diagram of a CDM sensing system……...25

Figure 2.9 Schematic diagram of SDM sensing system……..27

Figure 2.10 Schematic diagram of a FMCW multiplexing system…….28

Figure 2.11 Schematic of IWDM sensor system…….29

Figure 2.12 Conversion of wavelength to intensity using edge filter method……30

Figure 2.13 Schematic diagram of tunable filter method……....30

Figure 2.14 Principle of interferometric detection method…….31

Figure 3.1 Schematic diagram of a CDM sensor system……....38

Figure 3.2 Experimental setup of Hojoo Lee's proposed system……....40

Figure 3.3 Experimental setup of S. Abbenseth's proposed system……...41

Figure 3.4 Block diagram of a CDM based FBG sensor system…….43

Figure 3.5 Complementary code autocorrelations……...44

Figure 3.6 Complementary code OTDR algorithm…….45

Figure 3.7 Experimental setup of the proposed CDM based FBG sensor system…..58

Figure 3.8 Temperature against wavelength for FBG6……...64

Figure 3.9 Temperature against wavelength for FBG20…….65

Figure 3.10 Reflection points in the fiber sensor array……...66

Figure 4.1 Structure of VCSEL grown with MOCVD……....70

Figure 4.2 Experimental setup of the proposed FBG interrogation system 71

Figure 4.3 Normalized reflection power of FBG at different wavelength 72

Figure 4.4 Bragg wavelengths versus time delay 73

Figure 4.5 Spectra of VCSEL outputs with different tuning repetition rate 74

Figure 4.6 Schematic diagram of VCSEL-based TFBG vibration sensing system 78

Figure 4.7 TFBG spectra and its response to the fiber bending 79

Figure 4.8 Wavelength tuning characteristics of VCSEL 80

Figure 4.9 Comparison of TFBG reflections powered by a BBS and a wavelength matched VCSEL 81

Figure 4.10 System real-time outputs following a 200-Hz harmonic oscillation 82

Figure 4.11 Normalized system output following a 200-Hz harmonic oscillation 83

Figure 4.12 System frequency responses following a 200-Hz harmonic oscillation..83

Figure 5.1 Single-sideband modulation using Dual-Parallel-MZ modulator……..88

Figure 5.2 Optical output vs. Bias voltage……..89

Figure 5.3 Experimental setup of the proposed interrogation system…….92

Figure 5.4 Setup to test modulator loss and signal characteristic……..104

Figure 5.5 Signal after SSB modulator and after EDFA ……..105

Figure 5.6 The output series pulses in optical domain …….106

Figure 5.7 The output series pulses in time domain ……......106

Figure 5.8 The normalized reflection shape of grating filter ……109

Figure 5.9 The reflection pulses of grating filter in real-time scope…….....110

Contents

CERTIFICATE OF ORIGINALITY i

ABSTRACT ii

ACKNOWLEDGEMENTS iv

LIST OF ABBREVIATIONS v

LIST OF FIGURES vii

Chapter 1 Introduction 1

1.1 Optical Fiber Sensors 1

1.2 Optical Fiber Sensing Technologies 3

1.3 Research Motivation 4

1.4 Scope of Thesis 6

1.5 Statement of Contributions 8

1.6 Publications 9

Chapter 2 Fiber Bragg Grating Sensing Systems 11

2.1 Introduction 11

2.2 Principles of Fiber Bragg Gratings 11

2.3 Multiplexing Techniques for FBG sensor systems 18

2.4 Interrogation Techniques for FBG Sensor Systems 29

2.5 Summary 32

Chapter 3 CDM Based FBG Sensor System 33

3.1 Introduction 33

3.2 Review of CDM Based FBG Sensor Systems 36

3.3 Code Design of the Proposed Sensor System 42

3.3.1 Sequences with Zero Autocorrelation Sidelobes 43

3.3.2 Code Sequences in Which n is Power of 2 45

3.3.3 Code Sequences for n is Any Even Number 52

3.4 Operation Principle and Theoretical Analysis 56

3.5 Experimental Results and Discussion 63

3.6 Summary 68

Chapter 4 VCSEL Based TFBG Vibration Sensing System..... 70

4.1 Introduction 70

4.2 Vertical Cavity Surface Emitting Laser 71

4.3 VCSEL based Interrogation System 73

4.3.1Experimental Setup and Operating Principle 73

4.3.2 Experimental Results and Discussion 74

4.4 VCSEL Based Tilted Fiber Grating Vibration Sensing System 78

4.4.1 Tilted Fiber Bragg Grating Vibration Sensor Systems 78

4.4.2 Principle of Proposed VCSEL Based TFBG Vibration Sensing System 80

4.4.3 Experimental Results and Discussion 83

4.5 Summary 86

Chapter 5 SSB Modulation Based Interrogator for FBG Sensor Systems 88

5.1 Introduction 88

5.2 Optical Single-sideband Modulation 89

5.3 Single-sideband Modulation based Interrogation System 93

5.3.1 Experimental Setup and Operation Principle 93

5.3.2 Theoretical Analysis 95

5.3.3 Results and Discussion 106

5.4 Summary 115

Chapter 6 Conclusions and Future Work 116

6.1 Summary 116

6.2 Future work 118

Bibliography 119

Chapter 1 Introduction

Optical fibers have revolutionized the way we communicate. Over the past 40 years, optical fiber communication industry has experienced an explosive growth. High performance and reliable fiber links with tens of terabit per second data rate per fiber have been built all over the world to form an amazing information superhighway.

Benefitted from the development of optical fiber communication technology, optical fiber sensor technology [1-5] has also developed rapidly. During the early stage of fiber sensing technology development, most researches were focused on the markets that traditional sensor technology had been proven unsuitable. But the situation is changing with the fallen optical component price and the improvement of component quality. These changes have greatly increased the competitiveness of optical fiber sensors to traditional sensors and applications for optical fiber sensors have been developed in various areas.

1.1 Optical Fiber Sensors

Optical fiber sensing technology is, compared with optical fiber communication technology, a highly specialized, niche technology that typically takes long research and development times. Optical fiber sensor was first demonstrated in mid 1960s and developed rapidly in the following years [2]. In the 1970s, the most successful one

probably was the optical fiber gyroscope which was first reported in 1977 and then turned into an industry instrument in the mid 1990s. From 1977 to 1979, sensitivity of fiber acoustic sensors had been improved by about 100dB so that many of these sensors rival or surpass the performance of previous electroacoustic sensors. Fiber sensor for magnetic, acoustic, pressure, temperature, strain, acceleration, rotation, linear and angular position, fluid level, torque, photoacoustic, current, humidity and chemical measurements have since been investigated extensively.

The numerous types of fiber sensors can be loosely grouped into two basic categories as extrinsic sensors and intrinsic sensors. The main difference between extrinsic and intrinsic sensors is that whether the light keeps within the fiber at all times. For extrinsic sensors, a sensing region that modulates one of the light properties is placed between two fibers to reflect an environmental parameter. The light needs to go out from one fiber and then propagate to another fiber after the sensing region. In contrast, the light keeps in the fiber all the time for intrinsic sensing. Only environmental parameters that affect the light properties in the fiber can be measured. These light properties include optical delay, optical intensity and spectral properties. Usually the extrinsic sensors are used in biomedical and chemical measurements and intrinsic sensors are used in physical measurements.

1.2 Optical Fiber Sensing Technologies

There are many technologies developed for optical fiber sensing, and some approaches have been well studied and emerged into at least one commercial application. Dual path interferometer, Faraday rotation, spectroscopy and distributed measurement are the four major approaches that make great contributions to fiber sensing field.

Dual path fiber interferometer was the earliest intrinsic sensing technology to be thorough studied and developed. It measures the different delay between the signal arm and the reference arm in the interferometer. The resolution of this delay can be better than10^{-7} radians. And the signal can be detected it with optical powers about 1mW in a 1Hz bandwidth. The inherently balanced nature of the interferometer gives this remarkable sensitivity. Resolution around 1 micro radian can be achieved with careful engineering even in the configurations with less “perfect” balance such as the Michelson or Mach-Zehnder. One successful application of dual path interferometer is the optical fiber gyroscope.

Faraday rotation is well known as a magneto-optical phenomenon. The magnetic field along the direction of propagation will cause a linear rotation of polarization in the plane. This forms the basis of a successful current monitoring in single mode fiber. The typical use of optical fiber current sensor is to monitor the carrying currents of electrical power systems in the order of 100A. The electrically passive operation of the sensor system makes it electrical isolation in the current

measuring point and enhances the safety of power systems.

Optical fiber spectroscopy normally uses the fiber to illumination a remote sample and collects the reflection of light for analysis. There are two dominant formats in fiber based spectroscopy sensing. The first one uses broadband illumination and is mainly targeted on liquids and solids measurements and is frequently referred as optrode. The second one utilizes narrow band precisely controlled wavelength light source as input, typically focuses on measurements of gas absorption lines and is referred as gas spectroscopy.

Distributed sensing is a promising technology as multiple points can be sensed in one single fiber. The fully distributed sensing is based on the intrinsic effect of scattering. A specified environmental parameter can be detected continuously along the fiber line. And optical time domain reflectrometry (OTDR) is the widely used method for checking the connections of optical networks. Quasi-distributed sensing is to splice several sensors together to form one fiber sensor array and usually called multiplexing. The capability of multiplexing is one of the most important properties for optical sensors.

1.3 Research Motivation

Optical fiber sensors have been studied intensely for more than 40 years and their applications are developed rapidly in various areas in recent years. Initially, most of the fiber sensors remained at laboratory-based prototype stage and less commercial

successes have been achieved because their conventional electro-mechanical sensors counterparts are well established and have proven reliabilities and relatively low manufacturing costs. Only a few applications were applied successfully to the field that depended heavily on the inherent advantages of fiber sensor to offset the major disadvantage of high cost. In recent years, the manufacturing costs of fiber sensors and their basic component sets such as light sources and detectors are decreasing and more fiber sensors are implemented in industrial applications as competitive products. The inherent advantages of fiber sensors include EMI immunity, electrically passive operation, large bandwidth, high sensitivity, and large-scale multiplexing capability. The promising utilization of optical fiber sensors plays an important role in various areas include civil engineering structural monitoring, textile structural composites monitoring, railway, spacecraft, marine, nuclear and medical applications.

Fiber Bragg grating (FBG) represents a key element in the established and emerging fields of optical fiber sensing. FBG has been considered an excellent sensor element for quasi-static and dynamic measurements. For example, it can be used to detect the change of strain, temperature or pressure. The measurand information of FBG is usually wavelength encoded. This characteristic makes it self-referencing and independent to amplitude fluctuation causing by source power change or connector losses. The interrogation method of FBG sensor system is important with emphasis on the accuracy, resolution, and detection speed. For practical applications of FBG sensor, special requirements are required for certain sensor systems. These include high speed

interrogation, long-distance or quasi-distributed sensing, etc. The capability of multiplexing makes the FBG sensing applications much more attractive than other types of optical fiber sensors. Various multiplexing techniques are studied and developed to share the expensive optical components to cut down the cost.

In this thesis, we investigate the code division multiplexing based FBG sensor system which has its own advantages over the previously proposed FBG sensor systems. In addition, two approaches to generate wavelength tuning signals for sensing applications have been studied. One is driving a vertical cavity surface emitting laser (VCSEL) with ramp current to produce a narrow wavelength tuning source, another is utilizing single-sideband modulator in a loop to produce series of wavelength shifted pulses. A VCSEL based tiled FBG vibration sensing system has been studied and demonstrated.

1.4 Scope of Thesis

This thesis is structured as follows:

In chapter 2, the basic concepts of fiber Bragg grating (FBG) are reviewed including the development history, the fabrication, the optical properties, and their responses to some physical parameters including temperature and strain which make them the promising candidates in many sensing areas. The multiplexing techniques and the interrogation techniques for FBG sensors are also discussed.

In chapter 3, the detail literature reviews of CDM based FBG sensor systems are given. The proposed CDM based FBG sensing system is described and discussed. The code sequences with length of power of 2 are constructed and some rules for code sequences of even length are derived. A thorough theoretical analysis is then given. A 20-sensor array experimental setup gives results close to those obtained through theoretical analysis. Finally problems encountered during the experimental investigation are discussed.

In chapter 4, an interrogation system using a VCSEL as light source is proposed. Using saw tooth signal to drive the VCSEL input current, a continuous spectrum tuning range of 2nm can be obtained. Relationship between wavelength tuning range and scanning speed of the VCSEL is studied. AVCSEL based tilted fiber grating vibration sensing system is then investigated. Dynamic vibration measurement up to 200Hz has been achieved.

In chapter 5, an interrogation system using a SSB modulator in a fiber loop as light source is proposed. Theoretical analysis and experimental demonstration are given. In the proposed scheme, a single laser pulse is launched into the loop and generates a serial of frequency shifted pulses at the output port. The shift frequency between two adjacent pulses is equal to the RF driving frequency of the SSB modulator. The tuning range mostly depends on the bandpass filter in the loop and can be easily achieved in several nanometers. The performance of such a sensor system is investigated.

In chapter 6, conclusions of the thesis are presented and the future work is recommended.

1.5 Statement of Contributions

The original contributions made during the author's Ph.D. study are summarized as follows:

1. Investigation of code design for unipolar-bipolar correlation process. Code sequences with a length of 2^n that are suitable for CDM based FBG sensor systems are constructed. In addition, some rules for the more general code sequences with a length of 2n are investigated
2. Development of a Code Division Multiplexing based FBG sensing system. A thorough theoretical analysis of the proposed system is given and experiments were done to verify the system performance.
3. Development of a VCSEL based sensor interrogation system. VCSEL was driven by a ramp signal to act as a tunable light source. A VCSEL based TDM sensing system is proposed.
4. Development of a VCSEL based tilted FBG vibration sensing system. The VCSEL in this system enables the recoupled modes to work at a high power level to obtain better signal-to-noise ratio. Vibration measurement up to 200Hz has been achieved by the proposed cost-effective sensing system.

5. Development of a single-sideband modulation based interrogation system. A wavelength shifting pulse sequences is generated with a loop setup for sensing application.

1.6 Publications

The following publications arose during the research study:

1 **Yuheng Huang**, Tuan Guo, Chao Lu, and P. K. A. Wai, “Theoretical and experimental study of a CDM FBG Sensor System,” accepted by *Fiber and Integrated Optics*

2 **Yuheng Huang**, Chao Lu, and P. K. A. Wai, “Single-sideband Modulation Based FBG Sensor interrogation system,” to be submitted to *IEEE Photonics Technology Letters*

3 **Yuheng Huang**, Tuan Guo, Chao Lu, and Hwa-Yaw Tam, “VCSEL-Based Tilted Fiber Grating Vibration Sensing System,” *IEEE Photonics Technology Letters*, Vol. 22, No. 16, 2010

4 Tuan Guo, **Yu-Heng Huang**, Bai-Ou Guan, Chao Lu, Hwa-Yaw Tam and Jacques Albert, "VCSEL-based tilted fiber grating vibration sensing system," *Conference on Lasers and Electro-Optics (CLEO)*, 2011.

5 **Yuheng Huang**, Tuan Guo, Chao Lu, Hwa-Yaw Tam, and P. K. A. Wai, “Fiber-Optic Vibration Sensing System using a VCSEL-powered Tilted Fiber Grating,” *OptoElectronics and Communications Conference*, 2010.

6 **Yuheng Huang**, Tuan Guo, Chao Lu, P. K. A. Wai and Hwa-Yaw Tam, “VCSEL-based FBG Vibration Sensor,” *Asia-Pacific Optical Sensors Conference*, 2010.

7 **Y H Huang**, Chao Lu, P. K. A. Wai and H Y Tam, “Large-scale FBG sensors utilizing code division multiplexing,” *Conference on Lasers and Electro-Optics (CLEO)*, 2008.

Chapter 2 Fiber Bragg Grating Sensing Systems

2.1 Introduction

In this chapter, a background review on an important component for fiber optic sensor system investigated in the thesis, the fiber Bragg grating (FBG), is given. The basic principles together with their main properties will be described, and their applications for sensing will be introduced.

2.2 Principles of Fiber Bragg Grating

Fiber Bragg grating (FBG) is a key component in optical fiber communication systems and optical fiber sensing systems. The applications of FBG in optical communications include dispersion compensation, narrowband wavelength reflection in Raman amplifiers, pump locking in optical fiber amplifiers, etc. FBG is also commonly used as sensing components due to its inherent advantages such as EMI immunity, wavelength-encoded nature and the capability of multiplexing [5].

The basic principle of FBG is to modulate the refractive index along the fiber core to create a periodic perturbation. This can be done by exposing the fiber to an intense optical interference pattern. Fig 2.1 shows the uniform Bragg gratings, with the reflection spectrum and transmission spectrum under broadband incident light.

The wavelength of this specific reflection spectrum is named Bragg wavelength. FBG can be used as an optical filter to block unwanted wavelengths in optical communication systems, or be used as a wavelength reflector to select one specific communication channel.

In 1978, Hill et al. demonstrated the first permanent optical fiber gratings at the Canadian Communications Research Centre (CRC), Ottawa, Canada [6], [7]. With the radiation of a visible argon ion laser, the gratings were created in the Germania-doped silica fiber and known as “Hill gratings”. As exposing the doped fiber to the UV light with suitable energy and wavelength, a permanent refractive index change in the fiber core is created. This phenomenon is referred as photosensitivity and was thought to be only associated with the “Hill gratings”, but it has been observed though photo excitation at different UV wavelengths in a wide variety of different fibers in the following years of research. At present, various techniques can be used to inscribe different Bragg grating structures in the photosensitive optical fibers using ‘side-writing’ approach in which UV light is irradiated from the side of the fiber. And the phase-mask approach is one commonly used method to inscribe Bragg gratings.

Uniform gratings with constant gratings period and perpendicular phase fronts to the longitudinal axis of fiber are the basic building block in most Bragg grating structures. When a guided fiber mode is incident upon a fiber grating, a certain proportion of the incident light will be reflected backwards while goes through the grating planes. Upon the so-called Bragg condition, the reflections created by each

wavelet will be in phase and make up a strong backward-traveling mode.

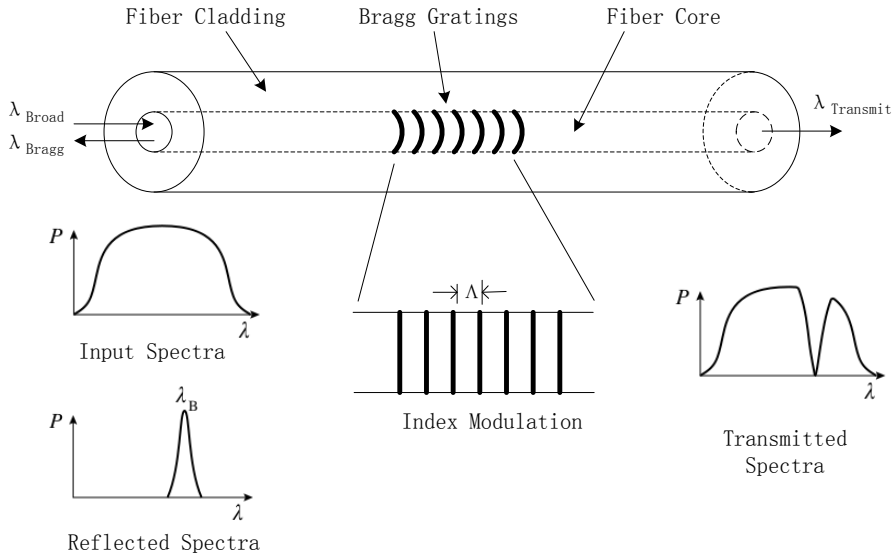

Figure 2.1 Schematic of uniform Bragg gratings.

Figure 2.1 shows the input and reflected spectra of a uniform FBG. The strongest reflection occurs at the first order Bragg condition and the Bragg wavelength is written as [8]:

$$\lambda_B = 2n_{eff}\Lambda\,, \tag{2.1}$$

where n_{eff} is the effective refractive index of the fiber core and Λ is the periodicity of the Bragg grating.

The impact of fiber Bragg grating in optical fiber sensing is enormous. FBG has all the advantages of common optical fiber sensing elements, such as EMI immunity and electrically passive operation. In addition, FBG has its own advantages, such as self-referencing and capability of multiplexing in one fiber line. The measurand information of FBG is usually wavelength encoded. So the sensing

information is self-referencing and independent to the amplitude fluctuation causing by source power change or connector losses. This characteristic makes FBG excelling than many other optical sensing elements. In addition, the narrow reflected spectra and low insertion loss give the capability for multiplexing numbers of FBGs in a single optical fiber. Thus many network topologies can be used for the sensor system to increase flexibility.

The wavelength of FBG depends on its grating period and the effective refractive index of the fiber core. And both the grating period and the effective refractive index of the fiber core will be affected by the change of. By using equation (2.1), the shift of Bragg wavelength caused by temperature and strain changes is expressed as [8]:

$$\Delta\lambda_B = 2(\Lambda\frac{\partial n_{eff}}{\partial l} + n_{eff}\frac{\partial\Lambda}{\partial l})\Delta l + 2(\Lambda\frac{\partial n_{eff}}{\partial T} + n_{eff}\frac{\partial\Lambda}{\partial T})\Delta T \qquad (2.2)$$

The first term of (2.2) gives the effect of strain, while the second term gives the effect of temperature on the gratings.

A change of strain in the fiber produces a shift of Bragg wavelength due to the change of grating periodicity and the change of refractive index caused by photoelastic. The shift of wavelength with applied strain can be written as:

$$\Delta\lambda_B = \lambda_B(1-p_e)\Delta\varepsilon \qquad (2.3)$$

where p_e is the effective photoelastic coefficient, $\Delta\varepsilon$ is the applied strain.

For silica fiber, the numerical value of p_e is about 0.22, thus the normalized strain response can be expressed as:

$$\frac{1}{\lambda_B}\frac{\Delta\lambda_B}{\Delta\varepsilon} = 0.78\times10^{-6}\,\mu\varepsilon^{-1} \tag{2.4}$$

For silica fiber operating at 1550nm, the typical wavelength-strain sensitivity of FBG is about 1.2 $pm/\mu\varepsilon$.

The shift of the Bragg wavelength due to temperature arises from both the change of the refractive index and the change of the grating period, of which the former one is the dominant effect. The Bragg wavelength shift induced by a temperature change ΔT is expressed as:

$$\frac{\Delta\lambda_B}{\lambda_B} = (\alpha+\zeta)\Delta T \tag{2.5}$$

,

where α is the thermal expansion coefficient and ζ is the thermo-optic coefficient.

The typical wavelength-temperature sensitivity of FBG written in Corning's SMF28 fiber at 1550nm is about 13 $pm/°C$.

The uniform Bragg gratings are seldom used in sensing applications because of its strong associated side-lobe structure apparent in the reflection spectrum. The approach for suppressing side lobes is apodization. The term of apodization here means that the grading of refractive index decreases from the center and approaches to zero at the end of the grating. Apodized gratings have a significant improved side-lobe suppression ratio and keep the narrow reflection spectrum shape. The typically used functions for apodization are Gaussian, Raised-cosine, Tanh, Sinc and Blackman. Figure 2.2 shows the effect of side-lobe suppression for different apodized gratings. The much lower side-lope reflection power makes them more suitable for optical fiber

sensing elements, especially in the case of multiplexing.

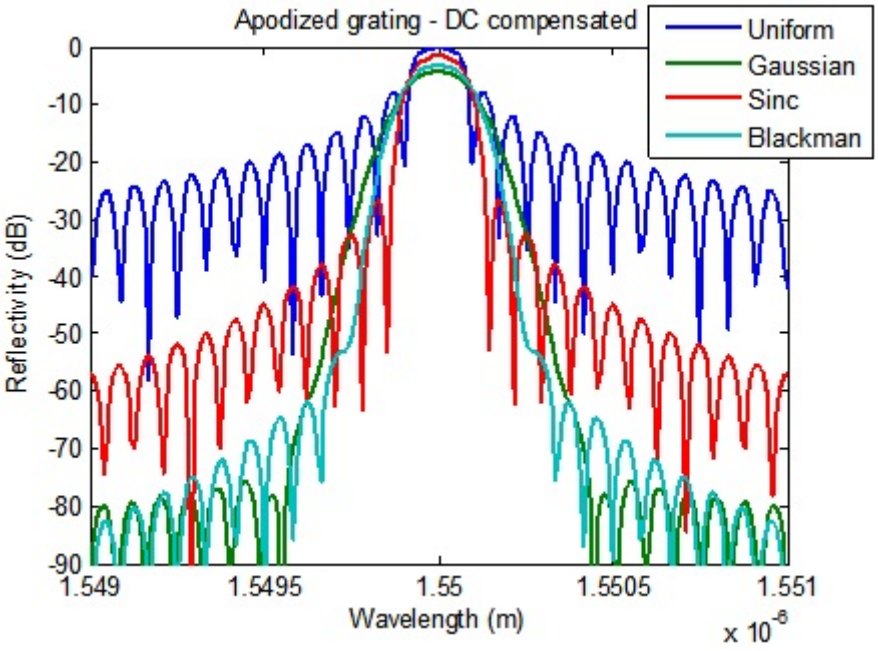

Figure 2.2 Reflection spectra of apodized Bragg gratings

Besides apodized gratings, there are many other commonly used structures for Bragg gratings such as chirped Bragg gratings, tilted Bragg gratings and long-period gratings. Figure 2.3 shows the changes of the refractive index in three different types of gratings.

In the chirped gratings, the refractive index profile is modified to add a variation of grating period along the fiber core. The wavelength of reflection will change as the incident light passes though the gratings, and reflected spectrum will be broadened. One property of chirped grating is adding dispersion. This property has been used in the development of dispersion compensation in high bit-rate telecommunication systems [9]. The chirped gratings as sensing elements also have been investigated [10], [11].

Tilted fiber Bragg grating (TFBG) are the gratings with its grating planes slanted with respect to the fiber axis [12], [13].The angle of tilt has an effect on the reflected power variation with fiber curvature and provides the possibility for vibration sensing.

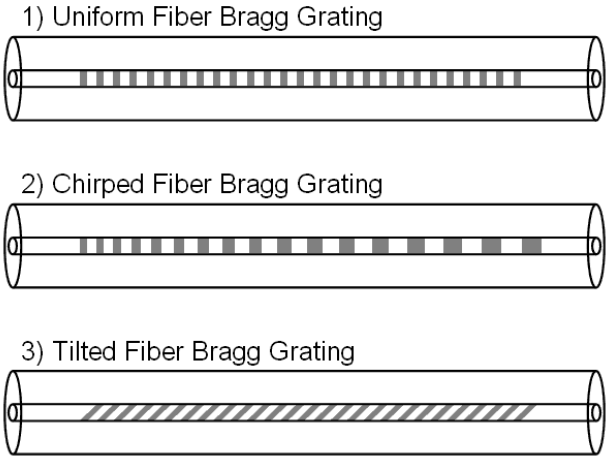

Figure 2.3 Structure of the refractive index along the fiber

The long-period fiber grating (LPG) usually has the grating periods of several hundred micrometers. A much broader response can be achieved by using the longer periods than a standard FBG. The principle of LPG is to couple the core guided mode to higher order cladding modes to realize a wavelength dependent loss which is due to scattering and absorption. So a spectrally selective loss can be obtained from the LPG. This characteristic of LPG make it suitable for applications in sensing temperature, strain, external index of refraction and bend radius [14].

2.3 Multiplexing Techniques for FBG sensor systems

A large number of multiplexing schemes [5], [8] have been reported, and generally they are grouped into one of the following categories: wavelength division multiplexing (WDM), time division multiplexing (TDM), code division multiplexing (CDM), spatial division multiplexing (SDM), frequency-modulated continuous wave multiplexing, or a combination of their hybrid approaches.

Wavelength-Division Multiplexing (WDM)

The commonly used technique for FBG sensor multiplexing is wavelength division multiplexing (WDM). FBG sensors with different Bragg wavelengths can be placed along a single optical fiber line. The separation distances between the sensors can be arbitrary or can be adjusted for desired locations. A dedicated spectral range must be allocated for each sensor to cover the operation range of the wavelength for temperature or strain measurements. This limits the maximum number of gratings that can be fitted within the spectrum of a given optical source. For example, a uniform spacing of 4nm between the Bragg wavelengths of the adjacent gratings corresponds to strain measurement range of about ±1500 με at 1550nm for each sensor. Consequently, the maximum sensor numbers that can be supported by a broadband source with a 40-nm spectrum width is 10.

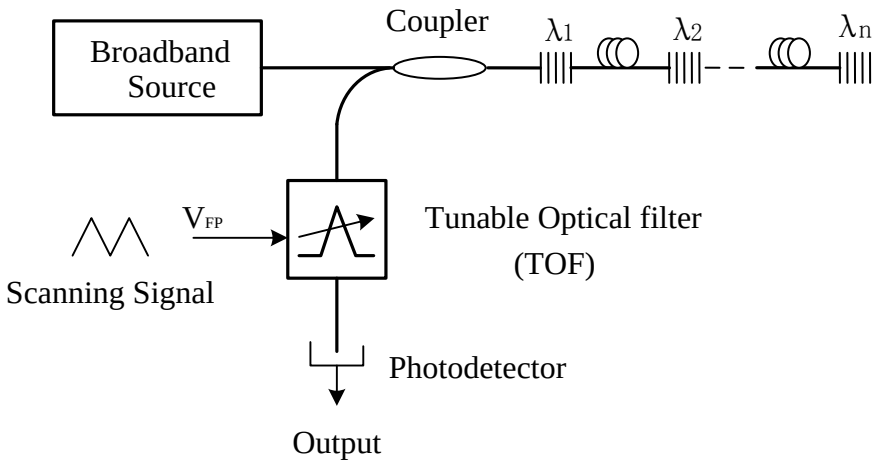

Figure 2.4 Schematic diagram of a WDM sensing system with tunable filter approach.

Figure 2.4 shows a WDM scheme with a tunable optical filter (TOF) to distinguish the different Bragg wavelengths of FBG sensors [15]. It uses a scanning signal to drive the TOF to scan the sensing wavelength range, making the system reliable, compact and easy to be used. As the TOF scans overlapped the reflection signals from the sensor, the highest power can be detected in the photodetector and then the Bragg wavelength can be obtained from the voltage of scanning signal applied to the filter. The level of crosstalk depends on the extinction ratio of the filter. If the cut-off of the TOF is sufficiently steep or the spectral separation between the gratings is large enough, the crosstalk can be negligible.

A combined WDM and interferometric detection system offers high wavelength shift resolution was reported in [16]. The light reflected from each grating is sent through a slightly unbalanced Mach-Zehnder interferometer (MZI) to convert the wavelength changes into phase changes. The signals are demultiplexed by use of WDM filter. The information is contained in the phase changes and can be extracted

using a phase-generated carrier technique. The interferometric technique is very sensitive to dynamic wavelength shifts, but its self bias phase drift limits the applications for quasi static measurements and needs to be handled carefully in system design.

Time-Division Multiplexing (TDM)

In the TDM system, a pulsed light is launched into the grating sensor array in the system along a single fiber. The sensors can be distinguished by the different time delays of the reflection signals due to the different placements of the sensors in the array. The minimal distance of two successive grating sensors depends on the pulse width of the input signal, and the reflection time delay between two FBGs should be larger than the time period of pulse. A high speed photodetector then can be used to detect the different reflections for analysis. In order to multiplex numbers of sensors in a single fiber, narrow pulses should be used and only one pulse can be sent with a round-trip time. Therefore, the performance of TDM based sensor systems is normally degraded by the limited reflection power of grating sensors.

TDM method allows the grating sensors to have the same wavelength range for sensing. As shown in Figure 2.5, the gratings FBG_1 to FBG_n can have the same reflection wavelengths. This greatly increases the bandwidth utilization of the light source, and let the Bragg grating fabrication become much easier because only one phase mask is needed to produce the same initial Bragg wavelength for FBG sensors.

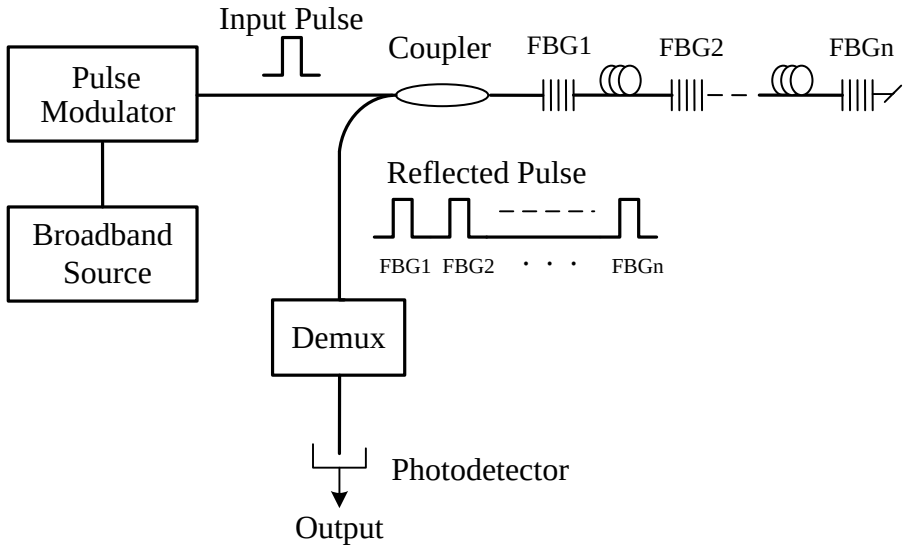

Figure 2.5 General diagram of a TDM sensing system

Combined with the interferometric wavelength shift detection method, A TDM sensing system with four FBG sensors spliced together, separated by 5 meters long fiber line between each other, has been demonstrated by Weis et al [17]. The strain resolution of about $1\,n\varepsilon/\sqrt{Hz}$ was reported. The grating elements in the sensor array can be either with the same Bragg wavelength or with different Bragg wavelengths. When combining TDM with WDM, reusing the source spectra can increase the number of sensors significantly. The sensors can be distinguished by both the different sensing wavelength ranges and the different time windows. The FBG sensors can be connected in serial, in parallel or in branching topology.

TDM method however suffers the disadvantages of lower reflected power and cross talk interference. It is apparent that one Bragg grating sensor should not reflect all the incident power backwards; otherwise, the grating sensors after it could not be detected because they have the same initial reflection wavelength. So the

reflectivity of the grating sensors is much lower than WDM method. For a 25-sensor TDM system, the reflectivity of about 2% is preferred to minimize the power depletion of the last sensor [18]. So the system performance is affected by the limited reflected power.

Another important factor that affects the system performance is cross talk. There are two kinds of cross talk in the TDM system, multiple reflections between grating sensors and spectral shadowing destruction [18], [19].

Multiple reflections will occur when two or more gratings have the same Bragg wavelength in the same fiber. Figure 2.6 gives a simple example of multiple reflections interference [18]. The launched pulse is partially reflected by grating sensor 2 and the reflection pulse is partially reflected back again by grating sensor 1 if sensor 1 and sensor 2 have the same Bragg wavelength λi at the reflected moment. Then this pulse is reflected by grating sensor 2 the second time and arrives at the detection unit in the same time with the desired reflected pulse from grating sensor 3 whose Bragg wavelength is λs. In the case that the number of sensors is large, multiple reflection interference will greatly degrade the system performance. In order to reduce the multiple reflections interference, the ratio of available time slots in a round-trip time to the total sensors is suggested to be greater than 24 [18].

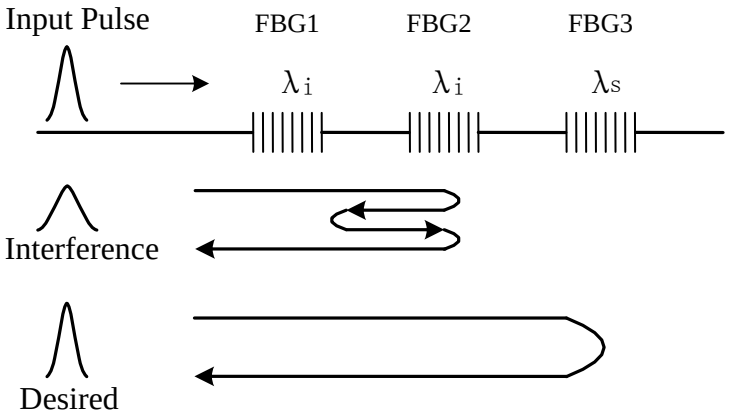

Figure 2.6 Multiple reflection cross talk.

Spectral shadowing is shown in Figure 2.7 [18]. After going through several numbers of sensors, the spectrum of the input interrogation pulse will be distorted, and the returned spectrum from the later sensors will be different from its true representation. This could introduce considerable detection error in the worst case scenario when the multiplexing sensor number is large. Reducing the grating reflectivity can slightly mitigate this form of cross talk.

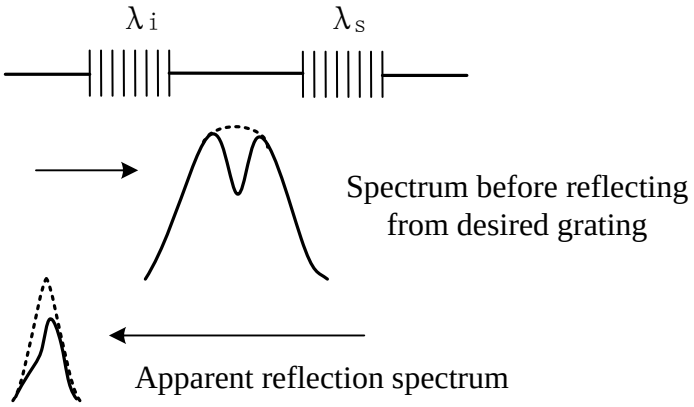

Figure 2.7 Interference caused by spectral shadowing.

TDM sensor multiplexing method has been studied widely in literatures such as in [18-24]. However, there is no any good solution to eliminate the cross talk yet.

In addition, we can see that in the TDM based FBG sensor system, only one short pulse can be sent into the serial Bragg grating sensor array in a round-trip time. Here a round-trip time is the time delay between reflected signals from the first and the last FBGs for the same input pulse. If we send more than one pulse into the sensor array within a round-trip time, some grating reflected signals from successive input pulses will arrive at the detection unit in the same time. Then the overlapped signals cannot be distinguished, so we must let the separation time between the input pulses be larger than the round-trip time. This leads to only one reflected pulse is detected for each FBG sensor in a round-trip time, and the average detected power is much lower comparing with the WDM method, especially in a large array with long round-trip time.

To improve the TDM sensor system performance, we can increase the incident optical power. However, this is limited by fiber nonlinearity as well as system component availability and cost. Alternatively, to find a way to send more pulses into the sensor array within a round-trip time is another method to increase the received power.

Code-Division Multiplexing (CDM)

CDMA technique is widely used in mobile communication system because it provides efficient radio frequency spectrum usage, excellent signal quality and large system capacity. CDMA technique is also being applied to the optical communication systems. Many researches have been done to develop practical optical CDMA

communication systems. Here we introduce code division multiplexing into FBG sensor systems. In a FBG sensor multiplexing system using CDM method, more than one pulse is sent into a sensor array in a round-trip time, the pulse sequence denotes a temporally encoded CDMA codeword. The reflected output from individual sensor can be obtained from the overlapped reflected signals of other sensors by utilizing the correlation property of CDMA codeword. Because the CDM approach delivers more signal pulses into the system and increases the average reflection power than the TDM approach, the overall performance of CDM sensor systems is expected to be better than that of the TDM sensor systems.

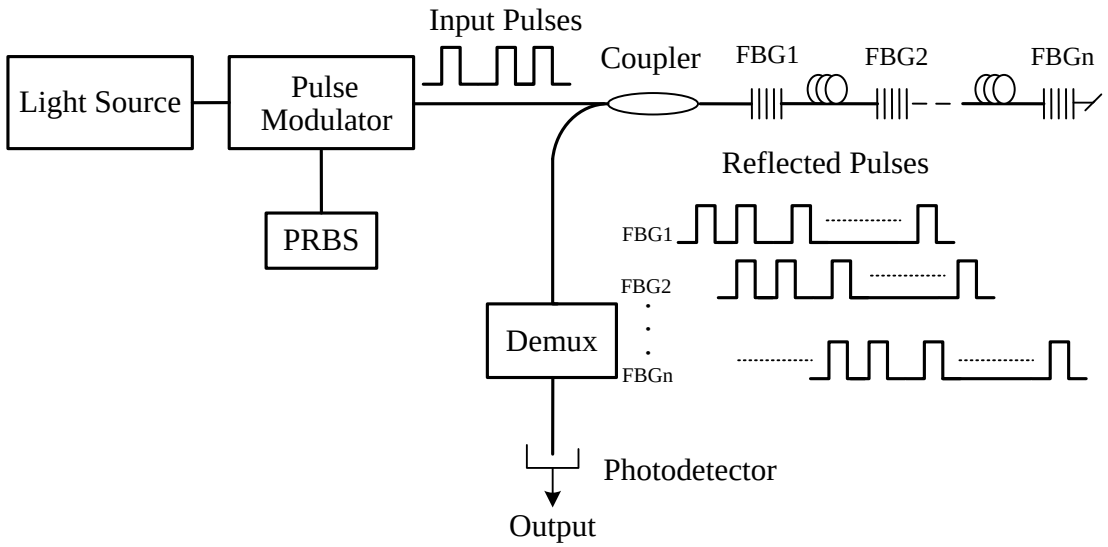

Figure 2.8 General diagram of a CDM sensing system.

A pseudorandom bit sequence (PRBS) is incorporated in the CDM sensing system as shown in Figure 2.8. The PRBS is used for simplicity of the experimental demonstration, while other bit sequences can also be used. A time shift version of the

PRBS sequence can be used to get the corresponding sensor information from the output.

Spatial-Division Multiplexing (SDM)

In many applications there is a need to use multiple fibers either to increase the number of sensing points or for improving the overall sensor system reliability. The sensors in these systems can be replace independently in the case of damage, and be interchangeable without the requirement of recalibration. Sensors with identical characteristics are quite feasible with FBGs. However, the serial WDM and TDM schemes prove unsuitable for interchangeability of sensors. SDM which is based on a parallel sensor topology is suitable for interchanging of sensors. Figure 2.9 shows one schematic diagram of SDM sensing system. In general, the FBG sensors in the SDM technique are located in different fiber branches and an optical switch can be used to select the desired fiber branch for monitoring. The SDM technique is a good candidate for combining with other multiplexing techniques such as TDM and WDM to increase the total number of sensors in a system. A state-of-the-art 60-sensor array system has been demonstrated by using a combined WDM and SDM approach [26].

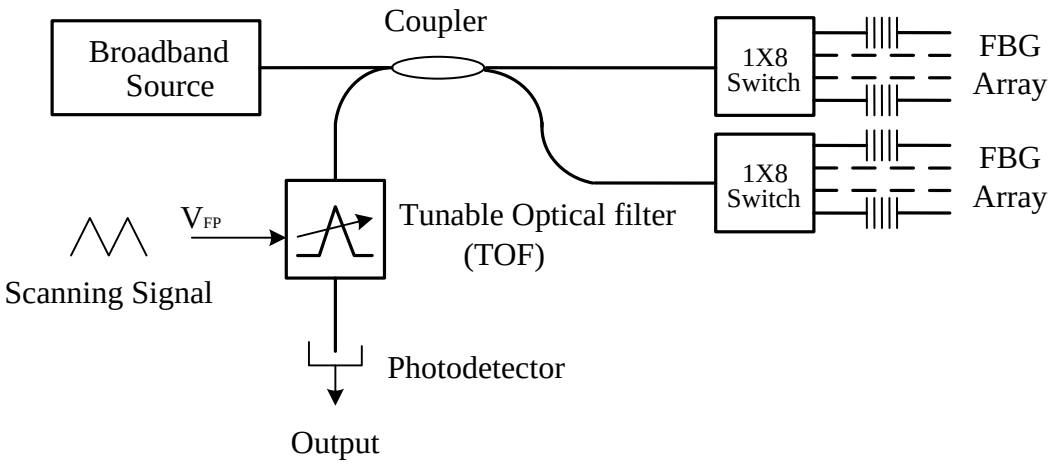

Figure 2.9 Schematic diagram of SDM sensing system.

Frequency-Modulated Continuous Wave (FMCW) Multiplexing

FMCW technique is using a linear frequency tuning radio frequency (RF) driver to modulate the intensity of the broadband source with demodulation achieved by using a tunable optical filter (Figure 2.10) [27].

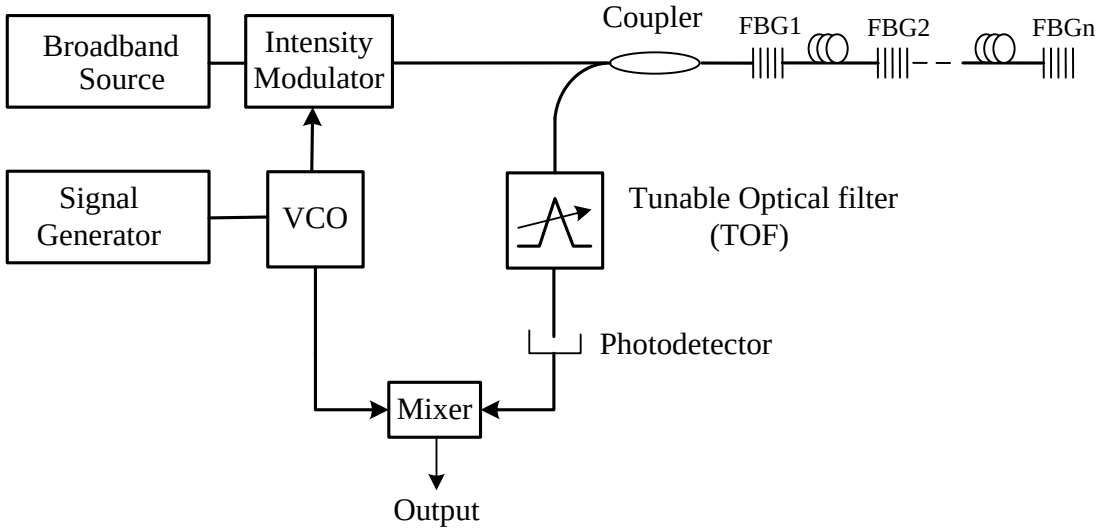

Figure 2.10 Schematic diagram of a FMCW multiplexing system.

The carrier is generated by a voltage-controlled oscillator (VCO). The

reflection signals of different FBG sensors in the array are distinguished in the frequency domain with the corresponding bandpass filters.

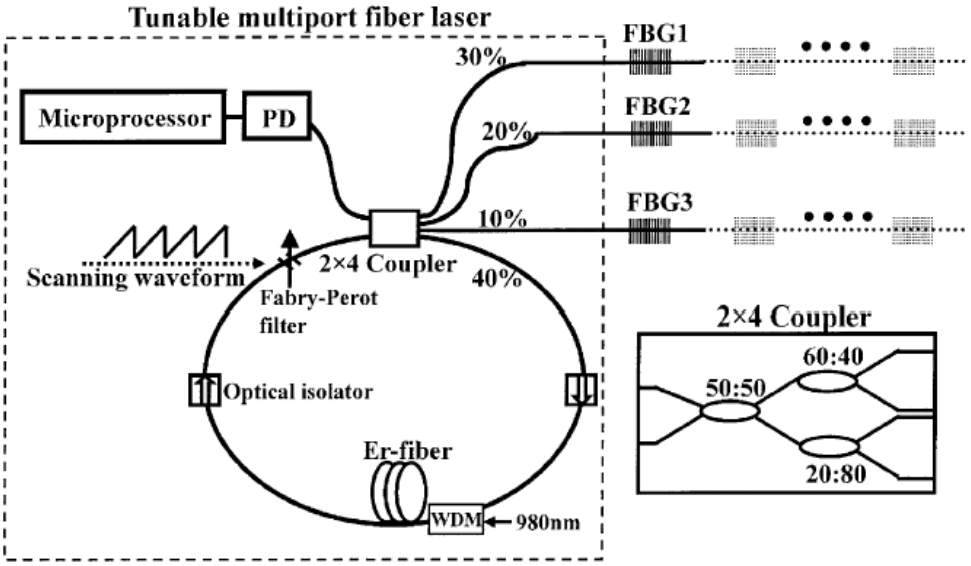

Figure 2.11 Schematic of a tunable multiport fiber laser for IWDM sensor system.

As multiplexing is a very important characteristic of FBG sensors, different multiplexing techniques are being continuously developed. Besides the common sensor multiplexing methods mentioned above, there are also other of less popular multiplexing technologies. There is a “bandwidth” constraint for WDM and a “time” constraint for TDM. Methods are proposed trying to overcome these constraints, such as intensity and wavelength dual-coding multiplexing (IWDM) technique [28]. It was shown that IWDM can double the sensor number for WDM by using two FBGs that allow wavelength overlap. One FBG has high reflectivity, while the other has low reflectivity with dual peak. Therefore, specially-designed FBGs are needed. Another research group proposed using different coupling ratios for FBGs with equal

reflectivity to achieve IWDM [29]. Figure 2.11 shows the proposed diagram of this approach.

2.4 Interrogation Techniques for FBG Sensor Systems

The sensor signal is usually wavelength encoded in FBG sensing systems. To demodulate the sensor signal, several techniques have been developed for performing wavelength shifting detection [30].

Edge filter is a wavelength-dependent loss device that provides a wavelength to intensity conversion. There is a tradeoff between the sensitivity and the measurement range (Figure 2.12). Using this approach, resolution of about $\pm 5\mu\varepsilon$ has been demonstrated [31]. The advantages of this approach are low cost and fast wavelength discrimination.

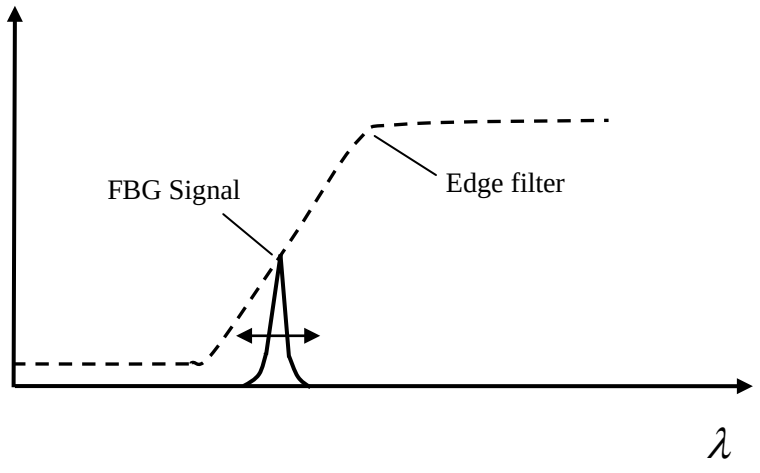

Figure 2.12 Conversion of wavelength to intensity using edge filter method.

As shown in Figure 2.13, the tunable filter approach for Bragg wavelength

detection is one of the most successful approaches in FBG sensor interrogation systems [32].

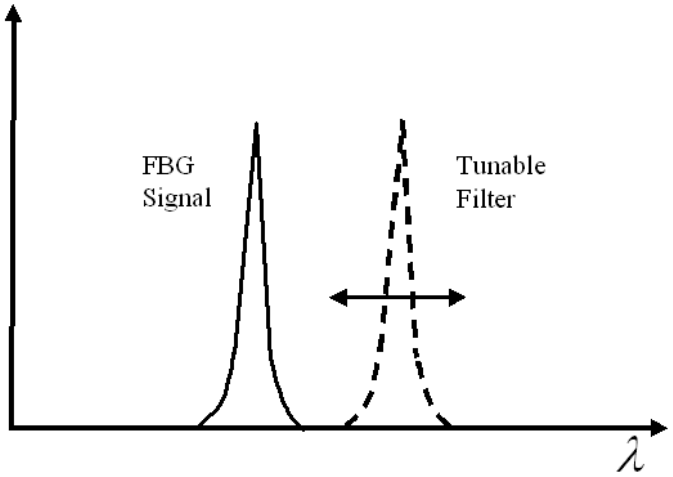

Figure 2.13 Schematic diagram of tunable filter method.

The tunable filter can be FBG-based filter, Fabry-Perot (FP) filter or acousto-optic filter or. The basic principle of the tunable filter approach is that the passband wavelength transmit through the filter depends on the voltage applied to the piezoelectric stacks that drive the filter. By tuning the filter, its passband will scan over the whole sensing wavelength range and cover the reflections of the FBGs. The wavelength can then be obtained by the corresponding voltage applied in the tunable filter when the maximum reflection power is detected. In strain measurement, resolution of the order about $\pm 1\mu\varepsilon$ has been demonstrated using FP approach [32].

The interferometric detection [33] is based on sinusoidal filtering effect. Figure 2.14 shows the sinusoidal transfer function of an interferometer. The wavelength of input signal will affect the phase term of the interferometer. This technique is very sensitive to small dynamic wavelength shifts. Dynamic shift

resolution on the order of about 10^{-3} pm has been experimentally demonstrated during weak mechanical perturbation of grating.

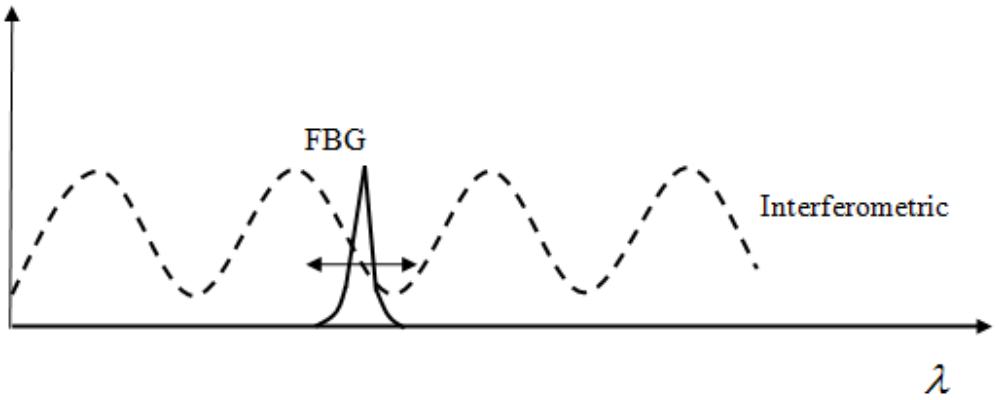

Figure 2.14 Principle of interferometric detection method.

A charge-coupled device (CCD) spectrometer [34] is a simple method for interrogation the gratings. The reflected light from the grating sensors is dispersed onto a linear CCD array using bulk grating and appropriate optics. The spectrometer reads the wavelength with a resolution determined by the product of the grating's linear dispersion at the detector plane with the pixel width, and the received wavelength is converted to intensity information in the CCD array along the detector elements. This instrument has demonstrated a strain sensitivity of ~1 $\mu\varepsilon$ and a bandwidth from static to 4kHz.

Fourier analysis is another tool for direct spectroscopic analyzing of the reflected FBG signals. The reflections from the array of FBG sensors are launched into an interferometer that one of its arms is moveable to adjust the relative optical path length. When the length of one arm is scanned, an interferogram between the two arms is produced at the detector as the relative path length goes to zero. A discrete

frequency component corresponding to the grating signal can be observed from frequency spectrum obtained by Fourier transforming the interferogram. Any Bragg wavelength shift of grating sensor can be detected by monitoring shifts in the Fourier frequency component. Bragg wavelength shift with resolution of ~0.015nm has been demonstrated [35].

2.5 Summary

We presented a brief review on FBGs which is the main fiber optical components investigated for sensing applications for the study presented in the thesis. The basic principle of FBGs is given with the development history, the fabrication, the optical properties, and their responses to some physical parameters including temperature and strain which make them promising candidates for many sensing applications. The multiplexing techniques and interrogation methods of FBG sensors are also introduced. Table 2.1 gives a brief comparison of several commonly used techniques for FBG sensor multiplexing.

multiplexing method	resolution	spectral efficiency	demodulation	system complexity
SDM	medium	low	moderate	moderate
WDM	high	low	moderate	simple
TDM	low	high	simple	moderate
CDM	medium	high	simple	moderate

Table 2.1 comparison of multiplexing techniques

Chapter 3 Code Division Multiplexing Based FBG Sensor System

3.1 Introduction

Fiber Bragg grating (FBG) has been developed to be a practical sensing component for environment parameter measurements, such as temperature, strain, load and vibration [5]. The unique advantages of FBG sensors make them the preferences for the applications that normal electrical sensors are unworkable. For example, they can be used in harsh environment of oil field or they can be embedded into constructions for structural health monitoring [36]. But the complexity and cost of system setup still limit the application of FBG sensors. To break this limitation, various multiplexing and interrogation schemes have been studied.

The purpose of multiplexing is to simplify the system setup and enhance the competitive. The sensors can be placed among many fibers and share the interrogation components spatially. This solution is limited by the optical switch which usually has high cost, slow switching time and few outputs. Another better solution is to place the sensors at different positions in a single fiber to setup the sensor array. This approach provides the quasi-distributed sensing capability and many different demodulation methods can be used to acquire the sensors' information along the fiber. It is simple and easy to implement multiplexing.

There are several technologies for Bragg grating sensor multiplexing in a single fiber. Two often used technologies are wavelength division multiplexing (WDM) and time division multiplexing (TDM) [19]. WDM is a widely used technique due to its good sensitivity and simple configuration. However, sensors in the array should be addressed with their dedicated wavelength range without any spectral overlap; therefore, the number of incorporated sensors is inherently restricted by the spectral bandwidth of the light source. In order to improve the spectral efficiency, an alternative method, TDM technique is explored. It utilizes the different time delays between reflected pulses to distinguish the multiplexed sensors. Thus the spectra of FBG sensors can overlap with each other and do not need to be separated, which greatly increases the utilization of the bandwidth, as reported [18], [38] for large-scale sensor array. There are many advantages of using TDM method to multiplex sensors, but drawbacks such as interference and cross talk also need to be considered and taken into account in the system implementation. In addition, the average detected power of TDM sensor system is extremely low because the pulse has to pass through all the sensors in the array and reflect back to the receiver before the next pulse can be sent and the sensor reflectivity must be low. This limits the interrogation speed for the sensing system which needs to meet a strict signal-to-noise ratio (SNR) requirement as well. Although high power laser and optical amplifier can be added to improve the input power and reflected power, the unwanted nonlinear effects and spectral shape distortion after amplifying should be treated carefully.

Trade off among these parameters has to be considered in a TDM system design.

Besides increasing input power, an alternative is to send more pulses into the sensor array. But the problem is that the reflected signals may spatially overlap and arrive at the detector at the same time if the reflection time delay between two FBG sensors is equal to the time delay between two pulses. In order to solve this problem, the sequence of input pulses should be coded carefully to let the sensor information be obtainable from the overlapped signals. This method is called code-division multiplexing (CDM). The CDM based FBG sensor systems were proposed and subsequently improved by K. P. Koo and Hyungdon Ryu [25], [39]. Based on the correlation processing, a sequence of pulses can be sent into the sensor array within the round-trip time and the individual sensor outputs can be exactly separated from the overlapped signals. However, in the above reports, additional time is needed for tunable laser to scan the whole wavelength range and it is not suitable for multiplexing large number of sensors. In addition, a standard PRBS sequence was used as the code sequence which is known to have nonzero cross-correlation with delayed version of the code, simple intensity modulation with direct detection results in a unipolar code and does not permit a completely cancelled interference. In order to solve above problem, improved method has been proposed by using two optical modulators at the receiver to realize balanced detection and convert the unipolar code to bipolar code [40]. But in this method, only one sensor can be detected in a round-trip time; meanwhile, the insertion loss of the optical modulators significantly reduces

the SNR at the receiver.

In this chapter, a novel scheme of CDM based sensor system is proposed and experimentally demonstrated. With special code design, it can achieve zero cross-correlation. A theoretical analysis is given to explain the operation principle of the proposed sensor system. The study shows that the proposed scheme enables simple sensor detection, improves signal to noise performance and offers the ability for cross talk compensation. In the proposed system setup, the codeword is unipolar, by using unipolar to bipolar conversion in electrical domain instead of in optical domain, a unipolar-bipolar correlation process can be achieved in the signal processing unit and all the sensors can be detected in a round-trip time. Experimental results demonstrated the feasibility of the proposed setup. The new scheme provides the potential for multiplexing hundreds of grating along a single fiber.

3.2 Review of CDM Based FBG Sensor Systems

In a CDM based sensor system, light pulse train representing a unique codeword is launched into the sensor array continuously. This means that the CDM approach can deliver more signal power than the TDM approach in a round-trip time and the system performance is expected to improve. Several schemes using CDM method in FBG sensor systems were proposed, the benefits and limitations of these schemes will be discuss in this section.

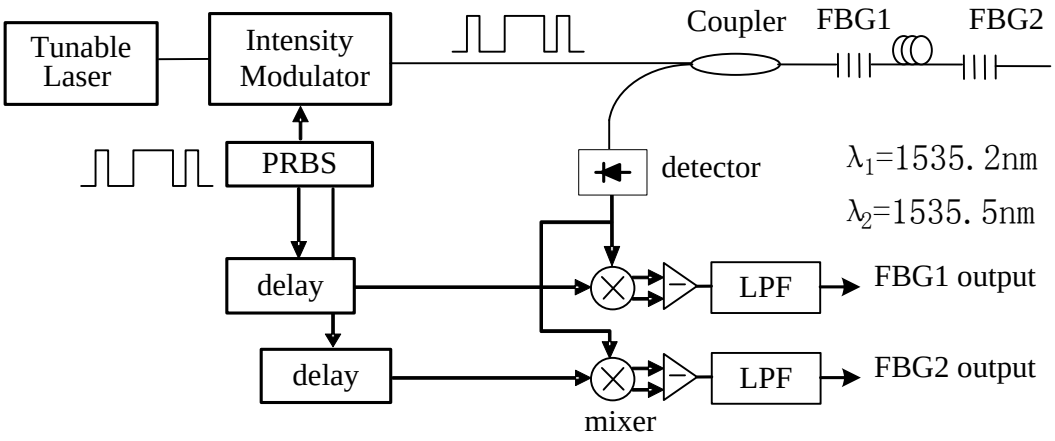

Figure 3.1 Schematic diagram of a CDM sensor system.

Figure 3.1 shows a scheme proposed by K.P. Koo [25]. A pseudorandom bit sequence (PRBS) is used for the CDM sensor system. A time shift version of the PRBS sequence is used to correlate with the reflections of FBG sensors to get the corresponding sensing information from the output. By placing the FBGs in the positions that the time delays between FBGs are equal to multiple times of the bit period of the PRBS, a selected grating sensor signal can be demultiplexed by correlating with a reference PRBS which has the same bit shifts. For decoding, two outputs were generated after the mixer, one is the correlation between the reflection of FBG sensor and the corresponding time delayed version of the PRBS sequence and the other is the correlation between the reflection of FBG sensor and the corresponding time delayed version of the complement PRBS sequence. By setting the proper time delays for the different channels, the information of FBGs can be selected. The maximum number of sensors in this CDM system depends on the length of bit sequence (2^m-1), which can be up to (2^m-1) by assuming a one-bit time delay

between sensors. For m = 8, it was expected the system can be used to multiplex up to 100 sensors.

In this system setup, a 0.3nm wavelength separation between sensors is needed to reduce the probability of multiple reflections between different sensors. In addition using the pseudorandom bit sequence as CDM codeword in the sensor system is not a good choice. The correlation between the PRBS and its one or multiply bit time-shifted version is always greater than zero even in the ideal bit synchronous condition. When the number of sensors increases, the multi-user interference will become dominant and affect the system performance. Also, using tunable laser as the light source will be time consuming when the tuning range is large.

But the decoding method here is very useful for incoherent optical system. this method uses the codeword subtract its complement as the decoding codeword, so the decoding process would be a unipolar-bipolar processing, and better multi-user interference cancellation could be obtained.

Figure 3.2 shows a scheme proposed by Hojoon Lee [40]. In this proposed system setup, he used the identical-chirped-grating interrogation to distinguish the center wavelength shift of the FBG [41] and the CDM method to separate different sensor signals. One pair of identical chirped gratings can be used to determine the external parameter change, such as strain or temperature. For the chirped grating pair sensor1 and filter1, in the initial state, both of them have the identical center wavelength. For this case, all reflected power is filtered by the chirped grating. In the

situation of applied strain, the wavelength of the sensor1 will shift and mismatch with the filter1. For this case, the optical power detected in the photodetector is proportional to the wavelength mismatch, and the mismatch is proportional to the applied strain, so the applied strain can be determined by the received power at the photodetector. Information of different sensors is separated by the different corresponding time-shifted correlation process.

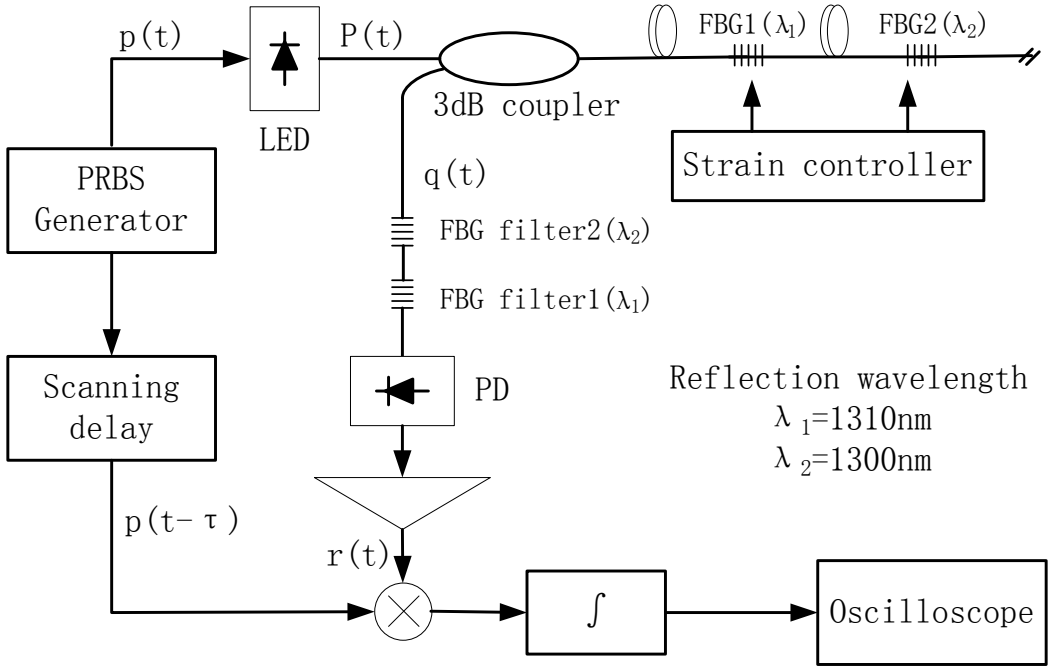

Figure 3.2 Experimental setup of Hojoo Lee's proposed system

In this scheme, a broadband source was used instead of tunable laser to overcome the wavelength scan rate limitation. Therefore, the wavelength demodulation needed to be done by a pair of chirped grating instead. The coding and decoding method was similar to the previous scheme and unipolar-bipolar correlation process was used. But the scheme also used PRBS which is not a good choice, and the chirped grating pairs must use different wavelength range, that means the wavelength

separation requirement is the same as the WDM sensor system, only a few sensors could be multiplexed.

Figure 3.3 shows another CDM based sensor multiplexing scheme proposed by S. Abbenseth [42]. In this scheme, they also use the unipolar-bipolar correlation process to get the intended information of the sensor, but the correlation is done in the optical domain through two modulators this time, and balanced code is used. Spectrometers are used to obtain the spectral information, so there is no spectral constraint between different sensors and they can have the same reflection wavelength. But spectrometers are expensive and have low detection speed. And only one sensor can be detected in a round-trip time. The system setup is not suitable to be extended to detect multiple sensors simultaneously.

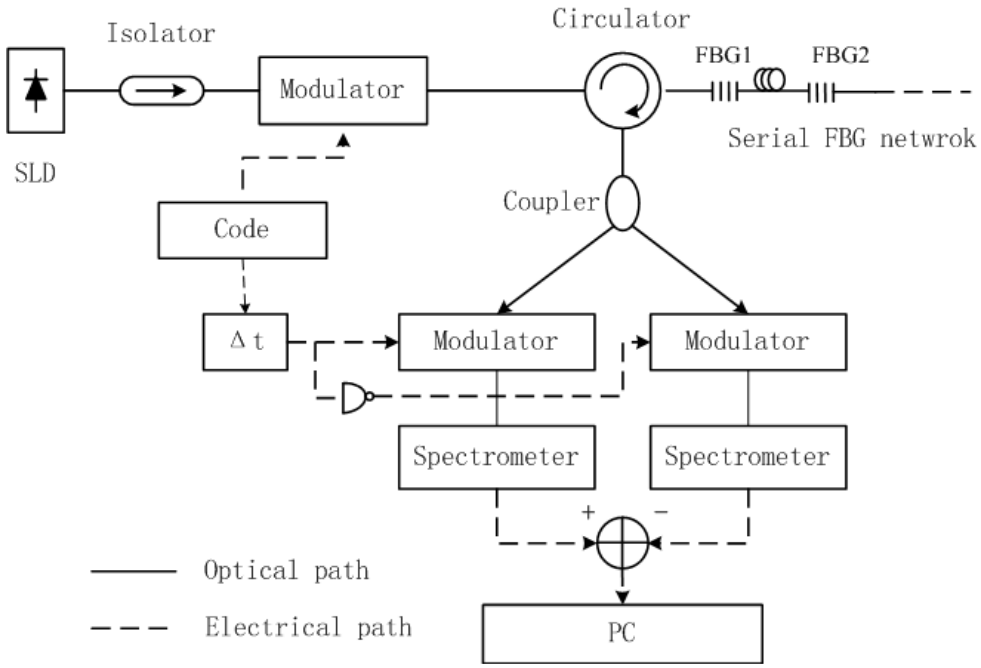

Figure 3.3 Experimental setup of S. Abbenseth's proposed system

From the reviews we can see that only preliminary study has been done in CDM based FBG sensor systems and no detailed analysis has been given. Further investigation of optimum system architecture and code design is needed. In order to design a simple and practical large scale FBG sensor multiplexing system using CDM method, several requirements are needed to be considered:

1. The wavelength demodulation method should allow FBG sensors with the same wavelength, which maximizes the bandwidth utilization. We will assume that all FBG sensors have the same sensing range and their spectra may be overlapped.

2. The wavelength demodulation method should allow fast wavelength discrimination.

3. The correlation between the codeword and its time-shifted version should ideally be zero. In CDM based FBG sensor systems, the input pulse sequence which denotes a CDMA codeword will be reflected by each sensor along the fiber. And the reflected sequences will arrive at the detector in different times which depend on the positions of the sensors along the fiber. So the reflected sequences could be considered as the time-shift versions of the codeword. Proper codeword design will reduce the correlation between the reflected sequences and improve the overall system performance.

In the next sections, we will describe our proposed system design and give thorough performance analysis of the system.

3.3 Code Design of the Proposed Sensor System

Figure 3.4 shows the block diagram of the proposed system setup. A light source generates broadband light pulses which are fed into the FBG array. The reflection spectra of the FBGs can be different, partially overlap or the same. The pulsed light is a unique sequence of “on” and “off” corresponding to the code patterns of “1” and “0” respectively. The light pulse sequence goes through the circulator and fed into the FBG sensors. The reflection signals will then go back to the signal processing unit via the circulator. The signal processing unit should consist of wavelength detection unit and electronic signal processing unit.

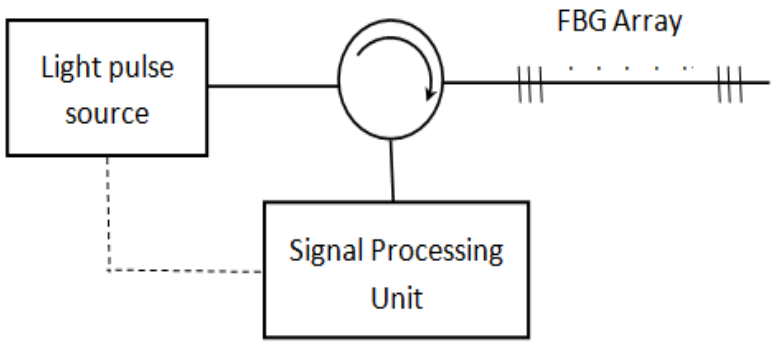

Figure 3.4 Block diagram of a CDM based FBG sensor system

By choosing sufficiently long pulse sequences, the reflected pulse sequences of sensors will overlap spatially and contain information of all the sensors in the array. The delay of the reflection pulse sequence generated by different sensors in the FBG array depends on the spatial position of the sensor. By placing the sensors in multiple time slot distances, one can keep the bit level synchronization of the reflection signals. With proper code design and sensor placement, signal of the specified sensor can be

decoded from the overlapped reflection pulses. Due to the on-off direct intensity modulation, there is no negative signal at the receiver. However, after converting optical signals into electrical signals, bipolar codeword can be used to do decoding in the signal process unit for interference cancelling and better system performance. So the coding and decoding process should better be unipolar-bipolar.

3.3.1 Sequences with Zero Autocorrelation Sidelobes

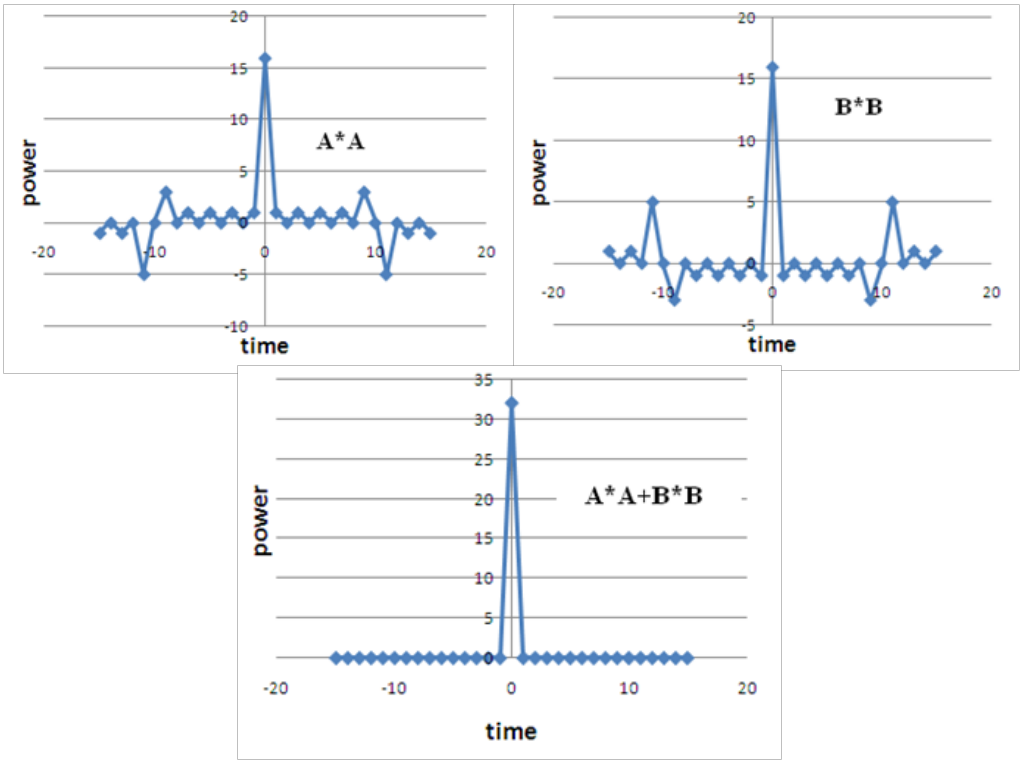

Figure 3.5 Complementary code autocorrelations

Complementary codes is a code pair A_k, B_k of L-element sequences whose element is either 1 or -1 and the sum of the autocorrelations of the two sequences is zero for all non-zero shifts. This kind of code sequences is first introduced by M. J. E. Golay in

late 1940's [43] and also called Golay sequences. For example, a code pair of 16 bit can be [1, 1, 1, -1, 1, 1, -1, 1, 1, 1, 1, -1, -1, -1, 1, -1] and [1, 1, 1, -1, 1, 1, -1, 1, -1, -1, -1, 1, 1, 1,- 1, 1].

Figure 3.5 shows the aperiodic autocorrelations properties of this code pair. The sidelobes are completely cancelled when the two individual autocorrelations added together. By using this code sequence pair, interferences from other signals can be cancelled exactly in an ideal system.

The complementary codes had been applied to an optical time domain reflectometer design to improve its system performance [44]. In order to utilize bipolar codes in a direct detection OTDR system where only positive optical intensity signals are generated in the photodetector, one bipolar code is decomposed into two unipolar codes and four successive probe "shots" are sent into the fiber. Figure 3.6 shows this algorithm.

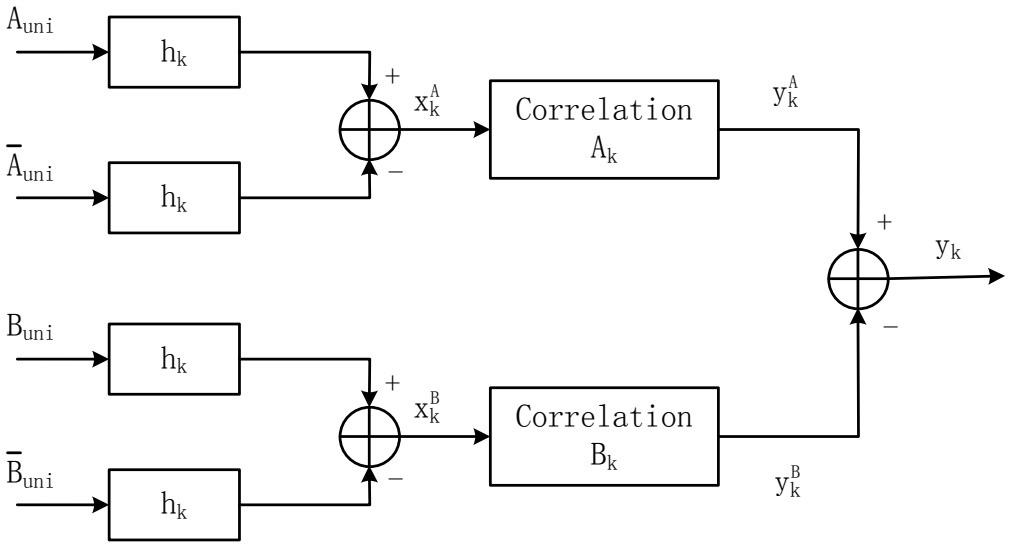

Figure 3.6 Complementary code OTDR algorithm

Four probe signals are injected into the fiber and the backscatter returns are detected: a unipolar version of the first code of a Golay pair and its 1's complement; a unipolar version of the second code of a Golay and its 1's complement.

The returns from the first two signals are subtracted from each other and correlated with a bipolar version of the first Golay code. The returns from the last two signals are subtracted from each other and correlated with a bipolar version of the second Golay code. The correlation outputs then are added up to yield an estimate y_k of the fiber response.

Although this method can also be adopted in the FBG sensor systems, a simpler code algorithm is needed that considering the characteristic of FBG sensor in its multiplexing systems.

3.3.2 Code Sequences in Which n is Power of 2

For unipolar-bipolar code design, the codeword contains "1" and "0", and the decoding codeword contains bipolar code "1" and "-1" for the correlation processing. This utilizes some properties of bipolar-bipolar process in electrical communication systems and is more suitable for intensity modulation optical systems. To completely cancel the multiuser interference, balanced code that has equal number of "1" and "0" is chosen.

Because in the proposed FBG sensor system, all reflected signal sequences are the time-shifted version of the input pulse sequence and they are synchronized in bit

level. We want to design a codeword such that the decoding codeword would be orthogonal with any cyclic time-shifted version of the codeword. Then in the ideal case, with the corresponding time-shifted decoding codeword, the signal of a sensor can be distinguished from the overlapped signal sequences. The interference from other sensors can be completely removed after the unipolar-bipolar correlation process.

It is easy to prove that the codeword whose bipolar version is orthogonal to all its single cyclic bit shift is nonexistent. So we should construct a cyclic unipolar-bipolar orthogonal codeword such that the bipolar version of which is orthogonal to its even cyclic bit shift version. This codeword has properties similar to the even-shift orthogonal sequences. Even-shift orthogonal sequences are a kind of binary sequences that its elements are either 1 or -1 and its autocorrelation functions are zero for all non-zero even bit shifts [45].

A codeword of length 2^n is defined as sequence $\mathbf{C_n}= [c_1,c_2,\ldots, c_2{}^n]$ whose element c_i (i=1,2,…, 2^n) is either 1 or 0. A method of constructing a 2^n bit codeword $\mathbf{C_n}$ may be described as follows:

First, a 2^{n-1} bit bipolar codeword $\mathbf{A_{n-1}}$ is constructed.

Then, the 2^n bit unipolar codeword $\mathbf{C_n}$ will be constructed from $\mathbf{A_{n-1}}$.

Let sequence $\mathbf{A_1}$ consists of two chips [1,-1], sequence $\mathbf{B_1}$ consists of two chips [1, 1], then [$\mathbf{A_1}$, $\mathbf{B_1}$] denotes [1,-1, 1, 1]; [- $\mathbf{A_1}$] means minus $\mathbf{A_1}$ and denotes [-1, 1]; $\mathbf{A_1}\cdot\mathbf{B_1}$ represents the cross-correlation between the sequences$\mathbf{A_1}$ and $\mathbf{B_1}$.

Therefore, from A_1 and B_1 given above, we have

$\mathbf{A_1 \cdot B_1 = 1*1 + (-1)*1 = 0}$
$\mathbf{A_1 \cdot A_1 = 1*1 + (-1)*(-1) = 2}$
$\mathbf{B_1 \cdot B_1 = 1*1 + 1*1 = 2}$

Subsequent sequences can be obtained using this procedure:

Let $\mathbf{A_2}=[\mathbf{A_1}, \mathbf{B_1}]= [1,-1, 1, 1]$, $\mathbf{B_2}=[-\mathbf{A_1}, \mathbf{B_1}]= [-1,1, 1, 1]$, $\mathbf{A_3}=[\mathbf{A_2}, \mathbf{B_2}] =[\mathbf{A_1}, \mathbf{B_1}, -\mathbf{A1}, \mathbf{B_1}]$ and $\mathbf{A_3}$ (n) denotes n bit shifts of $\mathbf{A_3}$, then the periodic autocorrelation and aperiodic autocorrelation property of sequence $\mathbf{A_3}$ can be showed in Table 3.1.

cyclic shifts					periodic autocorrelation
$\mathbf{A_3}(0)$	$\mathbf{A_1}$	$\mathbf{B_1}$	$-\mathbf{A_1}$	$\mathbf{B_1}$	$\mathbf{A_3 \cdot A_3}=8$
$\mathbf{A_3}(2)$	$\mathbf{B_1}$	$\mathbf{A_1}$	$\mathbf{B_1}$	$-\mathbf{A_1}$	$\mathbf{A_3}(0) \cdot \mathbf{A_3}(2)=0$, because $\mathbf{A_1 \cdot B_1}=0$
$\mathbf{A_3}(4)$	$-\mathbf{A_1}$	$\mathbf{B_1}$	$\mathbf{A_1}$	$\mathbf{B_1}$	$\mathbf{A_3}(0) \cdot \mathbf{A_3}(4)=2(-\mathbf{A_1 \cdot A_1}+\mathbf{B_1 \cdot B_1})=0$
$\mathbf{A_3}(6)$	$\mathbf{B_1}$	$-\mathbf{A_1}$	$\mathbf{B_1}$	$\mathbf{A_1}$	$\mathbf{A_3}(0) \cdot \mathbf{A_3}(6)=0$, because $\mathbf{A_1 \cdot B_1}=0$
acyclic shifts					aperiodic autocorrelation
$\mathbf{A_3}(0)$	$\mathbf{A_1}$	$\mathbf{B_1}$	$-\mathbf{A_1}$	$\mathbf{B_1}$	$\mathbf{A_3 \cdot A_3}=8$
$\mathbf{A_3}(2)$		$\mathbf{A_1}$	$\mathbf{B_1}$	$-\mathbf{A_1}$	$\mathbf{A_3}(0) \cdot \mathbf{A_3}(2)=0$, because $\mathbf{A_1 \cdot B_1}=0$
$\mathbf{A_3}(4)$			$\mathbf{A_1}$	$\mathbf{B_1}$	$\mathbf{A_3}(0) \cdot \mathbf{A_3}(4)=(-\mathbf{A_1 \cdot A_1}+\mathbf{B_1 \cdot B_1})=0$
$\mathbf{A_3}(6)$				$\mathbf{A_1}$	$\mathbf{A_3}(0) \cdot \mathbf{A_3}(6)=\mathbf{A_1 \cdot B_1}=0$

Table3.1 even autocorrelation property of a 8 bit sequence $\mathbf{A_3}$

From Table 3.1 we can see that $\mathbf{A_3}$ have the following properties:

(1) The even bit shift periodic autocorrelation will be zero

(2) The even bit shift aperiodic autocorrelation will be zero.

In general, for integer $n \geq 2$, $\mathbf{A_n}$ is constructed as $\mathbf{A_n}=[\mathbf{A_{n-1}}, \mathbf{B_{n-1}}]$, $\mathbf{B_n}=[-\mathbf{A_{n-1}}, \mathbf{B_{n-1}}]$,

It is clear that for any given integer k, where $1 \leq k < n$, $\mathbf{A_n}$ can be written as an array of alternated $\mathbf{A_k}$ and $\mathbf{B_k}$. Ignoring the sign of $\mathbf{A_k}$ and $\mathbf{B_k}$, then $\mathbf{A_n}$ would be:

$\mathbf{A_n}=[\mathbf{A_k}, \mathbf{B_k}, \mathbf{A_k}, \mathbf{B_k}, \ldots \mathbf{A_k}, \mathbf{B_k}]$

Supposing $\mathbf{A_{n-1}} \cdot \mathbf{B_{n-1}} = 0$, $\mathbf{A_{n-1}} \cdot \mathbf{A_{n-1}} = \mathbf{B_{n-1}} \cdot \mathbf{B_{n-1}} = 2^{n-1}$, then

$\mathbf{A_n} \cdot \mathbf{B_n} = \mathbf{A_{n-1}} \cdot (-\mathbf{A_{n-1}}) + \mathbf{B_{n-1}} \cdot \mathbf{B_{n-1}} = 0;$

$\mathbf{A_n} \cdot \mathbf{A_n} = \mathbf{B_n} \cdot \mathbf{B_n} = \mathbf{A_{n-1}} \cdot \mathbf{A_{n-1}} + \mathbf{B_{n-1}} \cdot \mathbf{B_{n-1}} = 2^n$

When n=2,

$\mathbf{A} \cdot \mathbf{B} = 1*1 + (-1)*1 = 0,$
$\mathbf{A} \cdot \mathbf{A} = 1*1 + (-1)*(-1) = 2,$
$\mathbf{B} \cdot \mathbf{B} = 1*1 + 1*1 = 2,$

satisfied the supposed conditions.

So from the mathematical induction, for integer $n \geq 1$, we have

$\mathbf{A_n} \cdot \mathbf{B_n} = 0$ and $\mathbf{A_n} \cdot \mathbf{A_n} = \mathbf{B_n} \cdot \mathbf{B_n} = 2^n$.

For any 2k bit shifts of $\mathbf{A_n}$, where $1 \leq 2k < 2^n$, 2k can be written in the form of $2k = q*2^m$, where q is an odd number and $m \geq 1$.

Because $\mathbf{A_n}=[\mathbf{A_{n-1}}, \mathbf{B_{n-1}}]$, $\mathbf{B_n}=[-\mathbf{A_{n-1}}, \mathbf{B_{n-1}}]$, so for a given $m \geq 1$, ignoring the signs, we can rewrite $\mathbf{A_n}$ as the form $[\mathbf{A_m}, \mathbf{B_m}, \mathbf{A_m}, \mathbf{B_m}, \ldots \mathbf{A_m}, \mathbf{B_m}]$. Then a 2k bit shifts of $\mathbf{A_n}$ means q step shifts in the form $[\mathbf{A_m}, \mathbf{B_m}, \mathbf{A_m}, \mathbf{B_m}, \ldots \mathbf{A_m}, \mathbf{B_m}]$.

Because q is an odd number, so the periodic and aperiodic correlation between $\mathbf{A_n}$ and $\mathbf{A_n}(2k)$ will be the sum of $\sum \mathbf{A_m} \cdot \mathbf{B_m}$.

Actually $\mathbf{A_m} \cdot \mathbf{B_m}$ always equal to 0, so the periodic and aperiodic correlation between $\mathbf{A_n}$ and $\mathbf{A_n}(2k)$ will be zero.

So for integer $n \geq 2$, $\mathbf{A_n}$ has the following properties:

(1) The even bit shifted periodic autocorrelation will be zero

(2) The even bit shifted aperiodic autocorrelation will be zero.

With $\mathbf{A_{n-1}}$, a 2^n bit unipolar codeword $\mathbf{C_n}$ can be generated for the proposed optical fiber sensor system.

Let a_i be the *i*th element of the 2^{n-1} bit codeword $\mathbf{A_{n-1}}$. Therefore we have

$$\mathbf{A_{n-1}} = [a_1, a_2, a_3, \ldots a_{2^{n-1}}]$$

Let $e_i = (1+ a_i)/2$, and a unipolar codeword $\mathbf{E_{n-1}}$ can be obtained as

$$\mathbf{E_{n-1}} = [e_1, e_2, e_3, \ldots e_{2^{n-1}}]$$

$\mathbf{E_n}$ is a unipolar code and all its elements will either be 1 or 0. Let $\overline{E}_{n-1}$ be the complement of $\mathbf{E_{n-1}}$, then $\mathbf{C_n}$ can be constructed as

$$\mathbf{C_n} = [\mathbf{E_{n-1}}, \overline{\mathbf{E}}_{n-1}]$$

And the decoding codeword $\mathbf{D_n}$ would be

$$\mathbf{D_n}=\mathbf{C_n}- \overline{\mathbf{C}}_n = [(\mathbf{E_{n-1}} - \overline{\mathbf{E}}_{n-1}) ,(\overline{\mathbf{E}}_{n-1}- \mathbf{E_{n-1}})] = [\mathbf{A_{n-1}}, -\mathbf{A_{n-1}}].$$

So $\mathbf{D_n}\cdot\mathbf{C_n}=[\mathbf{A_{n-1}}, -\mathbf{A_{n-1}}] \cdot[\mathbf{E_{n-1}}, \overline{\mathbf{E}}_{n-1}]= \mathbf{A_{n-1}} \cdot(\mathbf{E_{n-1}} - \overline{\mathbf{E}}_{n-1})= \mathbf{A_{n-1}} \cdot\mathbf{A_{n-1}} =2^{n-1}$.

We define an all "1"codeword$\mathbf{X_n}$ =[1,1,1, … 1], then $\mathbf{E_{n-1}}$ can be wrote as

$$\mathbf{E_{n-1}}=(1/2)*[\mathbf{X_{n-1}} + \mathbf{A_{n-1}}],$$

So $\mathbf{C_n}= (1/2)* [\mathbf{X_{n-1}} + \mathbf{A_{n-1}}, \mathbf{X_{n-1}} - \mathbf{A_{n-1}}] =(1/2)*\mathbf{X_n}+(1/2)* [\mathbf{A_{n-1}}, - \mathbf{A_{n-1}}]$.

In the unipolar-bipolar correlation process, correlation $\mathbf{D_n}$and$\mathbf{C_n}$would be

$$\mathbf{D_n}\cdot\mathbf{C_n}=[\mathbf{A_{n-1}}, -\mathbf{A_{n-1}}] \cdot[\mathbf{E_{n-1}}, \overline{\mathrm{E}}_{n-1}]= \mathbf{A_{n-1}} \cdot(\mathbf{E_{n-1}} - \overline{\mathrm{E}}_{n-1})= \mathbf{A_{n-1}} \cdot\mathbf{A_{n-1}} =2^{n-1}.$$

For any 2k bit shifts of $\mathbf{C_n}$, where $1 \leqslant 2k < 2^n$, we now calculate the correlation between $\mathbf{D_n}$ and $\mathbf{C_n}$(2k).

Because $\mathbf{D_n}=[\mathbf{A_{n-1}}, -\mathbf{A_{n-1}}]$, $\mathbf{C_n}=(1/2)*\mathbf{X_n}+(1/2)* [\mathbf{A_{n-1}}, - \mathbf{A_{n-1}}]$ and $\mathbf{X_n}$ is an all "1"s sequence, so

$$\mathbf{D_n}\cdot\mathbf{C_n}(2k)= (1/2)*\mathbf{D_n}\cdot\mathbf{D_n}(2k)$$

Because 2k can be written in the form of $2k=q*2^m$, where q is an odd number and $1\leq m\leq n-1$.

As described above, because $\mathbf{A_n}=[\mathbf{A_{n-1}}, \mathbf{B_{n-1}}]$, $\mathbf{B_n}=[-\mathbf{A_{n-1}}, \mathbf{B_{n-1}}]$,

For a given m<n-1, ignoring the signs, we can rewrite $\mathbf{A_{n-1}}$ as

$[\mathbf{A_m}, \mathbf{B_m}, \mathbf{A_m}, \mathbf{B_m}, \ldots\mathbf{A_m}, \mathbf{B_m}]$, and $\mathbf{D_n}=[\mathbf{A_{n-1}}, -\mathbf{A_{n-1}}]$, so $\mathbf{D_n}$ also can be expressed as the form $[\mathbf{A_m}, \mathbf{B_m}, \mathbf{A_m}, \mathbf{B_m}, \ldots\mathbf{A_m}, \mathbf{B_m}]$, then a 2k bit shifts of $\mathbf{D_n}$ means q steps shift in the form $[\mathbf{A_m}, \mathbf{B_m}, \mathbf{A_m}, \mathbf{B_m},\ldots\mathbf{A_m}, \mathbf{B_m}]$.

Because q is an odd number, so the periodic and aperiodic correlation between $\mathbf{D_n}$ and $\mathbf{D_n}(2k)$ will be sum up of $\sum \mathbf{A_m}\cdot \mathbf{B_m}$.

Actually $\mathbf{A_m}\cdot \mathbf{B_m}$ always equal to 0, so the periodic and aperiodic correlation between $\mathbf{D_n}$ and $\mathbf{D_n}(2k)$ will be zero.

This shows that the even bit shifts periodic correlation between codeword $\mathbf{C_n}$ and its bipolar version $\mathbf{D_n}$ is zero. After decoding process, the reflected sequences from these sensors ideally will have no interference to the intended reflected sequence.

But when m=n-1, q is equal to 1, then the 2^{n-1} bit shifts of $\mathbf{D_n}$, $\mathbf{D_n}(2k)$ would be

$\mathbf{D_n}(2k) =[-\mathbf{A_{n-1}}, \mathbf{A_{n-1}}]$, and $\mathbf{D_n}\cdot\mathbf{D_n}(2k)=-2\,\mathbf{A_{n-1}}\cdot\mathbf{A_{n-1}} = -2^n$.

This shows that the 2^{n-1}bitshiftsperiodiccorrelationbetweencodeword $\mathbf{C_n}$ and its bipolar version $\mathbf{D_n}$ would not be zero. So in the sensor system, the reflected time delay between any two sensors must not be 2^{n-1} bit period, or else they cannot be

distinguish from each other through the decoding process.

Hence we can place at most 2^{n-2} FBG sensors in the system by using the 2^n bit codeword $\mathbf{C_n}$ and unipolar-bipolar correlation process theoretically. But actually the number of sensors is limited by other factors such as multiple reflections and beating noise. One limitation should be considered is the cross talk from multiple reflections [13], the number of sensors that can be placed is significantly fewer than the number of time slot in the array. This shows that the constructed codeword is suitable for the proposed sensor system.

Here is an example for code length of 16 bit:

C=[1,0,1,1,0,1,1,1,0,1,0,0,1,0,0,0] and

D=[1,-1,1,1,-1,1,1,1,-1,1,-1,-1,1,-1,-1,-1]

In a real-world system, the extinction ratio of on-off modulation is finite. The input signal of “0” could not be ideally zero optical power, so there will also be some small power reflected back from the input signal “0”. Thus, the reflection sequence from a two bit time period delayed sensor can be expressed as:

R(2)= [r1,r1,r0,r1,r1,r1,r0,r1,r0,r0,r1,r0,r0,r0,r1,r0],

where r1 is the reflection from pulse “1”and r0 is the reflection from pulse “0”.

The correlation between R(2) and D is exactly zero in the ideal case that the wavelength of sensor remains the same at the moment thus its reflection power from pulse “1” and pulse “0” keeps the same respectively.

As mentioned previously, the correlation of R(8) and D wouldn't be zero, so the FBG sensor cannot be placed at the position of 8 bit time period reflection delay after the first sensor. For the same reason, if a sensor was placed at the position of 2 bit delay, the position of 10 bit delay should not be placed.

3.3.3 Code Sequences in Which n is Any Even Number

There are two disadvantages in the constructed codeword of the previous section:

1. The length of code sequences is restricted to a power of 2.
2. The 2^{n-1} bit shifts periodic correlation between codeword $\mathbf{C_n}$ and its bipolar version $\mathbf{D_n}$ is nonzero. So in the sensor system, more attention is needed for the placement of sensors to avoid 2^{n-1} bit period time delay between each other.

In this section, code sequences of length n where n is any even number has been further investigated. The correlation function between its bipolar version and the codeword itself is zero for all non-zero even shifts is achieved. This enhances the flexibility of system design.

Suppose a code sequence of length 2n is defined as $\mathbf{C} = [a_1, b_1, a_2, b_2,\ldots, a_n, b_n]$ whose elements a_i, b_i (i=1, 2, …,n) are either 0 or 1; and a decoding code sequence of length 2n is defined as $\mathbf{D} = [c_1, d_1, c_2, d_2,\ldots, c_n, d_n]$ whose elements c_i, d_i (i=1, 2, …,n) are either -1 or 1.

Then the cross-correlation between **D** and 2j bit even cyclic shift of **C** should satisfy:

$$\sum_{i=1}^{j} c_i a_{n-j+i} + d_i b_{n-j+i} + \sum_{i=j+1}^{n} c_i a_{i-j} + d_i b_{i-j} = 0, \quad (3.1)$$

where 0< j <n.

$$\sum_{i=1}^{n} a_i c_i + b_i d_i = \mathrm{m}, \quad (3.2)$$

where j=0 and m denotes the received power after correlation.

To increase the received power in the sensor system, the larger the value of m the better. So from (3.2) we can deduce that for any a_i, b_i equal to 1, the corresponding c_i, d_i should be 1 respectively. This means:

c_i=1 when a_i =1 and d_i=1 when b_i =1. (3.3)

And in order to completely cancel the interference from other sensors, m must be even and **D** needs to be a balance code, the sum of elements in **D** is zero. That is:

$$\sum_{i=1}^{n} c_i + d_i = 0. \quad (3.4)$$

Suppose the number of "1" in a_i is m_1, the number of "1" in b_i is m_2 and let $m_1$larger or equal to m_2, then (3.2) can be condensed to

m_1+ m_2=m. (3.5)

Using (3.1) to sum up from j=1 to n-1, we have:

$$\sum_{\mathrm{j}=1}^{\mathrm{n}-1} \left(\sum_{\mathrm{i}=1}^{\mathrm{j}} c_i a_{n-j+i} + d_i b_{n-j+i} + \sum_{\mathrm{i}=\mathrm{j}+1}^{\mathrm{n}} c_i a_{i-j} + d_i b_{i-j} \right) = 0 \quad (3.6)$$

And can be rewrite as:

$$\sum_{\mathrm{i}=1}^{\mathrm{n}} \left(c_i \sum_{\mathrm{j}=1}^{\mathrm{n}} a_j - c_i a_i + d_i \sum_{\mathrm{j}=1}^{\mathrm{n}} b_j - d_i b_i \right) = 0 \quad (3.7)$$

Suppose the sum of c_i is x, from (3.4) the sum of d_i will be –x. So (3.7) can be condensed as:

$$(m_1 - m_2)x = m \tag{3.8}$$

From equation (3.5), (3.8) we derive

$$m_1 = \frac{1}{2}(m + \frac{m}{x}) \tag{3.9}$$

$$m_2 = \frac{1}{2}(m - \frac{m}{x}) \tag{3.10}$$

Because the sum of c_i is x, the number of "1" in c_i then is (n+x)/2. With condition of (3.3), we can get：

$$(n+x)/2 \geq m_1 \tag{3.11}$$

The sum of c_i is -x, the number of "1" in d_i then is (n-x)/2. With condition of (3.3), we can get：

$$(n-x)/2 \geq m_2 \tag{3.12}$$

Replacing (3.9) into (3.11) and (3.10) into (3.12), we derive

$$m - n \leq x - \frac{m}{x} \leq n - m \tag{3.13}$$

So for a given a code length of 2n, the maximum of m should satisfy equation (3.13).

Because all the number here is integer, two more rules can be derived to help to find the maximum of m easier.

1. If n is even, x needs to be even, from (3.9) then $\frac{m}{x}$ must be even too. So m must be multiples of 4 for n is even.
2. If n is odd, x needs to be odd. m should a odd factor larger than 1.

Table 3.2 shows the maximum number of “1” for code length 6 to 32 from equation (3.13).

code length of 2n	6	8	10	12	14	16	18	20	22	24	26	28	30	32
maximum m	2	4	2	4	6	4	6	8	6	8	10	8	12	16

Table 3.2 Maximum of m for different code length

To verify table 3.2, a computer program is used to exhaustive search the possible codeword from length of 6 to 32. The result is just the same as table 3.2.

Some examples are:

6: C=[0,0,1,0,1,0] D=[-1,-1,1,-1,1,1]

8: C=[0,0,1,0,1,0,1,1] D=[-1,-1,1,-1,1,-1,1,1]

10: C=[0,0,0,0,0,0,1,0,1,0] D=[-1,-1,1,-1,-1,-1,1,1,1,1]

12: C=[0,0,0,0,0,0,1,0,1,0,1,1] D=[-1,-1,1,-1,-1,1,1,-1,1,-1,1,1]

For the code length of 32, the maximum number of “1” is 16, just equals to the half of code length which is the upper bound. So the codeword of length 32 constructed here has the same performance as it was constructed in the previous section but with less restrictions. Because all cyclic even shifts of the codeword are orthogonal to its decoding codeword, the sensors can be simply placed at any even bit time period delayed positions.

There is not any straightforward way to construct a codeword of any length. However, for a given codeword of length 2n, a codeword with length of 8n can be constructed.

Suppose a given code sequence of length 2n is **C** = [a_1, b_1, a_2, b_2,…, a_n, b_n] and its decoding code sequence is **D** = [c_1, d_1, c_2, d_2,…, c_n, d_n], it can be proved that

C=[a_1, a_1,$\bar{a}_1$, a_1, b_1,b_1,b_1,$\bar{b}_1$, …, a_n, a_n,$\bar{a}_n$, a_n, b_n, b_n, b_n, $\bar{b}_n$] and

D=[c_1, c_1, -c_1, c_1, d_1,d_1,d_1,-d_1, …, c_n, c_n, -c_n, c_n, d_n, d_n, d_n, -d_n] are the code sequence and its decoding sequence of length 8n.

By using this rule, a longer codeword may be constructed from the shorter codeword which is much easier to exhaustive search.

3.4 Operation Principle and Theoretical Analysis

The system setup is shown in Figure 3.7. As described in the above section, a proper code sequence is used to drive the SLED to generate a pulse sequence. The reflected power from different FBG sensors can be distinguished by using its corresponding delay version of the decoding codeword. This breaks the restriction of TDM sensor systems that only one pulse can be sent within a round trip time and more power can be detected at the receiver.

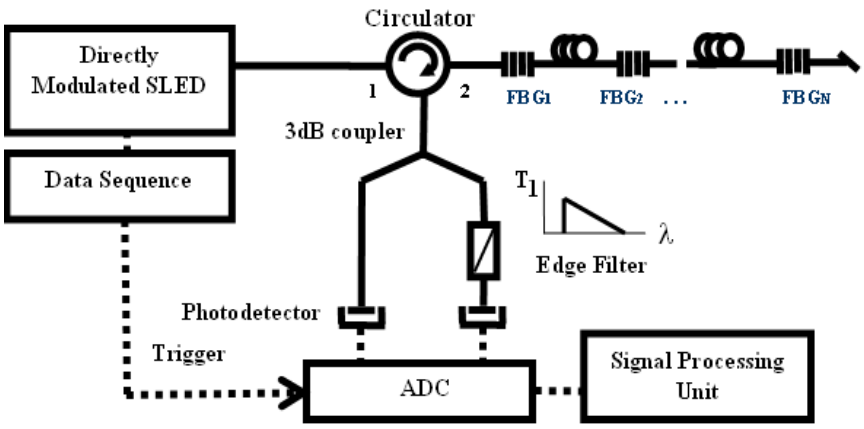

Figure 3.7 Experimental setup of the proposed CDM based FBG sensor system

In grating sensor systems, the change of measurand (such as temperature, strain) is usually wavelength encoded. There are various methods to measure the wavelength shift to demodulate the sensor signal in system, such as edge filter [46], scanning match filter [47], and interferometric detection [16]. In order to demodulate the wavelengths of different sensors in the overlapped signal, edge filter method is used in the proposed system setup. For the edge filter method, the reflected optical signals are divided into two paths by a 3dB coupler. The left path is unfiltered and optical power is measured with the photodetector directly as wavelength independent reference; the right path is filtered by the edge filter and the transmission power is wavelength dependent. With reference power, filtered power and the filter curve, one can obtain the wavelength information after signal processing. This passive wavelength-power ratio conversion method offers a high speed demodulation with simple configuration. The wavelength resolution of edge filter depends on the input signal-to-noise ratio (SNR) and the slope of filter curve. A simple way to improve resolution is to let the slope larger. But actually the maximum slope of the edge filter is limited by the input SNR [48]. The slope that exceeded the maximum will lead to worse system performance. So the edge filter slope should be optimized to improve the resolution under the estimation of reflected signal SNR and system requirement of discrimination wavelength range.

In the signal processing unit, signal of two paths need to be decoded separately to obtain the power of particular sensor before calculating its wavelength information.

Suppose the pulse period is T_b, the round-trip time is nT_b. Here round-trip time means the time for the pulse to travel from the first FBG to the last FBG and then goes back to the first one. So the number of time slots is n. Let the codeword also be n bits that equals to the round-trip time and the number of sensors in the array be m.

Considering a single reflected pulse from the FBG sensor in the TDM sensor system, since the output of SLED is amplified spontaneous emission (ASE) and the reflection spectral of FBG sensor is narrow, the dominant noise of the reflected pulse would be thermal noise and spontaneous-spontaneous beat noise at the photodetector. So the SNR of the single reflected pulse after left arm would be:

$$SNR_0 = \frac{I^2}{i_{th}^2 + i_{sp}^2}, \tag{3.14}$$

where *I* is the photodetector output generated by the reflected pulse power, i_{th}^2 is the thermal noise and i_{sp}^2 is the beatnoise between the various frequencies within the reflected spectrum of the ASE.

The thermally generated current noise is given by

$$i_{th}^2 = 4kTB_e/R, \tag{3.15}$$

where *R* is the resistance which the photocurrent first experiences, *k* is Boltzmann's constant and equals to $1.38*10^{-23}$ J/K, *T* is the temperature of the resistor in Kelvin and *Be* is the electric bandwidth of the signal, here $Be=1/T_b$, T_b is the bit period.

The intensity noise generated by spontaneous-spontaneous beating between various frequencies in the reflected signal is given by [48]:

$$i_{sp}^2 = I^2 \frac{0.66 B_e}{B_o} \ , \tag{3.16}$$

where B_o is the full width half maximum (FWHM) spectral width of the Gaussian shape reflected signal in Hertz and B_e is the electrical bandwidth of the signal.

SNR of reflected pulse after right arm with edge filter is:

$$SNR_{0R} = \frac{\alpha^2 I^2}{i_{th}^2 + \alpha^2 i_{sp}^2} \ , \tag{3.17}$$

where α is the transmission ratio of the edge filter.

Wavelength is obtained from the normalized power ratio between the two arms. So the SNR of wavelength signal would be:

$$\frac{1}{SNR_0} = \frac{1}{SNR_{0L}} + \frac{1}{SNR_{0R}} \tag{3.18}$$

Because more than one pulse is sent within a round-trip time, some reflected signals from different sensors would spatially overlap. If the spectra of the overlapped signals are partially overlap or the same, the beat noise of ASE will increase rapidly as proportional to the square of its dc current *I*.

For the worst case, all sensors have the same Bragg wavelength for a given time, the beat noise would be maximal in this case because all the overlapped signals have the same optical frequencies and beat with each other to enlarge the fluctuation of the detector output. For a given sensor, after decoding, the dc output would be n*I*/2 for an n bit length balanced codeword.

Because the noise is statistic independence for each pulse, it will simple add together in the decoding process after the ADC. The thermal noise would be:

$$i_{th-all}^2 = ni_{th}^2 \tag{3.19}$$

The spontaneous-spontaneous beat noise is proportional to the square of dc component. The power of the reflection pulses in the sequence is different due to the number of sensor signals that overlapped together in the pulse is different. Besides, the reflected power of each sensor is different caused by power depletion. To simplify the derivation, we suppose that for an m sensors array, the reflected power for each sensor is equal the number of "1"s overlapped in a reflected bit period would have a uniform distribution from 0 to m. The beat noise would be:

$$i_{sp-all}^2 = n\frac{(0^2+1^2+2^2+\cdots m^2)I^2}{m+1}\frac{0.66B_e}{B_o} \approx \frac{nm^2}{3}i_{sp}^2 \tag{3.20}$$

The signal to noise ratio of left arm after decoding would be:

$$SNR_{1L} = \frac{(nI/2)^2}{i_{th-all}^2+i_{sp-all}^2} = \frac{nI^2}{4i_{th}^2+\frac{4}{3}m^2i_{sp}^2} \tag{3.21}$$

And the SNR of right arm after decoding would be:

$$SNR_{1R} = \frac{n\alpha^2I^2}{4i_{th}^2+m^2\alpha^2i_{sp}^2} \tag{3.22}$$

So the SNR of wavelength using CDM method would be:

$$\frac{1}{SNR_1} = \frac{1}{SNR_{1L}} + \frac{1}{SNR_{1R}} \tag{3.23}$$

Comparing SNR_1 with SNR_0, one can get the performance improvement by using CDM based sensor system than the typical TDM sensor system.

In a typical system, the input power density of an SLED is 0.2mW/nm. The reflectivity of FBG is around 2% and FWHM is 0.2nm. The bandwidth B_e is 50MHz, the response of detector is 1A/W with thermal noise density $20\text{pA}/\sqrt{\text{Hz}}$. The code length is 1024 with 50 sensors in the array to keep n/m>20 to reduce the multiple reflections. After calculation, i_{th}^2 is $2*10^{-14}\text{A}^2$ and i_{sp}^2 is $8.44*10^{-16}\text{A}^2$. If α equals to

0.5, then SNR_0 is 6.4 and SNR_1 is about 141 in one round-trip time. That means CDM system gives about 13.4dB signal to noise ratio improvement. And in this situation, the sp-sp beat noise is about 26 times larger than the thermal noise. The thermal noise limited assumption will lead to overestimate of the system performance.

Actually in a real-world sensor system, the Bragg wavelengths of sensors vary randomly in the sensing range as their monitoring measurands change. The beat noise should be much smaller than the worst case. Considering the situation that Bragg wavelengths of sensors are evenly distributed in the sensing range with the difference between adjacent sensors is $B_o/2$. For two reflected signals with same power and Gaussian shape, the mutual beat noise causing by overlapped spectra is:

$$i_{sp-m}^2 = i_{sp}^2 e^{\frac{(-2ln\,2)\Delta B^2}{B_o^2}} \quad , \tag{3.24}$$

where ΔB is the frequency difference.

The total beat noise for an n bit length codeword with m sensors is:

$$\begin{aligned} i_{sp-all}^2 &= nm\left[i_{sp}^2 + 2i_{sp}^2(0.7071 + 0.25 + 0.0442 + 0.0039)\right] \\ &= 3.01nmi_{sp}^2 \quad , \end{aligned} \tag{3.25}$$

where the mutual beat noise is calculated with the frequency difference from $\pm B_o/2$ to $\pm 2B_o$, for frequency difference larger than $2B_o$, the mutual beat noise is small and negligible.

The SNR after decoding can rewrite as:

$$SNR_{2L} = \frac{(nI/2)^2}{i_{th-all}^2 + i_{sp-all}^2} = \frac{nI^2}{4i_{th}^2 + 3.01mi_{sp}^2} \tag{3.26}$$

$$SNR_{2R} = \frac{(nI/2)^2}{i_{th-all}^2 + i_{sp-all}^2} = \frac{n\alpha^2 I^2}{4i_{th}^2 + 3.01m\alpha^2 i_{sp}^2} \tag{3.27}$$

$$\frac{1}{SNR_2} = \frac{1}{SNR_{2L}} + \frac{1}{SNR_{2R}} \tag{3.28}$$

In this situation, 20 sensors can be placed within a spectral range of 2nm. The sp-sp beat noise is about 0.64 times of the thermal noise in this case for left arm. Both noises should be considered in the system performance estimation. SNR_2 is about 653 when the Bragg wavelength is in the middle of the edge filter with α equals to 0.5 and the code length is 512. The performance is much better than the worst case.

With a linear edge filter of half power loss per nm slope, the maximum resolution of 60pm in a round-trip time can be achieved. This equivalent resolution is 0.25pm/$\sqrt{\text{Hz}}$. To resolve a temperature change of 1℃, 10pm resolution is needed. So the maximal interrogation speed is about 1.6kHz. If better resolution with higher interrogation speed is needed, a standard Erbium-doped fiber amplifier (EDFA) can be placed after the SLED source to increase the input power.

To estimate the system performance for dozens of sensors within a spectral range, it can be assumed that the spectral differences between the sensors are multiple times of $B_o/2$. For a spectral range of 2nm, 20 spectral points can be located. If the number of sensors in each point is k, then for this 20k-sensor multiplexing array, the sp-sp beat noise will be:

$$\begin{aligned} i_{sp-all}^2 &= n\left[20(0.5k)^2 i_{sp}^2 + 40(0.5k)^2 i_{sp}^2 (0.7071 + 0.25 + 0.0442 + 0.0039)\right] \\ &= 15nk^2 i_{sp}^2 \end{aligned} \tag{3.29}$$

With a linear edge filter of half power loss per nm slope, the maximum k to keep a resolution better than 1pm/$\sqrt{\text{Hz}}$ is 8. So the maximum number of sensors in the

array should less than 160 to keep an acceptable resolution.

3.5 Experimental Results and Discussion

An experimental setup of the proposed CDM sensor system is shown in Figure 3.7. A 50MHz NRZ signal was generated by the PPG to drive the directly modulated SLED. The reflected signals of the FBG array are divided into two parts by the coupler. The left part of the light pulse signals goes into the photodetector directly while the right part goes through an edge filter before arriving at the photodetector. The output of the photodetectors will be converted into digital signals by a real-time scope and decoded by the signal processing unit.

A six-sensor array was used to examine the system performance in the situation of evenly distributed wavelengths. The gratings were around 1549nm with 0.2nm bandwidth and about 4% reflectivity. And the wavelength of FBG6 is at the central among the sensors. The distance between two adjacent grating sensors is set to multiples of 4.05 meters. So the reflection time delay between successive sensors is equal to multiple of 2-bit time period. The distance between the first and last sensors is 24.1 meters and the coded pulse sequence is 14 bit long. All the six sensors were put into a container of hot water and a thermometer with 0.1℃ accuracy was used to record the temperature change of water.

The temperature of hot water was recorded every second for the first hour,

then every minute for the second hour and every five minutes after that as the water cool down to ambient temperature. And the real-time scope captured the data simultaneously and the captured period is 20μs. As the temperature of water dropped, the change of reflected signals are captured and analyzed. Figure 3.8 shows the relationship between the wavelength and temperature of last sensor after data decoding and signal processing.

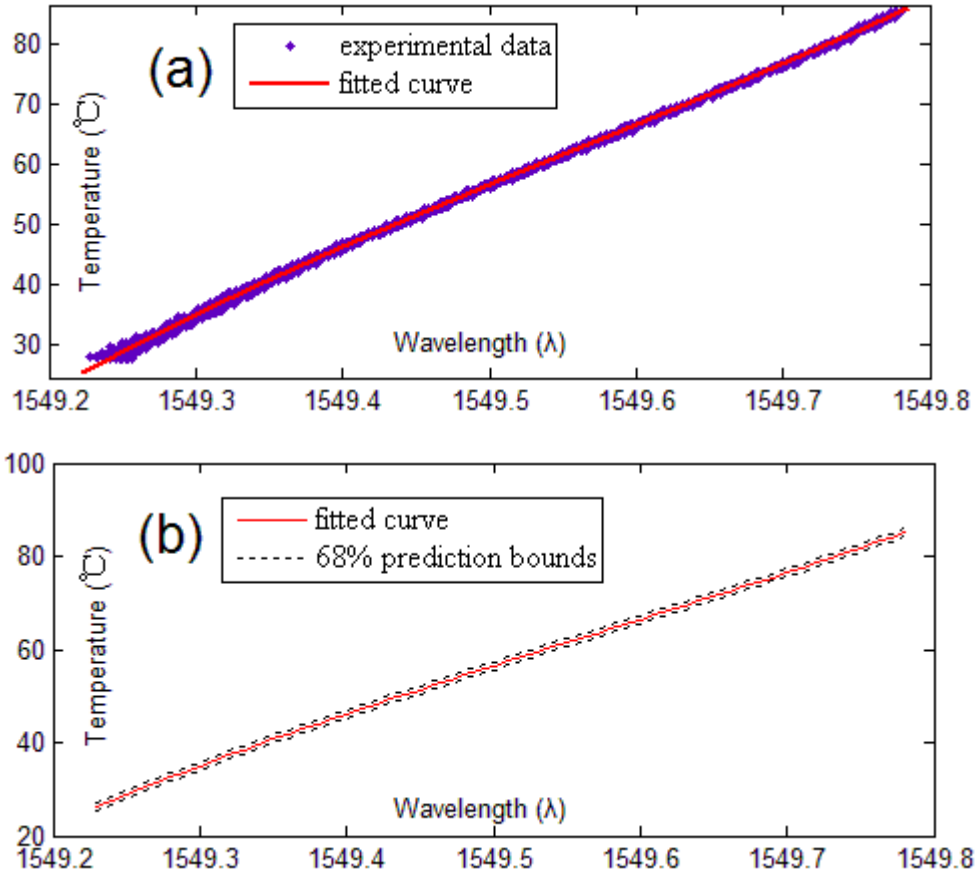

Figure 3.8 Temperature against wavelength for FBG6

In this experimental setup, the resolution is theoretically 14.3 pm by the given parameters and the temperature coefficient of the grating in water is 10.3pm per degree which is calculated by using the optical spectrum analyzer (OSA). That means

the resolution in temperature is about 1.38℃. Figure 3.8(a) gives the experimental data and the fitted curve between temperature and wavelength. Figure 3.8(b) shows the 68% prediction bounds for the fitted curve. In the normal distribution, the probability for a measurement to hit within the standard deviation of the true value is about 68% and the standard deviation is usually defined as the system resolution. The upper and lower bounds to the mean value are 0.95 times of standard deviation. The difference between lower and upper bounds is about 2.9℃ at 1549.5nm, so the resolution (equal to the standard deviation) is about 1.45℃. The experimental resolution is a little bit worse than the theoretical resolution but still fits the theoretical analysis well.

To investigate system performance of larger scale multiplexing for the proposed scheme, a 20-sensor array was used. The sensors were staggered along the fiber carefully to reduce the major multiple reflections. The distance between the first and last sensors is 1036.8 meters and the length of coded pulse sequence is 512 bits. An expected measurement resolution is 0.097pm/$\sqrt{\text{Hz}}$ by using the system parameters mentioned above. For a capture time of 40μs period, the resolution should be 15.3pm or about 1.48℃.

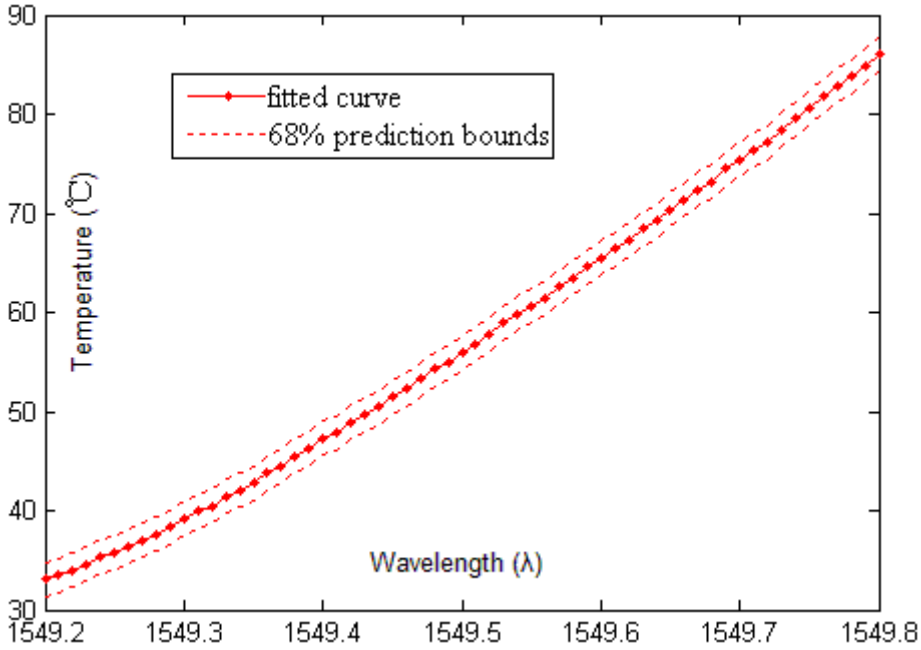

Figure 3.9 Temperature against wavelength for FBG20

Figure 3.9 shows the 68% prediction bounds of FBG20. The difference between lower and upper bounds is about 3.4℃ at 1549.5nm. Then the experimental resolution is 1.7℃, a bit worse than the expected resolution. This is mainly cause by power penalty and the spectral shadowing cross talk. After going through the first 19 sensors, the spectrum become nonuniform and the reflection shape of FBG20 will be distorted. This leads to power fluctuation and increases measurement error. One solution is to trace and calculate the actual transmitted spectral shape as it passes through every sensor. This can be done in the signal processing unit. After fixing the data, the bound difference reduces to 3.1℃. Considering the power penalty of the input signal, this result is very close to the expected resolution.

The reflectivity of FGBs in the system is very low, only 4% of the input power is reflected; the other unwanted reflection in the fiber may affect the signals of FBGs.

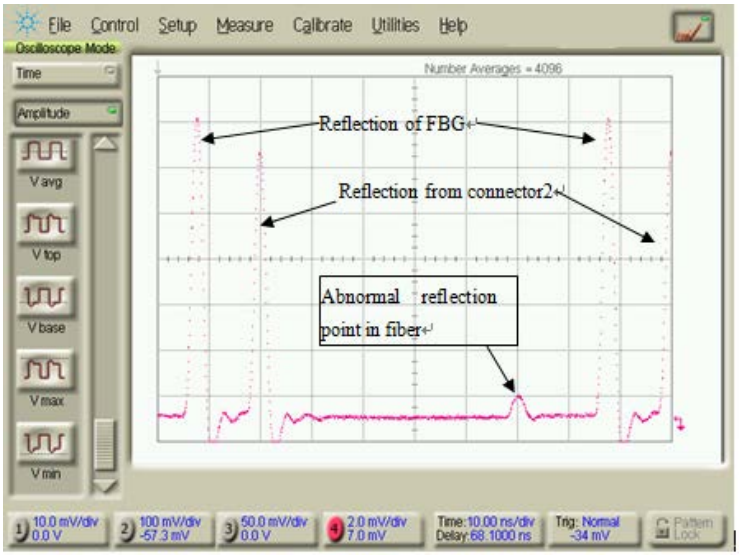

Figure 3.10 Reflection points in the fiber sensor array

Because the reflect bandwidth is narrow (0.1~0.2nm FWHM) and the input SLED is a broadband source (30~40nm), the power reflected from the connector is similar to the reflected power from FBGs. This will affect the accuracy and induce error. Figure 3.10 shows that the reflection power of the connector in front of the FBG is as strong as the FBG's. Besides, power also arises up from the bad splicing point between the fiber and FBG. To reduce connection reflection, splicing the fiber together instead of using a connector is the best choice. And making good splicing points is also important to minimize the unwanted reflections.

The refractive index of the single mode fiber used in our experiments is around 1.47 to 1.48. For a 50MHz NRZ signal, the transmission distance is 4.05 to 4.08 meters in one bit period. This is the ideal base distance for sensor placement. Actually it is neither easy nor necessary to keep the distance of adjacent sensors to be the multiples of base distance. Firstly, it is hard to cut and splice the fibers within

centimeter accuracy. Secondly, the sampling point is at the center of the bit period, margin for error in distance is loose. But when the number of sensors increases, the accumulated distance error may exceed the margin. So it is better to use a single pulse to test whether all the sensors are in their preset position before other experiments.

The drift of the edge filter also need to be considered for long-term accuracy. Drift will affect the measurement repeatability and accuracy. The dominant measurement error caused by drift in this system is the drift of edge filter. The drifts are about 2pm for 3 hours and 18pm for 24 hours. The induced measurement errors of wavelength shift will be 2pm and 18pm respectively. The drift of the edge filter is mainly caused by the change of ambient temperature and a less temperature sensitive edge filter can be used to mitigate this drift error for long-term accuracy.

3.6 Summary

In this chapter, we have studied the code-division multiplexing method for fiber Bragg grating sensing system thoroughly. Techniques of CDM based FBG sensor systems are reviewed and a new scheme has been proposed and experimentally demonstrated. The code sequences of length power of 2 are constructed and some rules for code sequences of even length are discussed. With the special code design, cross-correlation from other sensors can be completely canceled. Operation principle and theoretical analysis are given to understand the proposed sensor system.

Experimental results show good agreement with the theoretical analysis and demonstrate the great feasibility of the proposed setup. With spectral shape compensation to reduce the cross talk, the new scheme enabled multiplexing of 20 gratings along a single fiber while maintaining the sensing accuracy.

Chapter 4 VCSEL Based Tilted Fiber Grating Vibration Sensing System

4.1 Introduction

FBG based optical fiber sensor system has been used in many different applications nowadays because of its inherent advantages compared with conventional electrical sensor systems. In previous chapter, a sensor multiplexing scheme that can support a large number of sensors was presented. In this chapter, a high speed interrogation scheme for a single FBG sensor is discussed.

For an FBG sensor system, the key challenge is to determine the shift of the peak wavelength reflected from an FBG. Usually there are two kinds of methods to detect the wavelength shift. One is using a broadband ASE source as the input and a wavelength discriminator at the receiver side to detect the wavelength of received signal wavelength, and the other one is using a tunable laser as the source with known output wavelength to track the wavelength shift of the FBGs. However, when fiber ring laser based tunable laser or external cavity tunable laser is used as the source component in the second method, its high cost, large size and low tuning speed will have a significant impact on the cost and performance of the FBG sensor system.

Vertical cavity surface emitting laser (VCSEL) is one of the semiconductor lasers with the light emission through vertical direction. The laser structure is

consisting of vertically stacked mirrors with an active gain region. The influence of temperature and driving current on lasing wavelength of VCSELs has been widely studied [50-52]. Due to the short optical resonator, the emission wavelength of a VCSEL is determined by the cavity resonance. So the wavelength shift is mainly governed by the change of average refractive index in the resonator as the internal temperature change. And the input current will affect the internal temperature thus shift the emission wavelength. This property makes it a potential tunable light source for the practical fiber sensing systems with its low cost and simple configuration.

In this chapter, we present a fast FBG sensor interrogation system utilizing VCSEL laser as the light source. Using saw tooth signal to drive the VCSEL input current, a continuous spectrum tuning range of 2nm can be obtained. Relationship between wavelength tuning range and scanning speed of the VCSEL is studied. And the application for vibration sensing with tilted FBG is investigated and experimental demonstrated.

4.2 Vertical Cavity Surface Emitting Laser

Vertical Cavity Surface Emitting Laser (VCSEL) is one of the most favorable light emitting sources which has satisfied some major demands of today's industry: simple and reproducible devices processes, efficient wafer scale device test, low power consumption with compact device size, capability of high speed modulation, low packaging cost and high reliability.

The basic structure of a VCSEL is shown schematically in Figure 4.1. The top and bottom layers are composed of high reflectivity DBR mirrors. An active layer is sandwiched between them to form the cavity structure. The active layer is usually composed of multiple quantum wells. And normally an ion-implantation layer or selectively oxidized high-Al content AlGaAs layer is used in the topmost DBR to achieve electrical and optical confinement for high injection density and high conversion efficiency [53]. Photons are spontaneously generated by the recombination of electrons and holes as carriers are injected into the active layer from the ohmic contacts. Stimulated emission will then be triggered by the spontaneous emission to generate extra photons whose wavelengths are identical. This process is the principle mechanism of optical gain [5].

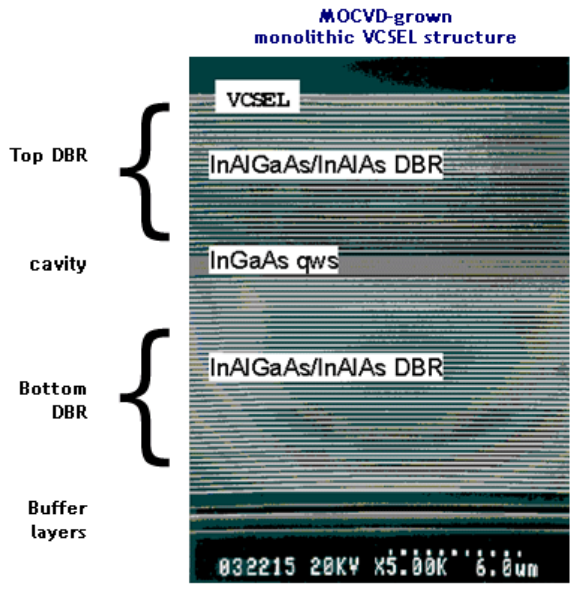

Figure 4.1 Structure of VCSEL grown with MOCVD

Long-wavelength VCSELs are developed rapidly recent years. The product

of 1550nm VCSEL for 10G bps modulation is already commercially available for metro area network, gigabit Ethernet and PON etc. The mass production further reduces the cost of VCSEL and makes it a suitable component for optical fiber sensing.

4.3 VCSEL based Interrogation System

4.3.1 Experimental Setup and Operating Principle

Figure 4.2 shows the block diagram of the proposed system. The spectrum tuning signal from VCSEL is divided into two parts by a 90:10 fused fiber coupler. One part of the signal which contains 10% signal power is measured by photodetector 2 (PD2) as the reference power. The other part of signal will go into the FBG sensor through a circulator and its reflected signal is measured by PD1. By normalizing the received power between PD2and PD1, the reflected peak wavelength of FBG can be determined.

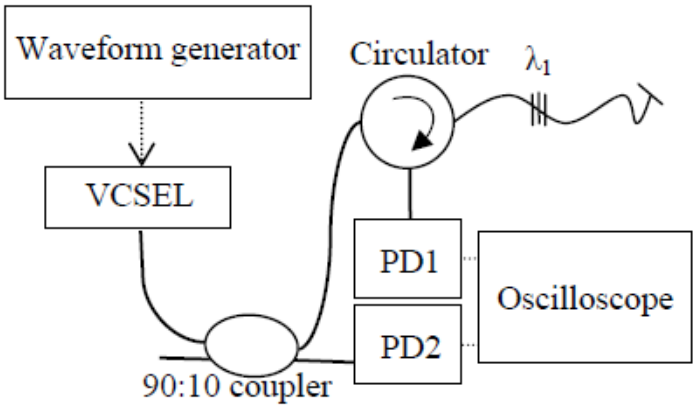

Figure 4.2 Experimental setup of the proposed FBG interrogation system

The output wavelength of VCSEL is a function of driving current and can be characterized beforehand. By tracking the power variation that obtained from the real-time oscilloscope, we can calculate the wavelength of FBG. The output power of VCSEL is not a constant as the input current varies. To get precise wavelength information, the received signal power is normalizes by the reference detected power of PD2.

4.3.2 Experimental Results and Discussion

In this proposed system, the wavelength is a function of the driving current, which needs to be plotted out first before other use.

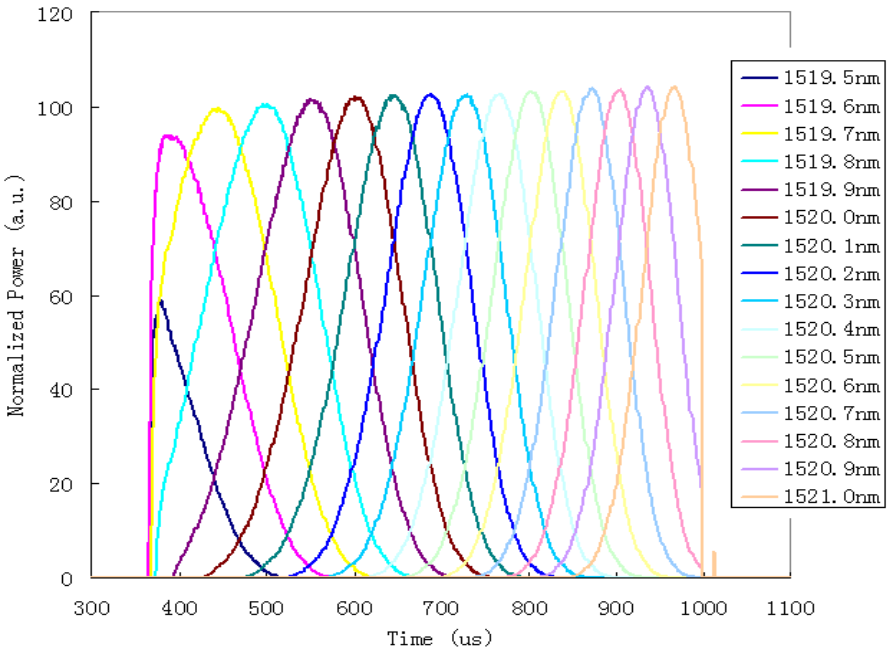

Figure 4.3 Normalized reflection power of FBG at different wavelength.

Figure 4.3 shows the variation of the normalized power that reflected from

different Bragg wavelength settings of the tunable FBG. Since the driving current for the VCSEL is a saw tooth wave repeatedly, the driving current is direct corresponding a fixed time within the signal period. The repetition rate of the saw tooth wave is 1kHz. As expected, the delay for the reflection peak increases as the centre wavelength of tunable FBG shifts towards longer wavelength.

The relationship between the wavelength shift and time delay is shown in Figure 4.4. There is an overestimation of time stamp for unnormalized peak power. This is because the output power of VCSEL increases as its driving current scans from the lowest at 0μs to the highest at 1000μs. This leads to the shift of the largest reflected power from the FBG Bragg wavelength to longer wavelength. After normalization, there will be a monotonic mapping between time and reflected wavelength. We can use this time and wavelength mapping to determine the wavelength shift in the sensing system.

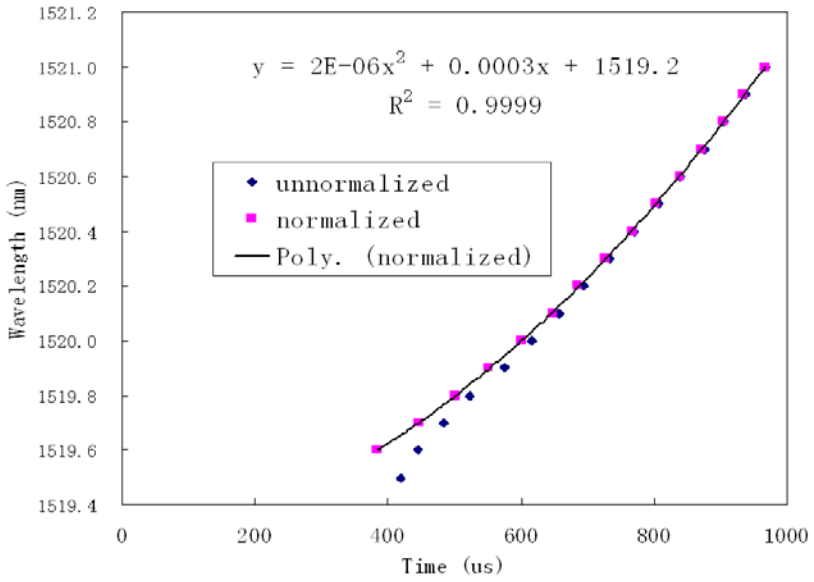

Figure 4.4 Bragg wavelengths versus time delay.

The repetition rate and amplitude range of the driving current will influence the tuning characteristic of VCSEL. We have characterized the output wavelength versus time for different tuning speed but the same tuning current range at room temperature. As the tuning speed increases, the spectral tuning range decreases.

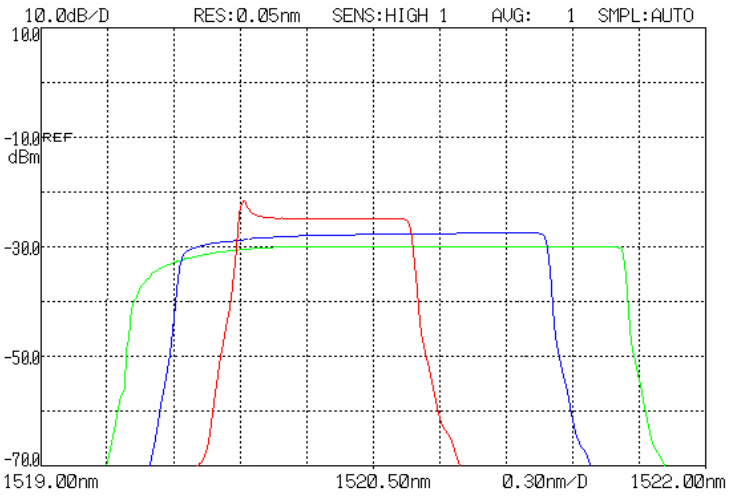

Figure 4.5 Spectra of VCSEL outputs with different tuning repetition rate.

The output spectra are shown in Figure 4.5 with an OSA using the max hold mode. Due to the short optical resonator of the VCSEL, the emission wavelength of a VCSEL is determined by its cavity resonance. The wavelength shift is mainly caused by the average refractive index changes in the resonator while its temperature changes. The thermal time constant of the VCSEL is in the range of microseconds. When the tuning speed is low, the cavity temperature will have plenty of time to rise up by the heat generated in VCSEL and drop down when the saw tooth scanning input current drops from the highest to the lowest value. But when the tuning speed is high and the period of the saw tooth signal is comparable to the thermal time constant, the

scanning input current will drop before the cavity temperature rise to its steady-state value. The scanning current will increase to become larger than the threshold before the cavity cool down to ambient temperature. As a result, the cavity temperature variation range will be smaller than that at lower tuning speed, so the wavelength tuning range will be smaller. This can be seen clearly in Figure 4.5. Another feature is that compared with that for lower tuning speed, the cavity temperature at higher tuning speed will be lower for the same tuning current, the output power will be larger as shown in Figure 4.5 because of the better alignment of cavity mode and gain peak.

For better resource utilization, Time Division Multiplexing method can be applied to the system to increase the number of FBG sensors that can be placed along a single fiber. The ramp signal from the waveform generator is changed to pulsed ramp signal by introducing steps of current that is below the threshold current between two consecutive steps of the original ramp signal to form the pulsed ramp signal. So there will be no output power during these time slots and TDM method can be used to distinguish different sensors with the same nominal Bragg wavelength.

So far we assume that the ambient temperature remains the same in the lab. But in the real world, it is not easy to keep this assumption. The VCSEL's ambient temperature will change in a certain range. The wavelength shift is about 80 pm/℃. This affects the relationship of wavelength and time, and induces measurement error. To deal with this issue, we propose to adopt time division multiplexing method and with one temperature insensitive FBG as the reference. So this makes the system more

robust and more sensors can be used.

4.4 VCSEL Based Tilted Fiber Grating Vibration Sensing System

4.4.1 Tilted Fiber Bragg Grating Vibration Sensor Systems

Tilted fiber Bragg grating (TFBG) is a kind of grating with its grating planes slanted with respect to the fiber axis [55], [56]. TFBG shows a lot of special characteristics compared with simple fiber Bragg grating (FBG) and long-period gratings (LPG). The tilt of the grating planes enhances the coupling of the light from the forward-propagating core mode to backward-propagating cladding modes and maintains a reduced backward core mode coupling. Among the backward-propagating cladding modes, there are a group of low-order cladding modes, known collectively as the “ghost” modes, which interact much with the fiber core but little with the cladding boundary. These strongly guided low-order cladding modes can be effectively recoupled to the fiber core via a lateral-offset splice [57], an abrupt-biconical taper [58], or a short section of multimode fiber [59] upstream the grating. The amount of above cladding-to-core recoupling varies strongly with fiber curvature, providing the possibility for vibration sensing using the mechanism.

Besides the compact tip-reflection sensing feature, these schemes offer the advantage of a cost-effective power-referenced demodulation for real-time vibration

measurements. However, in all the works above, the light sources used are erbium amplified spontaneous emission broadband sources (BBSs). Because the BBS emits light over a broad wavelength range (C band or L band), the average power over the wavelength range of interest is relatively low, resulting in a very weak TFBG cladding-to-core recoupling (hundreds of nanowatts). At the same time, a bandpass filter centered at the recoupled band is necessary for demodulation which further weakens the detected power.

Here we propose an alternative approach by using a commercial vertical-cavity surface-emitting laser (VCSEL) as the light source. The VCSEL's unique characteristics of low power consumption, high efficiency, circular beam spot, and low manufacturing cost make it a good candidate for light sources in optical sensor systems [60-62]. The special advantages of VCSEL we explore here are that high-speed (10kHz) continuous wavelength tuning (1~2nm) of the VCSEL perfectly covers the strongest TFBG cladding recoupling band, permitting the recoupling at a much higher power level (50 μW) and making the demodulation filter unnecessary. A dynamic vibration measurement up to 200Hz via cost-effective normalized power detection has been achieved so far. The proposed VCSEL-based TFBG vibration sensing system with simplified detection scheme and better signal-to-noise ratio is a good candidate for vibration measurement in various engineering applications.

4.4.2 Principle of Proposed VCSEL Based TFBG Vibration Sensing System

Figure 4.6 shows the experimental setup of the proposed system. The vibration sensing mechanism we used here is based on recapturing the TFBG excited low order cladding modes ("ghost" modes) via a lateral-offset-splice located at a short distance upstream from the grating

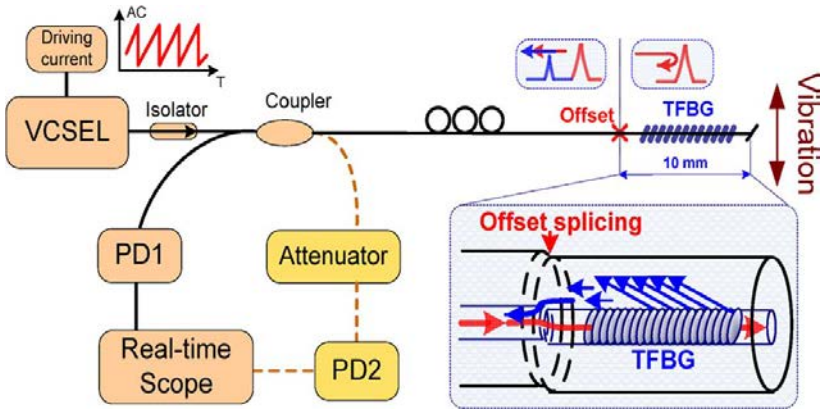

Figure 4.6 Schematic diagram of VCSEL-based TFBG vibration sensing system. Inset shows the sensor tip containing a TFBG with a lateral-offset splice.

The amount of TFBG cladding-to-core recoupling varies strongly with pure fiber bending and keeps its wavelength un-shift, as shown in the black and red spectra in Figure 4.7. Instead of using BBS as a light source, a high-speed continuous wavelength tuning VCSEL is utilized. Combining with two PIN power detectors and a real-time scope, the VCSEL-based TFBG vibration sensing system has been demonstrated, as shown in Figure 4.6. The original wavelength of VCSEL is selected to locate at the left-edge-side of the "ghost" resonances. Varying the driving current,

the laser output provides a fast but narrow range wavelength tuning over 1~2nm, which perfectly covers the whole strongest recoupled band, as shown in the dashed green curve in Figure 4.7 (a continuous VCSEL turning recorded at the optical spectrum analyzer using maximum hold mode).

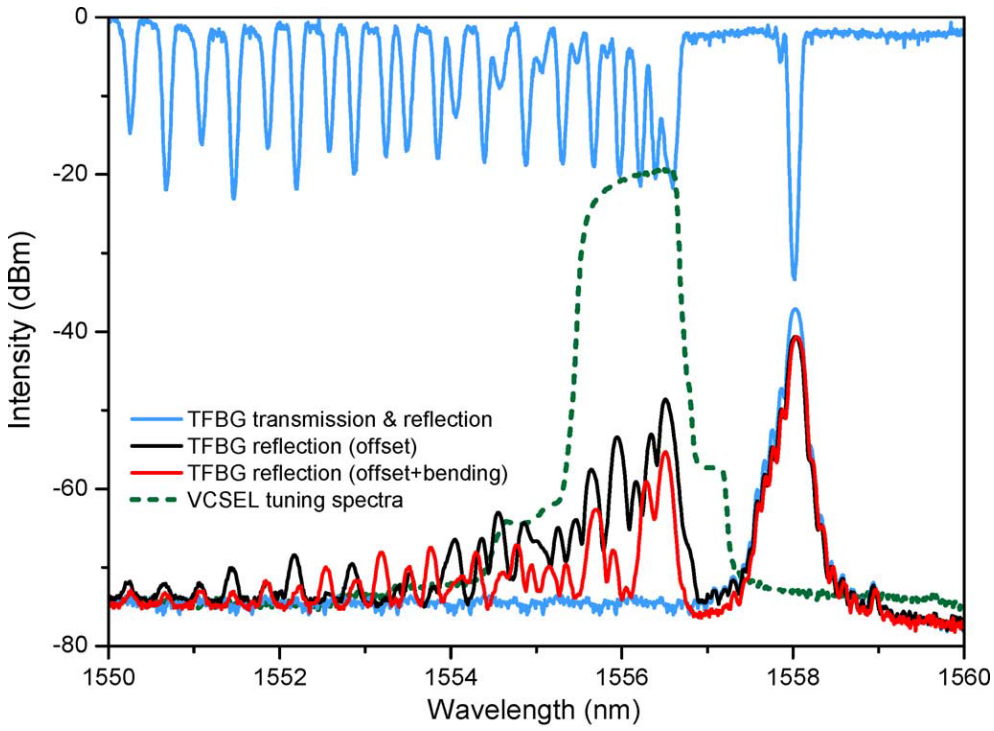

Figure 4.7 TFBG spectra before (light blue line) and after (black line) lateral-offset splice and its response to the fiber bending (red line). The dashed green line shows the VCSEL tuning spectra recorded by the OSA maximum hold mode.

The tuning characteristic of VCSEL is determined by the modulation of its driving current. Figure 4.8 gives a detailed observation on the effect of the driving current (amplitude range and repetition rate) on the VCSEL's wavelength range swept and power level spectrum. The VCSEL wavelength tuning range increases with the rise of the driving current amplitude and decreases with the increase of the tuning

speed, as shown in Figure 4.8(a) and (b), respectively. The slight power variation in Figure 4.8(b) is due to the temperature dominated refractive index modulation in the VCSEL resonator. With a fast tuning speed, the input scanning current will drop before the cavity temperature rises to its "steady-state" value, resulting in a narrower tuning band and a slightly increased power level because of the power concentration. However, the slight power fluctuations (versus wavelength) should not matter since the measurement result at each wavelength is normalized to the power emitted by the VCSEL at the same time (as described in Figure 4.10). The selection of amplitude and repetition rate of driving current in turn depends on the spectrum bandwidth to be interrogated and the vibration frequency under-measured.

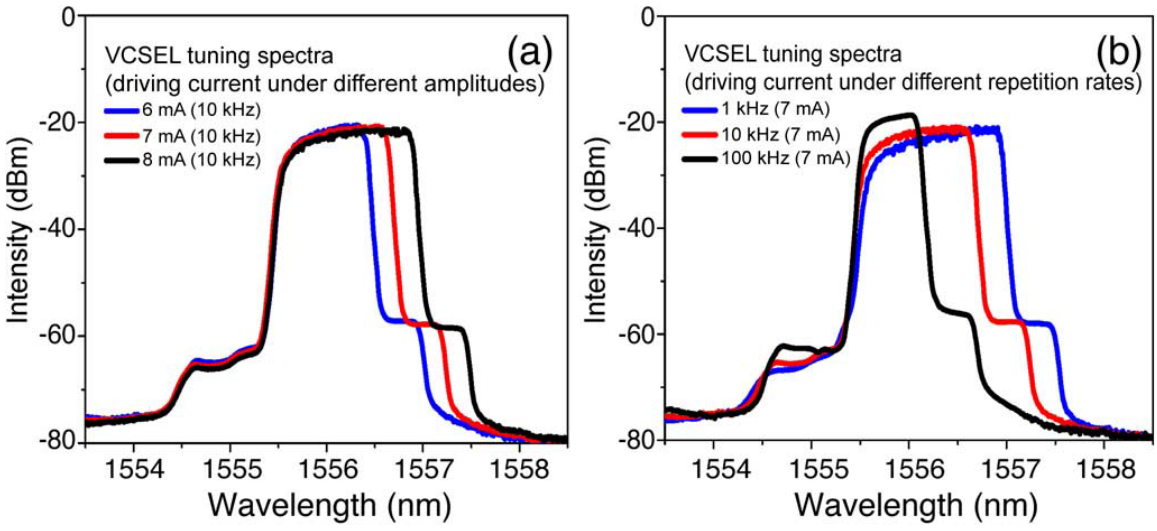

Figure 4.8 Wavelength tuning characteristics of VCSEL versus driving currents at different (a) amplitudes and (b) repetition rates.

4.4.3 Experimental Results and Discussion

The VCSEL used in our experiment is a commercial product from RayCan. The bias current of the VCSEL is driven by a 10-kHz saw-tooth-signal with amplitude less than 10mA.The average power output of the VCSEL is 0.3mW. With this light source, the TFBG recoupling are now working at a much higher power level with 15dB improvement compare to BBS and an optical signal-to-noise ratio of 40dB can be achieved, as shown in Figure 4.9.

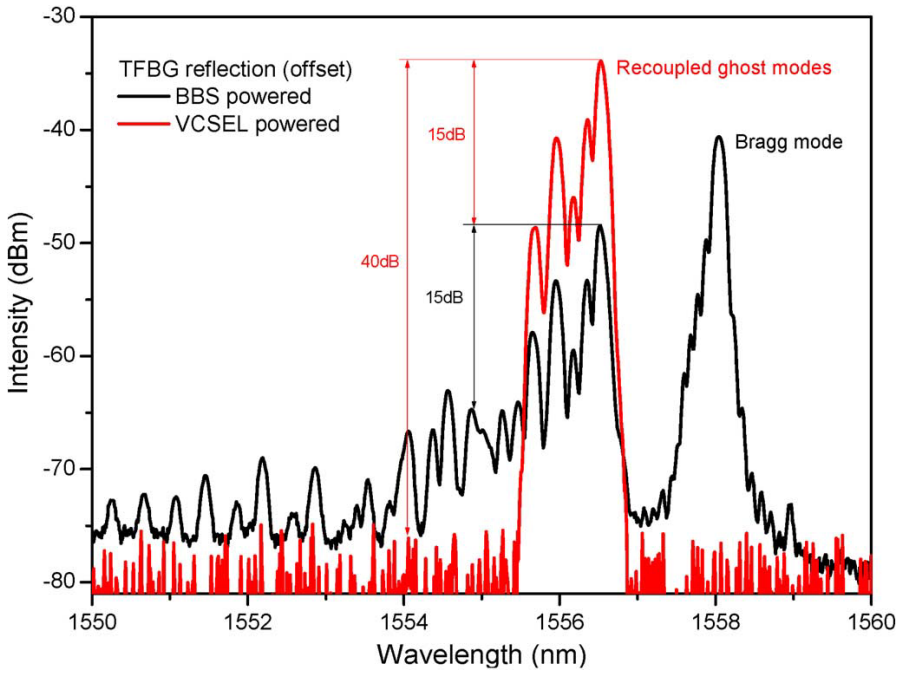

Figure 4.9 Comparison of TFBG reflections powered by a BBS (black line) and a wavelength-matched VCSEL (red line).

Figure 4.10 shows the continuous power output of the vibration sensing system under a 200Hz harmonic oscillation and the inset presents the details of real-time power output within one VCSEL sweep period over 100μs (VCSEL repetition rate of 10kHz). For each vibration period (5ms), 50 VCSEL sweep periods have been

recorded, providing a sufficient amount of data for an accurate amplitude monitoring. The real-time scope used in the system has a sampling rate of 100 MS/s. Then, for the VCSEL with a repetition rate of 10kHz, 10000 sampling points can be recorded in each VCSEL sweep period, drawing the response lines in the inset of Figure 4.10. For data processing, we select 128 sampling points concentrated in the reflection peak and give an average to obtain the amplitude power of this sweep period. The data processing speed is quick enough to meet 100kHz sweeping rate. Since the VCSEL output power also varies with the periodically modulated driving current, as shown in the inset of Figure 4.10 (black line), a reference power detector (PD2) with proper attenuation is utilized for the normalization of the system output.

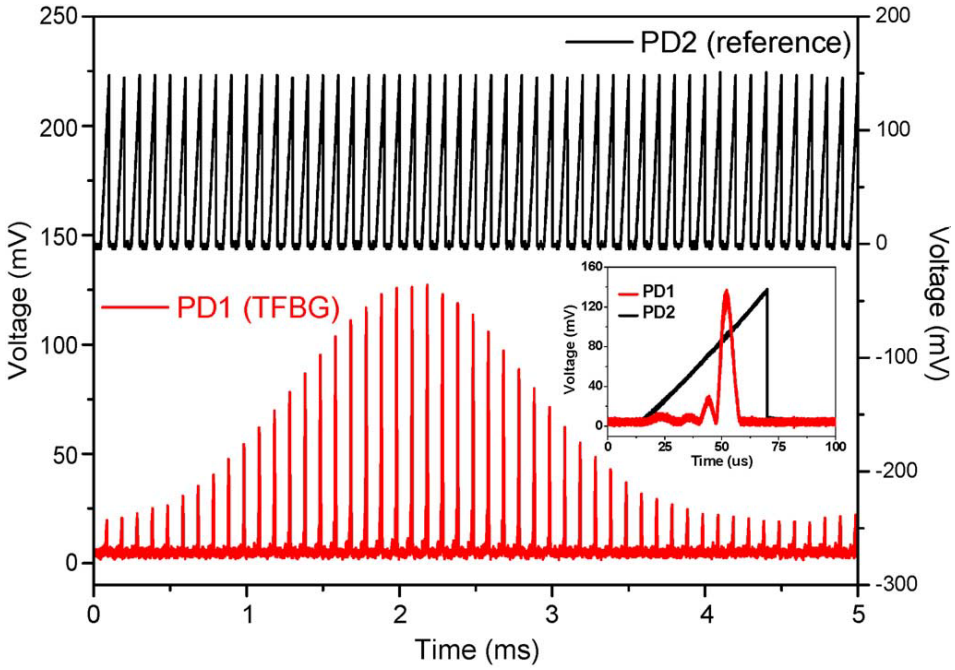

Figure 4.10 System real-time outputs following a 200-Hz harmonic oscillation. Inset zooms in the detail response within one VCSEL sweep period over 100μs.

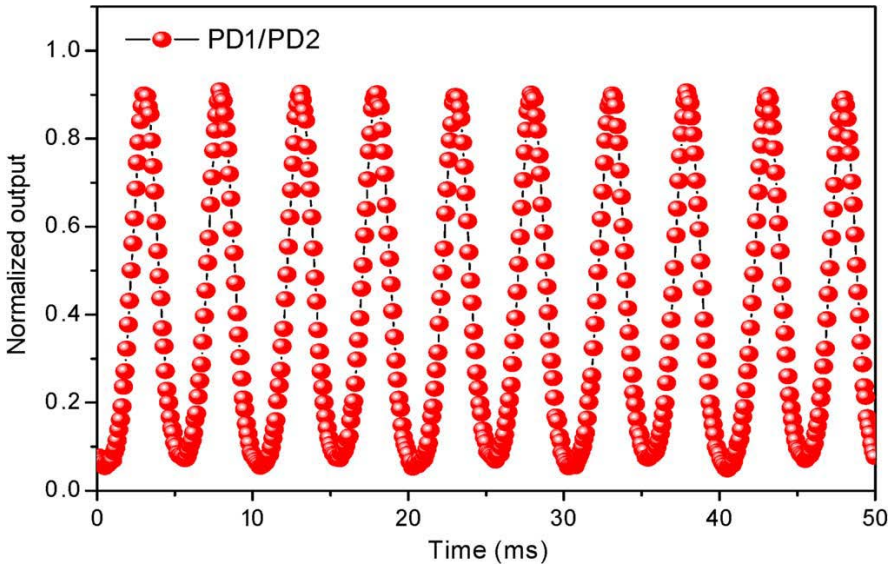

Figure 4.11 Normalized system output following a 200Hz harmonic oscillation

Figure 4.11 shows the normalized system output of the ratio of PD1/PD2. And Figure 4.12 presents its frequency response recorded by the electrical spectrum analyzer.

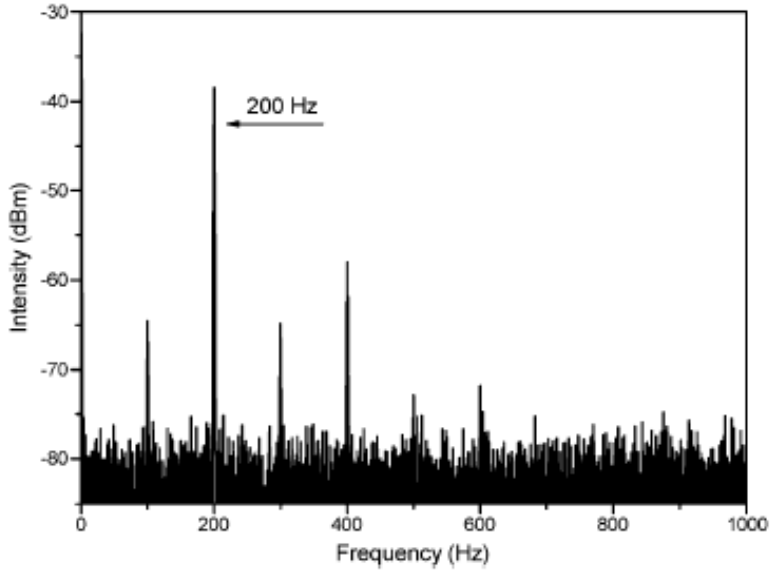

Figure 4.12 System frequency responses following a 200Hz harmonic oscillation

The small signals at double and half frequencies may be due to the slightly nonaxial alignment between the vibration generator and the sensing fiber tip.

Finally, it should be noted that angular dependence is quite an important question in any application where the direction of the vibration is not predetermined. Compared to the erbium-doped amplified spontaneous emission broadband source and LED, VCSEL emits a polarized light. Therefore, besides the directionality of the grating tilt and dependence of the cladding-to-core recoupling at the lateral offset junction (as discussed in [57], [58]), the orientation sensitivity of the offset TFBG vibration sensor also depends on the polarization state of the VCSEL. The VCSEL used here is of a single polarization state with a polarization mode suppression ratio (PMSR) up to 15 dB. Experimental tests show that a VCSEL with polarization control will induce a maximum of 4.5dB sensitivity difference between x and y-axis vibrations, which may potentially enhance the orientation-recognized ability of the offset TFBG vibration sensor.

4.5 Summary

A novel and simple VCSEL-based TFBG vibration sensing system is presented and demonstrated experimentally. The sensor comprises a short optical fiber stub containing a weakly tilted Bragg grating spliced to another slightly offset fiber. The tip-reflection sensing feature enables the sensor head to be fabricated as small as 10 mm (possibly less). The high-speed continuous wavelength tunable VCSEL

enables the recoupled modes to work at a high power level to obtain better signal-to-noise ratio at the output. The interrogation unit requires only two power detectors and a real-time scope. The light source power fluctuations can be effectively eliminated via a normalized power output. Vibration measurement up to 200Hz has been achieved by the proposed cost-effective sensing system. As the modulation frequency of the VCSEL can be raised up to several hundreds of kilohertz, the maximum detectable vibration frequency is mainly dominated by the acoustic resonance frequency of the sensor head (a 10-mm bare fiber stub used here), which potentially can be increased to kilohertz with proper material, structural and packaging design.

Chapter 5 Single-sideband Modulation Based Interrogator for FBG Sensor Systems

5.1 Introduction

Wavelength shift detection is the key issue for most of the fiber sensing systems because their measurands are wavelength encoded. As mentioned in the previous chapter, two approaches can be adopted to realize FBG wavelength interrogation. One is based on broadband source and wavelength discriminator. Techniques using this approach are reviewed in chapter 2.Wavelength discriminator implementations include edge filter discriminator [31], tunable filter [32], interferometric detection [33] and CCD spectrometer [34], [35].Another approach uses tunable laser as light source with calibrated wavelength tuning characteristics. There are several advantages of using tunable laser such as high output power, large tuning range and high tuning resolution. However, it was seldom used in the fiber sensing systems due to its high cost and low tuning speed.

In chapter 4, a VCSEL based interrogator and its application to tilted fiber grating vibration measurement is introduced. About 1.8nm tuning range at 1kHz repetition rate can be achieved by the interrogator. This proposed interrogation scheme is compact and has a better system performance than the broadband source approach. But one disadvantage of this interrogator is that the whole tuning

wavelength range shifts as the ambient temperature change. The shift is up to about 80pm/℃. For normal FBG sensing applications, TDM method with one temperature insensitive grating as reference is preferred. And this interrogator is especially suitable for the tilted grating vibration sensing system because vibration is encoded with the reflection power of "ghost" mode but not the wavelength shift. In this chapter, an interrogation system that utilizes single-sideband (SSB) modulation is discussed and experimentally demonstrated. Stable wavelength output and larger tuning range can be achieved by this scheme.

5.2 Optical Single-sideband Modulation

Single-sideband modulation (SSB) is first introduced by John Renshaw Carson in 1915 [63] and widely used over long distance telephone lines in the old days. It is also the radio standard for long-distance voice radio transmissions of aircraft since 1957. In communication systems, SSB modulation is the improvement of amplitude modulation (AM) with more efficiently utilized bandwidth. The output signal of amplitude modulation occupies twice the bandwidth compared with its baseband signal. In order to reduce the bandwidth occupation, SSB modulation is proposed. It suppresses one of the modulation sidebands at the cost of increasing system complexity.

SSB modulation can be achieved in optical communication systems by using a Dual-Parallel-Mach-Zehnder modulator. The Dual-Parallel-MZ modulator is a

multifunctional modulator which consists of two sub-MZ interferometers embedded in a main MZ interferometer. This nested MZ interferometers design gives more flexibility to generate optical signals in various modulation formats. It can be used as IQ modulator in the high speed DQPSK or DPSK optical transmission systems. It can also be used for SSB modulation.

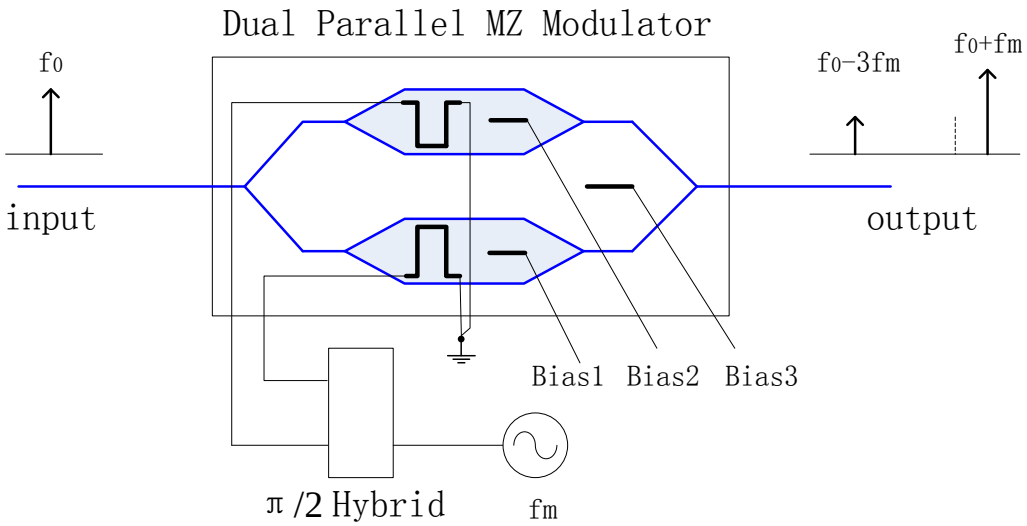

Figure 5.1 Single-sideband modulation using Dual-Parallel-MZ modulator. Bias1 and Bias 2 are set at the NULL point and Bias 3 is set at quadrature point. The output contains a major upper sideband whose frequency is f_0+f_m with a undesired third order harmonic f_0-3f_m.

The schematic of SSB modulation is shown is Figure 5.1. An input lightwave with amplitude A and frequency f_0 is modulated by an RF signal with peak-to-peak amplitude $2\sqrt{2}V_f$ and frequency f_m through a $\pi/2$ Hybrid. The phase differences between sub-MZ and main MZ interferometers are controlled by the input DC voltages of Bias1, Bias2 and Bias3. The relationship of optical output intensity and bias voltage is shown in Figure 5.2.

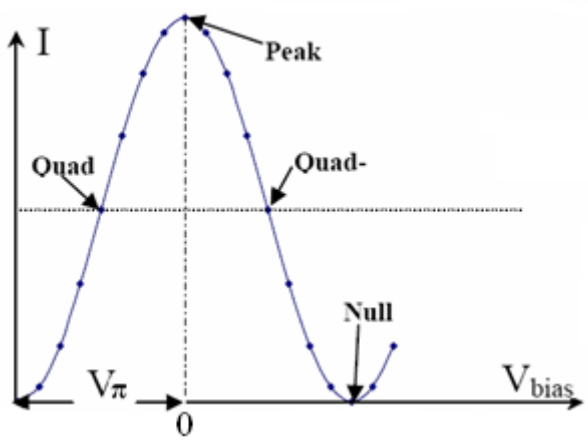

Figure 5.2 Optical output vs. Bias voltage

Then the outout optical field of the lower sub-MZ is represented by

$$E_1(t) = \frac{A}{4}\{\cos(\omega_0 t + \alpha\pi\cos\omega_m t + \beta\pi) + \cos(\omega_0 t + \alpha\pi\cos[\omega_m t + \theta])\}, \quad (5.1)$$

where $\omega_0=2\pi f_0$, $\omega_m=2\pi f_m$, $\beta\pi$ is the bias phase and θ is the phase difference between the interferometers, α is normalized amplitude of drive signal after hybrid (V_f/V_π).

Because bias 1 is set at NULL point, $\beta\pi$ is equal to π. θ is always euqal to π in this setup, then equation (5.1) can be expanded by the Jacobi-Anger expansion as:

$$E_1(t) = \frac{A}{2}\sin\omega_0 t \sin(\alpha\pi\cos\omega_m t) = -A\sin\omega_0 t \sum_{n=1}^{\infty}(-1)^n J_{2n-1}(\alpha\pi)\cos([2n-1]\omega_m t), \quad (5.2)$$

where $J_n(\alpha\pi)$ is the n-th first Bessel function.

For the upper sub-MZ, the RF drive signal is 90 degrees shift, and the outout optical filed is expressed as:

$$E_2(t) = \frac{A}{4}\{\cos(\omega_0 t + \alpha\pi\cos[\omega_m t + \pi/2] + \beta\pi) + \cos(\omega_0 t + \alpha\pi\cos[\omega_m t + \pi/2 + \theta])\} \quad (5.3)$$

and can be expaned as:

$$E_2(t) = \frac{A}{2}\sin\omega_0 t \sin(\alpha\pi\cos[\omega_m t + \pi/2])$$
$$= -A\sin\omega_0 t \sum_{n=1}^{\infty}(-1)^n J_{2n-1}(\alpha\pi)\cos([2n-1][\omega_m t + \pi/2]) \quad (5.4)$$

While the signals go through the main MZ interferometers, the lower arm adds additional π/2 phase shift. So from equation (5.2) and (5.3) we can get the final output signal:

$$E_o(t) = -A\sin(\omega_0 t + \frac{\pi}{2})\sum_{n=1}^{\infty}(-1)^n J_{2n-1}(\alpha\pi)\cos([2n-1]\omega_m t)$$
$$-A\sin\omega_0 t \sum_{n=1}^{\infty}(-1)^n J_{2n-1}(\alpha\pi)\cos([2n-1][\omega_m t + \pi/2])$$
$$= AJ_1(\alpha\pi)\cos(\omega_0 + \omega_m)t - AJ_3(\alpha\pi)\cos(\omega_0 - 3\omega_m)t$$
$$+ AJ_5(\alpha\pi)\cos(\omega_0 + 5\omega_m)t - AJ_7(\alpha\pi)\cos(\omega_0 - 7\omega_m)t \ldots \quad (5.5)$$

The first term of the output signal is the first order upper sideband we wanted, the frequency shift is equal to the driving frequency. The second term is 3-th order harmonic of the input signal and it is the dominant side mode noise. The side mode suppression ratio (SMSR) is the power between the wanted sideband and the 3-th order harmonic as $[J_1(\alpha\pi)/J_3(\alpha\pi)]^2$. Other high-order harmonics are so small and neglectable comparing with the first two terms. In oder to get a good power conversion efficiency with acceptable SMSR, the RF driving signal after hybrid with Vpp around Vπ is preferred.

5.3 Single-sideband Modulation based Interrogation System

Optical SSB modulation is widely used in optcial communication systems as it can reduce dispersion penalty and increase optical bandwidth efficiency. A optcial subcarrier multiplexings schemeutilizing SSB modulation was proposed [64]. Optical SSB modulation as high SMSR wavelength shifter also has been demonstrated [65].And with a loop setup, optical frequency comb generation using SSB modulation wasstudied [66], [67]. In this section, a wavelength tuning light source using SSB modulater in a fiber loop for sensing applications is proposed and experimentally investigated.

5.3.1 Experimental Setup and Operation Principle

Figure 5.3 gives the scheme of the proposed system setup. A laser output lightwave is modulated by a Mach-Zehnder modulator (MZM), the modulation pattern is NRZ signals that consisting only one “1” at the beginning and with all “0”in the remaining sequence. This optical pulse output is then fed into loop frequency shifter through a 3dB coupler. The polarization controller (PC) PC1 is used to maintain the same polarization state between the input pulse and the wavelength shifted pulse before they go into the SSB modulator and PC2 is used to adjust the polarization alignment with the SSB modulator. The optical band pass filter (BPF) is used to determine the

tuning range and suppress the out band noise from the EDFA. The SSB modulator is set to shift the wavelength to upper sideband (shift the frequency lower in frequency domain). The EDFA is used to compensate the power loss after modulation; it should be set to operate slightly under saturation to maintain low noise figure. A series of pulses with frequency shift equals to the RF driving frequency is generated and outputted from port3 of the 3db coupler1.

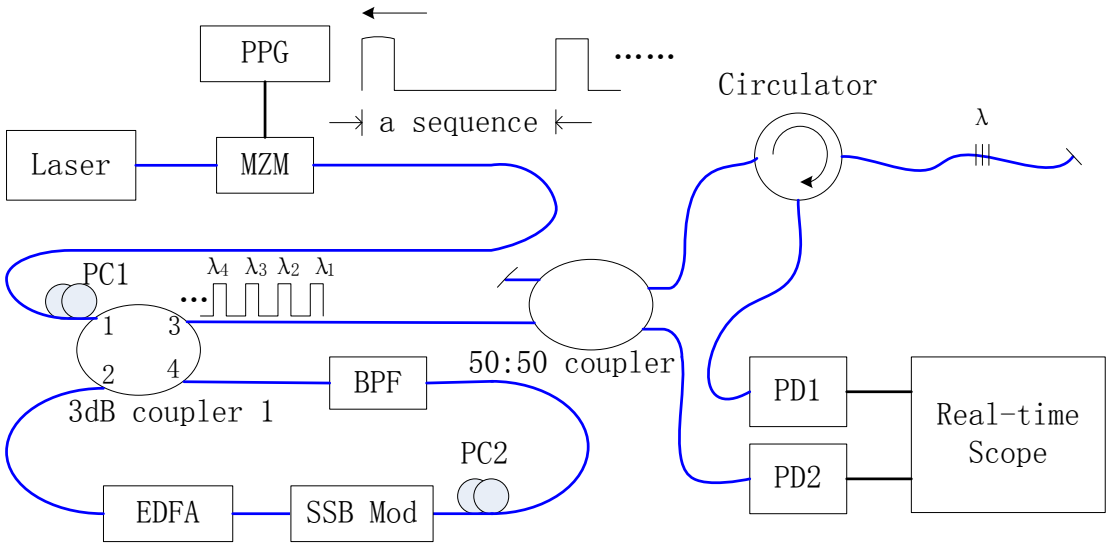

Figure 5.3 Experimental setup of the proposed interrogation system using SSB modulation

By carefully turning the PCs, EDFA and SSB modulator, a series of flat top pulses with wavelength tuning range being equal to the bandwidth of BPF can be generated and the tuning step can be easily changed by changing the RF driving frequency. For temperature or strain sensing applications, a reference power is needed to deal with power variation over tuning range and over long time period. So the series pulses will be divided into two paths by another 3 dB coupler and half of the signal power is detected by photodetector PD2 as the reference power. For vibration

sensing application, the reference power may not be needed as the vibration frequency is encoded in the relative power changes.

5.3.2 Theoretical Analysis

As there is an EDFA in the loop, the ASE noise will accumulate after every cycle. Assuming that the gain of EDFA compensates exactly the total loss in the loop and the spectrum shape of BPF is Gaussian shape with standard deviation σ equals 54GHz, the input laser pulse frequency is +54GHz higher than the center frequency of the bandpass filter (BPF). We can calculate the accumulated ASE noise after every loop cycle.

The ASE noise power density is assumed to be flat and equal to:

$$S_{sp}(\gamma)=n_{sp}(G-1)h\gamma \,, \tag{5.6}$$

where n_{sp} is the inversion parameter, G is the EDFA gain, h is the Planck constant and γ is the frequency.

After this ASE noise goes through the 3dB couple, BPF and EDFA again, the total noise power density would be:

$$S_1(x)=S_{sp}(\gamma)+e^{\frac{-(x+\Delta f)^2}{2\sigma^2}}S_{sp}(\gamma) \,, \tag{5.7}$$

where x is the frequency difference to the center frequency of BPF and Δf is the frequency shift cause by the SSB modulator.

And for the second round trip loop after the EDFA, the total noise power density would be:

$$S_2(x)= S_{sp}(\gamma)(1+e^{\frac{-(x+\Delta f)^2}{2\sigma^2}}+e^{\frac{-(x+\Delta f)^2}{2\sigma^2}+\frac{-(x+2\Delta f)^2}{2\sigma^2}}) \quad (5.8)$$

So after n round loop, the total noise power density would be:

$$S_n(x)=S_{sp}(\gamma)(1+e^{\frac{-(x+\Delta f)^2}{2\sigma^2}}+e^{\frac{-(x+\Delta f)^2}{2\sigma^2}+\frac{-(x+2\Delta f)^2}{2\sigma^2}}+\cdots+ e^{\frac{-(x+\Delta f)^2}{2\sigma^2}+\frac{-(x+2\Delta f)^2}{2\sigma^2}+\cdots+\frac{-(x+n\Delta f)^2}{2\sigma^2}}) \quad (5.9)$$

Let $$a_n(x) = (x+\Delta f)^2 + (x+2\Delta f)^2 + \cdots + (x+n\Delta f)^2 \quad (5.10)$$

$$b_n(x) = e^{-a_n(x)/2\sigma^2} \quad (5.11)$$

Then $$S_n(x)= S_{sp}(\gamma)[b_0(x) +b_1(x) +b_2(x)+ b_3(x) +\dots +b_n(x)] \quad (5.12)$$

From equation (5.10) we have

$$a_n(x) = n(x+\frac{n+1}{2}\Delta f)^2 + \frac{(n-1)n(n+1)}{12}\Delta f^2 \quad (5.13)$$

When x=0, we have

$$b_n(0) = (e^{-\Delta f^2/2\sigma^2})^{\frac{n(n+1)(2n+1)}{6}} \quad (5.14)$$

For the frequency shift Δf is equal to 6GHz, we have

$b_1(0)=e^{-1/162}=0.99384617$

$b_2(0)= (e^{-1/162})^5=0.9696$

$b_3(0)= (e^{-1/162})^{14}=0.9172$

$b_4(0)= (e^{-1/162})^{30}=0.8310$

$b_5(0)= (e^{-1/162})^{55}=0.7121$

$b_6(0)= (e^{-1/162})^{91}=0.5702$

$b_7(0)= (e^{-1/162})^{140}=0.4214$

$b_8(0)= (e^{-1/162})^{204}=0.2839$

$b_9(0)= (e^{-1/162})^{285}=0.1722$

$$b_{10}(0)= (e^{-1/162})^{385}=0.0929$$

$$b_{11}(0)= (e^{-1/162})^{506}=0.0440$$

$$b_{12}(0)= (e^{-1/162})^{650}=0.0181$$

$$b_{13}(0)= (e^{-1/162})^{819}=0.0064$$

$$b_{14}(0)= (e^{-1/162})^{1015}=0.0019$$

$$b_{15}(0)= (e^{-1/162})^{1240}=0.0005$$

$$b_{16}(0)= (e^{-1/162})^{1496}=0.0001$$

$$b_{17}(0)= (e^{-1/162})^{1785}=0.0000$$

For any n>17, $b_n(0)$ is negligible. The total noise power density would be:

$$\begin{aligned} S(0) &= S_{sp}(\gamma)\sum_{k=0}^{\infty} b_k(0) \\ &= S_{sp}(\gamma)(1+0.9938+0.9696+\cdots) \\ &= 7.0352\,S_{sp}(\gamma) \end{aligned}$$

S(0) is the total noise power density in the loop after EDFA of the frequency position at the center of BPF. For the output pulses, the dominant noise is the signal-spontaneous (s-sp) beat noise and only the ASE noise that close to the signal frequency will contribute to the s-sp beat noise due to the narrow bandwidth of the photodetector. So the s-sp beat noise can be obtained with the assumption that the ASE noise power density is flat within the narrow bandwidth range near the pulse frequency. The frequency difference between the pulse and the center of BPF is

$$x_m=m\Delta f \qquad (5.15)$$

For m>0, $b_n(x_m)= b_{n+m}(0)/ b_m(0)$

So we have

$$S_n(x_m)= S_{sp}(\gamma)[b_m(0) +b_{m+1}(0) +b_{m+2}(0)+ b_{m+3}(0) +\dots +b_{n+m}(0)]/b_m(0) \quad (5.16)$$

For n is large enough, we can obtain

$$S(x_1)=6.0726S_{sp}(\gamma)$$

$$S(x_2)=5.1994S_{sp}(\gamma)$$

$$S(x_3)=4.4393S_{sp}(\gamma)$$

$$S(x_4)=3.7963S_{sp}(\gamma)$$

$$S(x_5)=3.2629S_{sp}(\gamma)$$

$$S(x_6)=2.8261S_{sp}(\gamma)$$

$$S(x_7)=2.4710S_{sp}(\gamma)$$

$$S(x_8)=2.1837S_{sp}(\gamma)$$

$$S(x_9)=1.9516S_{sp}(\gamma)$$

For m<0,

$$b_n(x_m)= b_{n+m}(0)* b_{-m-1}(0) \text{ when } n+m>=0$$

$$b_n(x_m)= b_{-m-1}(0) /b_{-m-1-n}(0) \text{ when } n+m<0$$

$$S_n(x_m)= S_{sp}(\gamma)[1+ b_{-m-1}(0) /b_{-m-2}(0) + b_{-m-1}(0) /b_{-m-3}(0)+\dots+b_{-m-1}(0)/ b_0(0)$$

$$+b_0(0)* b_{-m-1}(0)+ b_1(0)* b_{-m-1}(0)+\dots+ b_{n+m}(0)* b_{-m-1}(0)] \quad (5.17)$$

So we can have

$$S(x_{-1})=8.0352S_{sp}(\gamma)$$

$$S(x_{-2})=8.9858S_{sp}(\gamma)$$

$$S(x_{-3})=9.7665S_{sp}(\gamma)$$

$$S(x_{-4})=10.269S_{sp}(\gamma)$$

$$S(x_{-5})=10.276S_{sp}(\gamma)$$

$$S(x_{-6})=9.8065S_{sp}(\gamma)$$

$$S(x_{-7})=8.8518S_{sp}(\gamma)$$

$$S(x_{-8})=7.5420S_{sp}(\gamma)$$

$$S(x_{-9})=6.0810S_{sp}(\gamma)$$

So the ASE noise power density can be written as

$$S(x_m)=\beta S_{sp}(\gamma)\,, \tag{5.18}$$

where β is in the range of 2~10.

The single side band s-sp beat noise power density at PD1 will be

$$N_{s-sp}(x_m)=4R^2\cdot\frac{1}{2}\alpha P(x_m)\cdot\frac{1}{4}\alpha S(x_m)\,, \tag{5.19}$$

where $P(x_m)$ is the output pulse power,R is the PD response, R= q/hγand α is the grating reflectivity at x_m.

$$I_s(x_m)=R\cdot\frac{1}{2}\alpha P(x_m)$$

$$\delta_{s-sp}^2(x_m)=N_{s-sp}(x_m)\cdot B_e$$

So the signal-to-noise ratio will be

$$SNR(x_m)=\frac{I_s(x_m)^2}{\delta_{s-sp}^2(x_m)}=\frac{P(x_m)}{2S(x_m)\cdot B_e} \tag{5.20}$$

The grating sensor reflectivity is

$$\alpha(x)=ae^{\frac{-(x-b)^2}{2\sigma_2^2}}\,, \tag{5.21}$$

where *a* represents the insertion loss and input power relative fluctuation，*b* is Bragg wavelength of the grating sensor and σ_2 is 12GHz.

From equation (5.15) it's clear that the SNR is independent of the grating

sensor reflectivity at the s-sp noise limited situation. So the SNR will remain the same at the same frequency position as the grating sensor shifts or even without the grating sensor.

There are two ways to get the value of parameter *b*. One method is using the reflectivity ratio between two different reflected pulses from the grating sensor. So the parameter *a* can be eliminated and *b* can be obtained from the ratio because the signal frequency of the two pulses are 100 resented. Another method is using all the reflection points from the grating sensor to do a curve fitting to find out the value *a* and *b*. Here we will compare the performance of these two methods.

The reflectivity can be obtained from the reflection power at PD1 and the reference power at PD2. So

$$\alpha(x_m) = \frac{R \cdot \frac{1}{2}\alpha P(x_m)}{R \cdot \frac{1}{2} P(x_m)} = \frac{I_s(x_m)}{I(x_m)} \quad , \tag{5.22}$$

where $I_s(x_m)$ is the reflection power and $I(x_m)$ is the reference power at frequency x_m.

In error propagation theory, for independent variables x_1 to x_n,

$$N = f(x_1, x_2, x_3, ...x_n)$$

$$\delta_N^2 = \left(\frac{\partial f}{\partial x_1}\right)^2 \delta_1^2 + \left(\frac{\partial f}{\partial x_2}\right)^2 \delta_2^2 + ... + \left(\frac{\partial f}{\partial x_n}\right)^2 \delta_n^2$$

$$\frac{\delta_N^2}{N^2} = \left(\frac{\partial \ln f}{\partial x_1}\right)^2 \delta_1^2 + \left(\frac{\partial \ln f}{\partial x_2}\right)^2 \delta_2^2 + ... + \left(\frac{\partial \ln f}{\partial x_n}\right)^2 \delta_n^2$$

So

$$\begin{aligned}\frac{\delta_\alpha^2}{\alpha^2} &= \frac{\delta_{Is}^2}{I_s(x_m)^2} + \frac{\delta_I^2}{I(x_m)^2} \\ &= \frac{2}{SNR(x_m)}\end{aligned} \tag{5.23}$$

For two different reflections at x_{m1} and x_{m2}, the ratio r is

$$r = \frac{\alpha(x_{m2})}{\alpha(x_{m1})} = e^{\frac{-(x_{m2}-b)^2}{2\sigma_2^2} - \frac{-(x_{m1}-b)^2}{2\sigma_2^2}} \tag{5.24}$$

So from equation (5.24), we can derive *b* from the two normalized reflectivity.

$$b = \frac{\sigma_2^2}{x_{m2} - x_{m1}}[\ln\alpha(x_{m2}) - \ln\alpha(x_{m1})] + \frac{x_{m2} + x_{m1}}{2} \tag{5.25}$$

The noise will be

$$\begin{aligned}\delta_b^2 &= \frac{\sigma_2^4}{(x_{m2} - x_{m1})^2 \alpha_{m1}^2}\delta_{m1}^2 + \frac{\sigma_2^4}{(x_{m2} - x_{m1})^2 \alpha_{m2}^2}\delta_{m2}^2 \\ &= \frac{\sigma_2^4}{(x_{m2} - x_{m1})^2}[\frac{2}{SNR(x_{m1})} + \frac{2}{SNR(x_{m2})}]\end{aligned} \tag{5.26}$$

This indicates that the larger frequency difference between two pulses, the smaller δ_b and better system performance can be obtained.

In the case that there are n reflection pulses from the grating sensor, doing an average of several independent *b* will get a smaller δ_b and more precise *b*. To simplify the calculation, all SNR(x_m) are assumed to be the same and given an average value SNR(0). So equation (5.21) can be written as

$$\begin{aligned}\delta_b^2 &= \frac{\sigma_2^4}{(x_{m2} - x_{m1})^2}\frac{4}{SNR(0)} \\ &= \frac{\sigma_2^4}{(m_1 - m_2)^2 \Delta f^2}\frac{4}{SNR(0)}\end{aligned} \tag{5.27}$$

For n points, the maximum frequency difference is (n-1)Δf. If we use 4 points to get 2 independent *b*, there are two grouping combinations that may get the best

performance.

One is x_1 and x_n to get b_1, x_2 and x_{n-1} to get b_2, after average, δb will be

$$\delta_b^2 = \frac{\sigma_2^4}{\Delta f^2 SNR(0)}[\frac{1}{(n-1)^2} + \frac{1}{(n-3)^2}]$$

Another is x_1 and x_{n-1} to get b_1, x_2 and $x_n$to get b_2, after average, δb will be

$$\delta_b^2 = \frac{\sigma_2^4}{\Delta f^2 SNR(0)}[\frac{1}{(n-2)^2} + \frac{1}{(n-2)^2}]$$

Because $[\frac{1}{(n-2)^2} + \frac{1}{(n-2)^2}]$ is always smaller than $[\frac{1}{(n-1)^2} + \frac{1}{(n-3)^2}]$, the second grouping is better.

So for 2k points to get k independent b for average, the best δb will be

$$\begin{aligned}\delta_b^2 &= \frac{4\sigma_2^4}{\Delta f^2 SNR(0)} \frac{1}{k^2} \frac{k}{(n-k)^2} \\ &= \frac{4\sigma_2^4}{\Delta f^2 SNR(0)} \frac{1}{(n-k)^2 k}\end{aligned} \tag{5.28}$$

When k=n/3, we can obtain the smallest δb in the case of n points as

$$\delta_b^2 = \frac{\sigma_2^4}{\Delta f^2 SNR(0)} \frac{27}{n^3} \tag{5.29}$$

For the curve fitting method, we first deal with a simple case that only 3 points are used to fit the parameters. Suppose the fitted curve of grating sensor is

$$y = ae^{\frac{-(x-b)^2}{2\sigma_2^2}}$$

So

$$Y = \ln y = \ln a - \frac{-(x-b)^2}{2\sigma_2^2}$$

$$\overline{Y_1} = A - \frac{-(x_{m1}-b)^2}{2\sigma_2^2}$$

$$\overline{Y_2} = A - \frac{-(x_{m2}-b)^2}{2\sigma_2^2}$$

$$\overline{Y_3} = A - \frac{-(x_{m3}-b)^2}{2\sigma_2^2}$$

where $\overline{Y_1}, \overline{Y_2}, \overline{Y_3}$ are the fitted values at x_{m1}, x_{m2}, x_{m3} respectively and A is equal to $\ln a$.

We can get the value of b by using the method of least squares. So

$$\varepsilon = (Y_1 - \overline{Y_1})^2 + (Y_2 - \overline{Y_2})^2 + (Y_3 - \overline{Y_3})^2 \tag{5.30}$$

$$\frac{\partial \varepsilon}{\partial A} = 0 \tag{5.31}$$

$$\frac{\partial \varepsilon}{\partial b} = 0 \tag{5.32}$$

where Y_1 is $\ln\alpha(x_{m1})$, Y_2 is $\ln\alpha(x_{m2})$ and Y_3 is $\ln\alpha(x_{m3})$.

From equation (5.31), we can derive

$$\overline{Y_1} + \overline{Y_2} + \overline{Y_3} = Y_1 + Y_2 + Y_3$$

$$\overline{Y_1} = \frac{Y_1 + Y_2 + Y_3}{3} + \frac{(x_{m2}-b)^2 + (x_{m3}-b)^2 - 2(x_{m1}-b)^2}{6\sigma_2^2}$$

$$\overline{Y_2} = \frac{Y_1 + Y_2 + Y_3}{3} + \frac{(x_{m1}-b)^2 + (x_{m3}-b)^2 - 2(x_{m2}-b)^2}{6\sigma_2^2}$$

$$\overline{Y_3} = \frac{Y_1 + Y_2 + Y_3}{3} + \frac{(x_{m1}-b)^2 + (x_{m2}-b)^2 - 2(x_{m3}-b)^2}{6\sigma_2^2}$$

From equation (5.27), we can derive

$$(1-\frac{1}{3}+\frac{(x_{m2}-b)+(x_{m3}-b)-2(x_{m1}-b)}{3\sigma_2^2}\frac{\partial b}{\partial Y_1})x_{m1}+$$
$$(-\frac{1}{3}+\frac{(x_{m1}-b)+(x_{m3}-b)-2(x_{m2}-b)}{3\sigma_2^2}\frac{\partial b}{\partial Y_1})x_{m2}+$$
$$(-\frac{1}{3}+\frac{(x_{m1}-b)+(x_{m2}-b)-2(x_{m3}-b)}{3\sigma_2^2}\frac{\partial b}{\partial Y_1})x_{m3}=0$$

So

$$\frac{\partial b}{\partial \alpha(\mathrm{x_{m1}})}=\frac{\partial b}{\partial Y_1}\frac{\partial Y_1}{\partial \alpha(\mathrm{x_{m1}})}=\frac{(2x_{m1}-x_{m2}-x_{m3})\sigma_2^2}{(x_{m1}-x_{m2})^2+(x_{m2}-x_{m3})^2+(x_{m3}-x_{m1})^2}\frac{1}{\alpha(\mathrm{x_{m1}})}$$

$$\frac{\partial Y_1}{\partial \alpha(\mathrm{x_{m2}})}=\frac{(2x_{m2}-x_{m1}-x_{m3})\sigma_2^2}{(x_{m1}-x_{m2})^2+(x_{m2}-x_{m3})^2+(x_{m3}-x_{m1})^2}\frac{1}{\alpha(\mathrm{x_{m2}})}$$

$$\frac{\partial Y_1}{\partial \alpha(\mathrm{x_{m3}})}=\frac{(2x_{m3}-x_{m1}-x_{m2})\sigma_2^2}{(x_{m1}-x_{m2})^2+(x_{m2}-x_{m3})^2+(x_{m3}-x_{m1})^2}\frac{1}{\alpha(\mathrm{x_{m3}})}$$

$$\delta_b^2=(\frac{\partial b}{\partial Y_1})^2\delta_{m1}^2+(\frac{\partial b}{\partial Y_2})^2\delta_{m2}^2+(\frac{\partial b}{\partial Y_3})^2\delta_{m3}^2$$
$$=\frac{(2x_{m1}-x_{m2}-x_{m3})^2\sigma_2^4}{[(x_{m1}-x_{m2})^2+(x_{m2}-x_{m3})^2+(x_{m3}-x_{m1})^2]^2}\frac{2}{SNR(x_{m1})}+$$
$$\frac{(2x_{m2}-x_{m1}-x_{m3})^2\sigma_2^4}{[(x_{m1}-x_{m2})^2+(x_{m2}-x_{m3})^2+(x_{m3}-x_{m1})^2]^2}\frac{2}{SNR(x_{m2})}+$$
$$\frac{(2x_{m3}-x_{m1}-x_{m2})^2\sigma_2^4}{[(x_{m1}-x_{m2})^2+(x_{m2}-x_{m3})^2+(x_{m3}-x_{m1})^2]^2}\frac{2}{SNR(x_{m3})}$$

For the case that the number of points to fit the parameters is n, it is easy to get:

$$\delta_b^2=\sum_{i=1}^{n}(\frac{\partial b}{\partial Y_i})^2\delta_i^2$$
$$=\frac{2\sum_{i=1}^{n}[(nx_i-\sum_{j=1}^{n}x_j)^2\sigma_2^4/SNR(x_i)]}{[\sum_{i=1}^{n-1}\sum_{j=i+1}^{n}(x_i-x_j)^2]^2} \quad (5.33)$$

To simplify the calculation, we assume that all the SNR(x_i) are the same, then

$$\delta_b^2 = \frac{\frac{2}{12}n^3(n^2-1)}{[\frac{1}{12}n^2(n^2-1)]^2} \cdot \frac{\sigma_2^4}{\Delta f^2 SNR(0)} = \frac{24\sigma_2^4}{n(n^2-1)\Delta f^2 SNR(0)} \tag{5.34}$$

From equation (5.29) and (5.34) we can see that the performance of these two methods is similar, however, the curve fitting method will be slightly better when n is larger than 4. And the larger n will give a better system performance.

The reflection power should be large enough to keep the s-sp beat noise to be the dominant noise in the system. In the experiment setup, P(x_m) is about -10dbm, G is 25dB to compensate the loop loss. The reflection power then should larger than 10% of input to maintain the s-sp beat noise dominant assumption. When grating sensor of σ is 12GHz, 6 signal pulses can locate in the reflection range where the reflectivity is larger than 0.1 as the sensor shifts. So from equation (5.20), we can derive

$$SNR(x_m) = \frac{P(x_m)}{2S(x_m)\cdot B_e} = \frac{8260}{\beta} \tag{5.35}$$

SNR(0) is approximately1376 when β=6. From equation (5.28), δ_b will be

$$\delta_b = 228\text{MHz} \tag{5.36}$$

In the wavelength range around 1550nm, 1pm equals to about 125MHz, so the ideal precision of this system is 2pm.

5.3.3 Results and Discussion

In the experiment, the bit rate of the pulse pattern generator (PPG) is set to 40MHz and there are 128 bits for one sequence. The first bit is “1” then followed by 127 “0”s. The repetition rate of the pulse sequence is thus 312kHz. The RF driving frequency is 6GHz and the BPF bandwidth is about 1nm. The laser output wavelength is set to 1550.0nm and is 1550.042nm or 193409.310GHz measured by a APEX optical spectrum analyzer AP2440. The AP2440 have a ±3pm wavelength absolute accuracy after warm up and self calibrated and with a 20MHz resolution at FWHM.

To measure power loss of SSB modulation and investigate the signal characteristic, an open loop test setup is performed as shown in Figure 5.4.

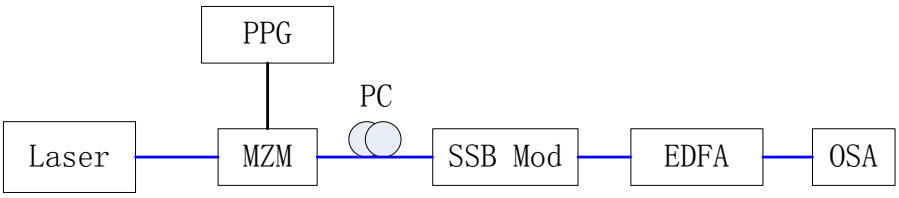

Figure 5.4 Setup to test modulator loss and signal characteristic

The signal power after MZM is -23dBm. Figure 5.5(a) shows the ouput signal spectrum after SSB modulator. The singal power is about -43dBm after SSB modulation and the dominant sideband is the residual input signal but not the 3-rd order harmonic due to the imperfect parameters for a real world modulator.The power loss is -20dBm after SSB modulation. Figure 5.5(b) shows the spetrum after EDFA. The sideband signals of the first and 3-rd order harmonic become comparable to the

residual input signal power after amplification, but they are still more the 35dB smaller than the signal power and negligible.

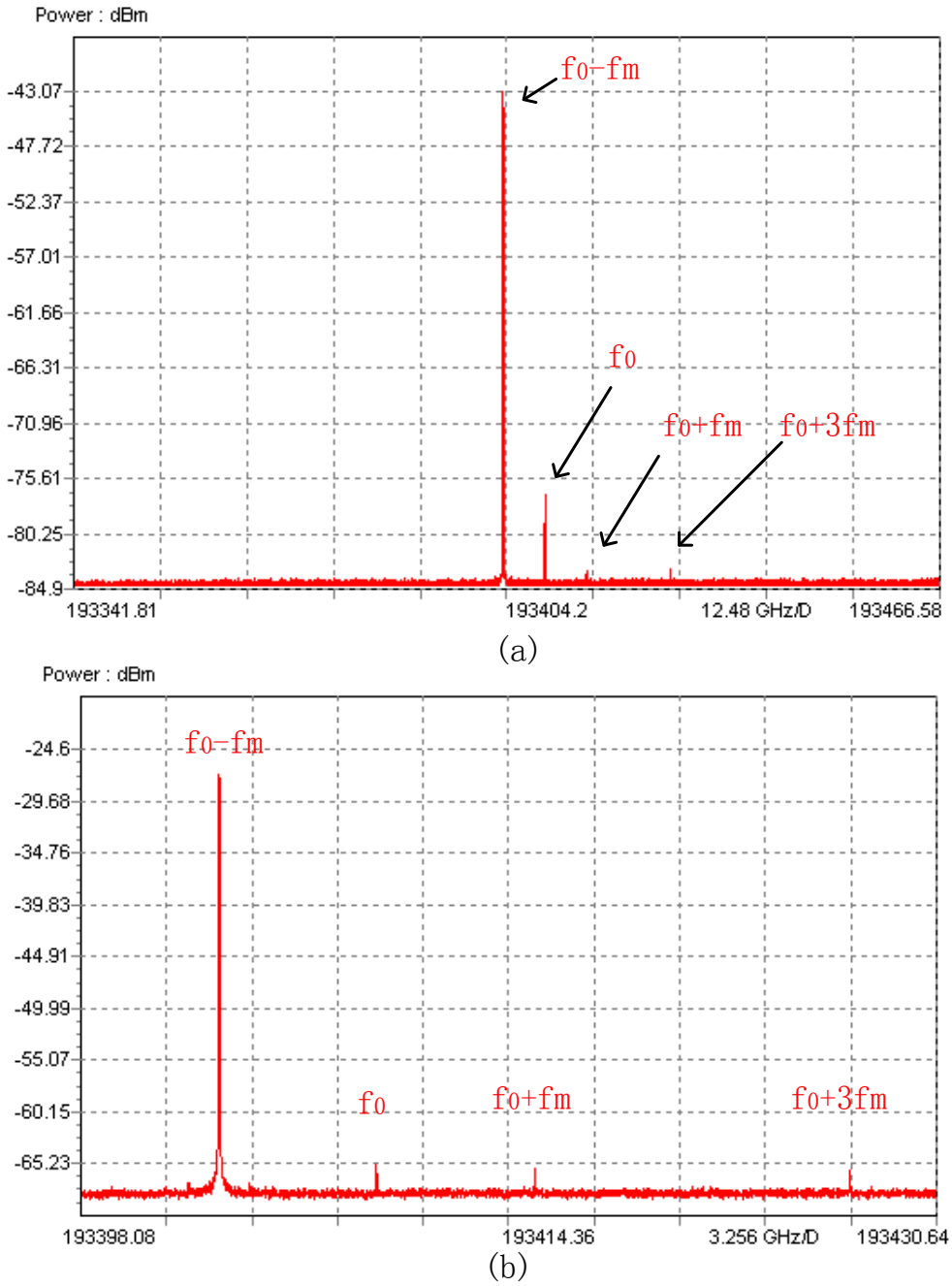

Figure 5.5 Signal after SSB modulator (a) and after EDFA (b)

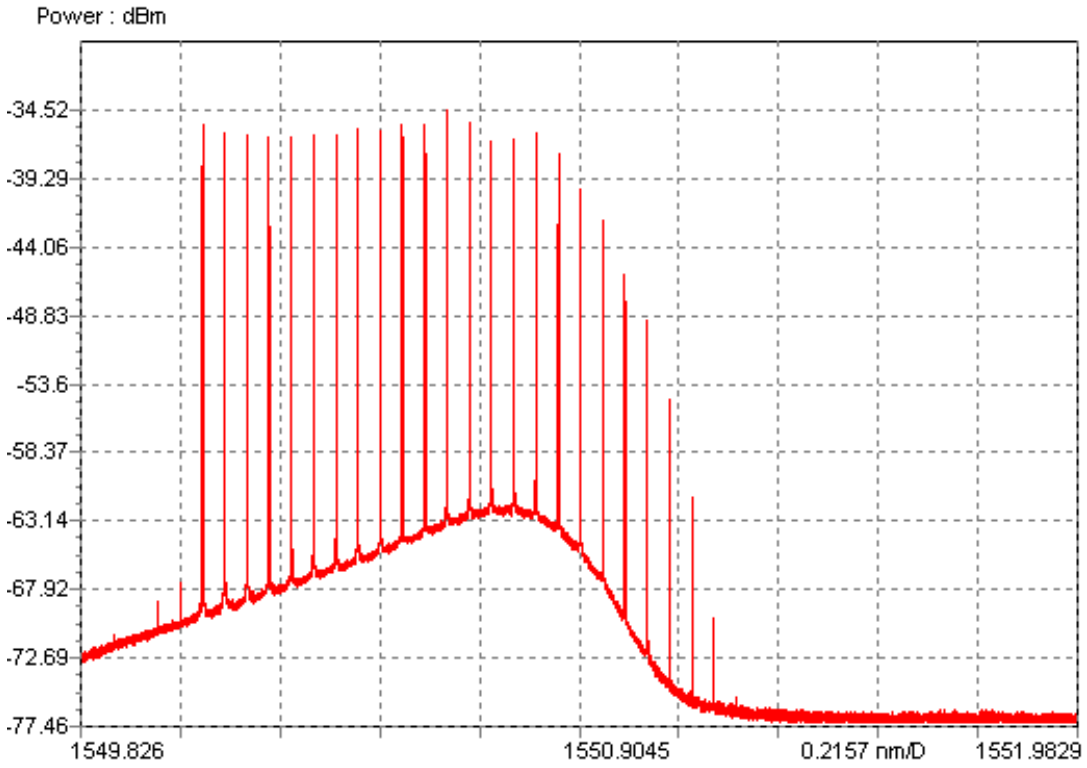

Figure 5.6 The output series pulses in optical domain

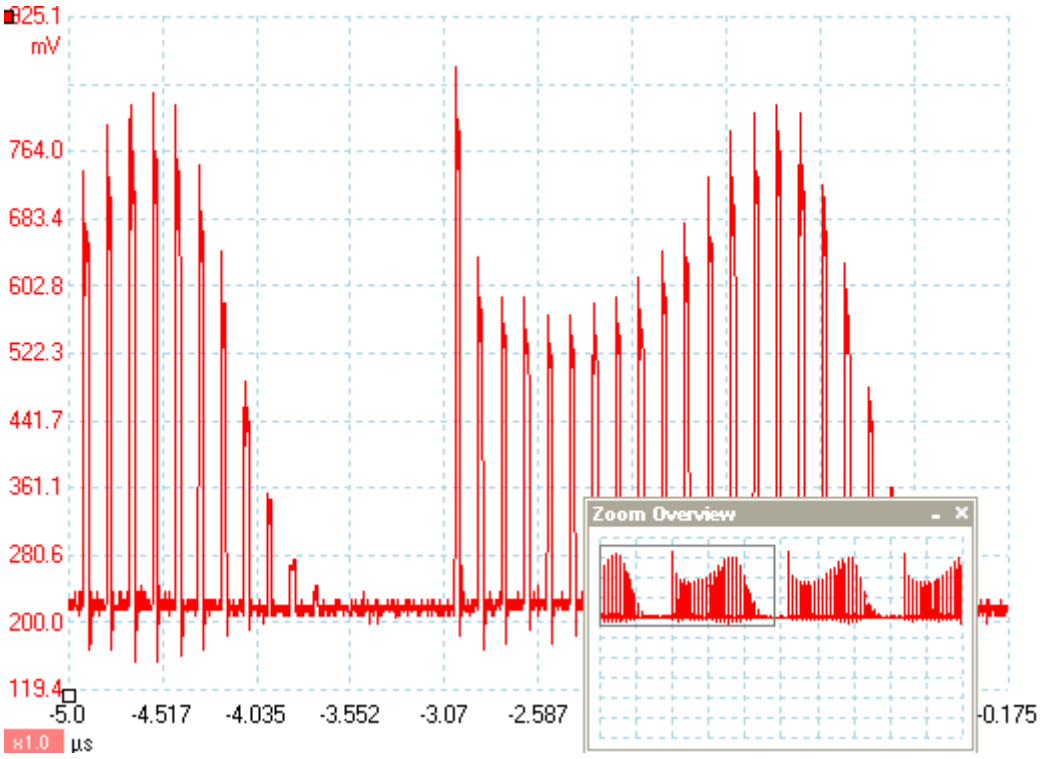

Figure 5.7 The output series pulses in time domain

Figure 5.6 shows the spectrum of port 3 of the 3dB coupler in the proposed system setup and Figure 5.7 shows its time domain output after the photodetector in a real-time scope. About 0.8nm wavelength tuning range has been achieved.

Because of the limited extinction ratio of MZM, some of lightwave will still propagate through the MZM at the “off” state. The power ratio between “on” and “off” is defined as extinction ratio for NRZ modulation. In our setup, the extinction ratio of MZM is about 20dB. So when the pulse go through the loop and comes to port 3 of the 3dB coupler, it will add the lightwave from the “off” state via port 1. It is about -20dB less than the desired signal and becomes the dominant sideband interference (other sidebands are about -35dB less from Figure 5.5). This will affect the normalized power ratio and degrade the final wavelength accuracy of the system. Another interference is the DC power of the ASE spontaneous-spontaneous beat noise. it is about 1% of the input power and will greatly affect the normalized power ratio when the reflection power from grating is around 10% of input. To eliminate the interference, one solution is to keep the pulse width less than half of the loop time and then the output of the following bit period from port 3 will contain the wavelength shifted “off” state power from port 2 with EDFA noise and the “off” state power from port 1. By subtracting the detection power of its following bit from the detection power of itself, the interference component from port 1 together with the DC component of ASE noise can be eliminated. This will greatly improve the measurement accuracy. However, the penalty is that the noise power doubles and SNR

decreases 3dB.

A tunable grating filter with 0.22nm FWHM bandwidth is used as sensor to test this interrogation system. The tuning step is 0.1nm with tuning range from 1550.2nm to 1551.2nm. To test the accuracy and linearity of this filter, an APEX2440 is used to measure the output wavelength of the filter while tuning the wavelength in 0.1nm step. The result shows that the output wavelength is about 0.16nm lower than the setting but the linearity is quite good that less than $\pm$2pm error in the range of 1550.2nm to 1551.2nm.

A method to extract the wavelength of sensor from its normalized reflection pulse series is to use the ratios between the two pulses. The grating reflection spetrum shape can be measured beforehand and will not change with tuning. By finding the same ratio point in the grating reflection spetrum shape with the same frequency seperation between the two pulses (multiple of 6GHz in this case), the relative wavelength positions of the pulses in the grating spetrum shape is confirmed. And the wavelength of the pulses are preseted, the grating wavelength then can be obtianed. To simplify the calulation, only one group of two pulses are used to estimate the grating wavelength and the frequency seperation between the two pulses is 24GHz

In this experiment, the reflection spectrum shape of the tunable grating filter is measured by an APEX2240 with resolution of 10MHz. The data is smoothed using local regression method and 5001 data points are selected to form the grating shape. Figure 5.8 shows the normalized reflection shape. The peak is at point 2501 and

frequency difference for adjacent points is 10MHz. For example, the power ratio between 6GHz frequency difference can be obtaind from the power ratio of 600 points difference.

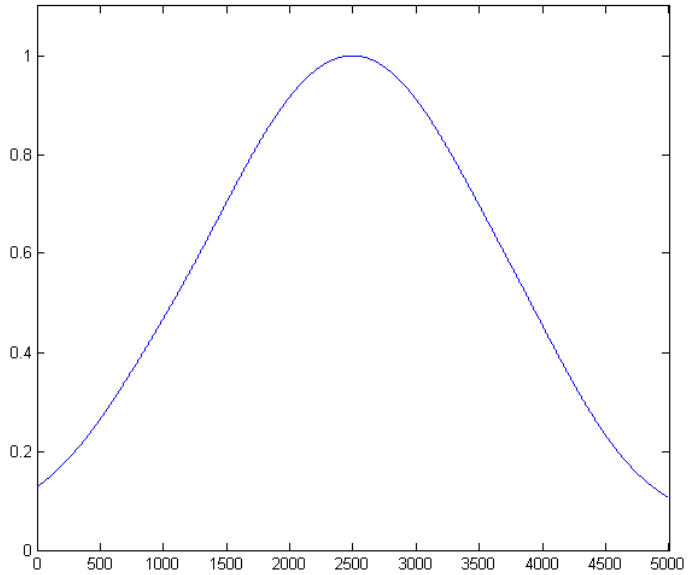

Figure 5.8 The normalized reflection shape of grating filter

Figure 5.9 shows the reflection pulses of grating filter at 1550.5nm. The time period between the adjacent pulses is equal to the loop time and the pulse width is about one quarterloop time. To reduce the noise and increase the measurement accuracy, average of 100 adjacent sequences is implemented before other signal processing.

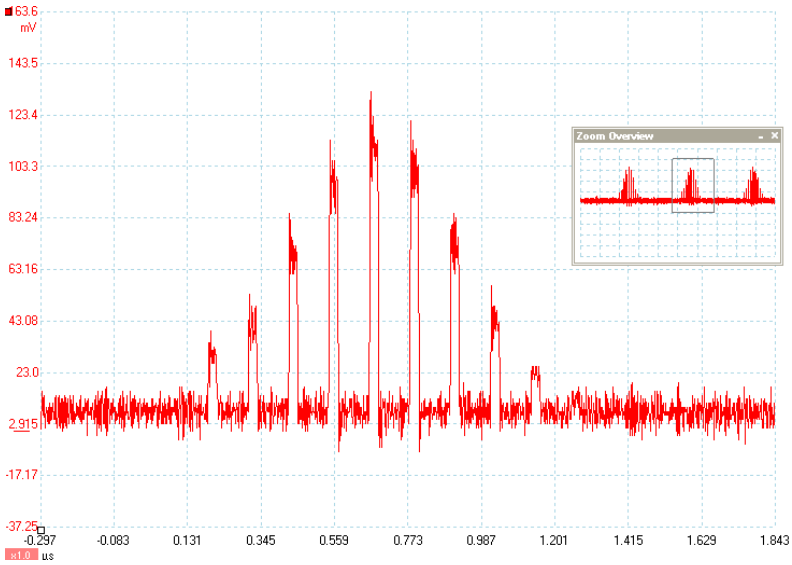

Figure 5.9 The reflection pulses of grating filter in real-time scope

After eliminated the sideband interference and normalized the power, the largest reflection power appears in the 7-th pulse whose frequency is f_0-6f_m. So we can use either ratio of 9-th and 5-th normalized reflection power to obtain the relative position of the filter.

For example, when P9/P5=1.2275, P9 corresponds to point 1424 in Figure 5.8 and P5 corresponds to point 3824. And the peak wavelength is at point 2501, so the measurement sensor frequency is 1323 points lower than P5, which means 13230MHz lower. So the measurement frequency will be f_0-4f_m-13230MHz and equal to 193372.08GHz or 1550.340nm.

	P9/P5	P9	P5
1	1.2275	1424	2824
2	1.2295	1426	2826
3	1.2323	1427	2827
4	1.2368	1429	2829
5	1.2325	1427	2827
6	1.2292	1426	2826

Table 5.1 power ratios of pulses and its corrosponding relative positions

Table 5.1 shows the results in six measurements. The maximum position difference of P9 is 13 points, which means 130MHz frequency difference.

Table 5.2 shows the maximum position difference, mean frequency and standard deviation in six measurements for different grating filter wavelength. The maximum is at 1550.9nm with 320MHz difference. For wavelength around 1550nm, 1pm is equivalent to about 125MHz. Based on the experimental results, a resolution better than 2pm can be expected.

	diff (MHz)	mean (MHz)	δ (MHz)
1550.3	130	193397.1	68.1
1550.4	220	193384.4	96.6
1550.5	130	193372.1	61.1
1550.6	160	193359.5	53.9
1550.7	70	193347	24.2
1550.8	240	193334.7	89.1
1550.9	320	193322.2	140.3
1551.0	300	193309.6	120.5

Table 5.2 standard deviation at difference wavelegths

Table 5.3 shows the relationship between the measurement results of

APEX2440 and the proposed SSB modulation based interrogator for the same tunable filter wavelength. The error between these two is within ±2pm in the whole wavelength range. The absolute accuracy can be considerd the same as APEX2440.

APEX	1550.14	1550.24	1550.34	1550.44
SSB	1550.139	1550.241	1550.33994	1550.4401
Diff	0.000634	-0.00053	6.4679E-05	-7.9E-05
APEX	1550.54	1550.64	1550.74	1550.84
SSB	1550.542	1550.639	1550.74003	1550.8393
Diff	-0.00192	0.000798	-2.627E-05	0.0006608

Table 5.3 SSB modulation based interrogator measurements vs. APEX measurements

One of the most important characteristics for this proposed setup is the stable relative wavelength accuracy. Because the optical tuning step is determined by the RF driving frequency, it is much easier to guarantee the frequecy shift accuracy of light. The tuning repeatability of normal tunable laser is typical ±5pm, which means that 5pm wavelength error may induce while tuning. Because the initial tuning wavelength is the wavelength of the input laser source, the absolute wavelength accuracy of the proposed setup is depended on the light source. Commercial laser source with frequency locking mechanism usually can have a better than ±10pm long-term accuracy, this would be quite enough for FBG sensing applications. Most of the time, people are interested in how the mesurand changes but not the absolute value.

And the tuning range of the proposed setup can be easily changed with different bandpass filters. This gives more flexibility for system design.

5.4 Summary

In this chapter, an interrogation system based on single-sideband (SSB) modulation in a loop setup is investigated. A laser lightwave is modulated by a 40MHz 128 bit NRZ pattern with only one “1” at the beginning to generate a pulse lightwave. This pulse cycles in the loop to produce a series of pulses at the output. And the SSB modulator shifts the cycling pulse every cycle, so the series of pulses are wavelength tuned. By carefully dealing with the sideband interference, a 5pm resolution can be obtained after 100 times average of the detected signals in the real-time scope. So the equivalent tuning speed is 3.125kHz at 5pm resolution, it can be applied to some high speed sensing applications. The advantages of this setup are more stable wavelength output and flexible tuning range adjustment.It is a practical scheme as tunable source in fiber sensor systems.

Chapter 6 Conclusions and Future Work

6.1 Summary

Fiber Bragg grating (FBG) has been used in various kinds of sensing applications with significant advantages over other fiber optic sensors. The multiplexing capability is important for enhancing the performance and increasing the cost effectiveness of an optical FBG sensor system. We proposed a code-division multiplexing technique for the FBG sensor system. Special codeword was constructed to meet the system requirement. Both code lengths of 2^n and 2n were studied. For the code length of 2^n, the number of '1's in the codeword can reach the maximum of half code length; this is the maximum power that can be launched into the fiber array with in a round-trip time. But the disadvantage is that the 2^{n-1} bit shifts periodic correlation between codeword $\mathbf{C_n}$ and its bipolar version $\mathbf{D_n}$ would not be zero. So in the sensor system, the reflected time delay between any two sensors must not be 2^{n-1} bit period, or else they cannot be distinguish from each other through the decoding process. For the more general case, code sequences with a length of (where n is any even number) also has been investigated. The maximum number of '1's of a given code length 2n is derived. And the rule to construct a 8n bit code sequence from a 2n bit code sequence is given. Based on the unipolar-bipolar correlation processing, a sequence of pulses can be sent into the sensor array within the round-trip time and the individual sensor outputs can

be exactly separated from the overlapped signals. Operation principle and theoretical analysis are given to understand the proposed sensor system. Experimental results show good agreement with the theoretical analysis and demonstrate the great feasibility of the proposed setup. With spectral shape compensation to reduce the cross talk, the new scheme achieved multiplexing of 20 gratings along a single fiber while maintaining the accuracy

Besides using the multiplexing method to reduce the cost per sensor, reducing the cost of light source is also desirable. A novel and simple VCSEL-based TFBG vibration sensing system is presented and demonstrated experimentally. The sensor comprises a short optical fiber stub containing a weakly tilted Bragg grating spliced to another slightly offset fiber. The tip-reflection sensing feature enables the sensor head to be fabricated as small as 10 mm (possibly less). The high-speed continuous wavelength tunable VCSEL enables the recoupled modes to work at a high power level to obtain better signal-to-noise ratio at the output. Vibration measurement up to 200Hz has been achieved by the proposed cost-effective sensing system.

And another more stable wavelength tuning light source utilizing single-sideband modulation to tune the wavelength has also been studied and experimentally demonstrated. The good relative wavelength tuning accuracy makes it more practical than other tunable light sources in fiber sensing applications.

6.2 Future work

Through the study of CDM method in FBG sensing system, it was found that the spontaneous-spontaneous beat noise from overlapped signals is the dominant noise source because it is proportional to the square of the number of overlapped signals within a reflected bit period. This is the inherent drawback of CDM method. One possible solution is to use a high speed tunable laser as the light source instead of SLED and using the coherent detection method to mitigate the beat noise. The tunable laser increases wavelength every round-trip time, the sequence of reflected signals with the same wavelength then mixes with a local laser whose wavelength is slightly different. A band pass filter can be used after the photodetector to remove the beat noise from the overlapped signals.

Further studies of the SSB modulation interrogation system are needed. Some simulation and theoretical analysis can be done to find out a better system setup such as the relationship between noise and the resolution of wavelength shift and the driving frequency.

Bibliography

[1] T. G. Giallorenzi, J. A. Bucaro, A. Dandridge, G. H. Sigel, Jr., J. H. Cole, S. C. Rashleigh, and R. G. Priest, "Optical fiber sensor technology," *IEEE J. Quant. Elec.*, QE-18, p. 626, 1982.

[2] J. Dakin and B. Culshaw, "Optical Fiber Sensors: Principles and Components," Vol. 1, Artech, Boston, 1988.

[3] B. Culshaw and J. Dakin, "Optical Fiber Sensors: Systems and Applications," Vol. 2, Artech, Norwood, MA, 1989.

[4] E. Udd, ed., "Fiber optic sensors," *Proc. SPIE*, CR-44, 1992.

[5] A. D. Kersey, M. A. Davis, H. J. Patrick, M. LeBlanc, K. P. Koo, C., G. Askins, M. A. Putnam, and E. J. Friebele, "Fiber grating sensors," *Journal of Lightwave Technology*, vol. 15, no. 8, pp. 1442–1463, Aug. 1997.

[6] K.O. Hill, Y. Fujii, D. C. Johnson and B. S. Kawasaki, "Photosensitivity in optical fibre wavelength: application to reflection filter fabrication," *Applied Physics Letters*, Vol.32, pp.647-649, 1978.

[7] B. S. Kawasaki, K. O. Hill, D. C. Johnson, and Y. Fujii, "Narrow-band Bragg reflectors in optical fibre," *Optics Letters*, Vol.3, pp.66-68, 1978.

[8] A. Othonos and K. Kalli, "Fiber Bragg gratings: fundamentals and applications in telecommunications and sensing," Artech House Publishers, 1999.

Bibliography

[9] F. Ouellette, “All-fiber filter for efficient dispersion compensation,” *Opt. Lett*., vol. 16, pp.303, 1991.

[10] M. A. Putnam, G. M. Williams, and E. J. Friebele, “Fabrication of tapered, strain-gradient chirped fiber Bragg gratings,” *Electron. Lett*., vol. 31, pp. 309, 1995.

[11] A. D. Kersey, M. A. Davis, and T. Tsai, “Fiber optic Bragg grating strain sensor with direct reflectometric interrogation,” *OFS*, Sapporo, Japan, pp.634, 1996.

[12] T. Erdogan and J. E. Sipe, “Tilted fiber phase gratings,” *J. Opt. Soc*. Amer. A, vol. 13, pp. 296–313, 1996.

[13] K. S. Lee and T. Erdogan, “Fiber mode coupling in transmissive and reflective tilted fiber gratings,” *Appl. Opt*., vol. 39, pp. 1394–1404, 2000.

[14] Stephen W James and Ralph P Tatam, “Optical fibre long-period grating sensors: characteristics and application,” *Meas. Sci. Technol*., vol. 14, 2003.

[15] A. D. Kersey, T. A. Berkoff and W. W. Morey, “Multiplexed fiber Bragg grating strain-sensor system fiber Fabry-Perot wavelength filter,” *Optics Letters*, Vol.18, pp.1370-1372, 1993.

[16] T. A. Berkoff and A. D. Kersey, “Fiber Bragg grating array sensor system using bandpass wavelength division multiplexer and interferometric detection,” *IEEE Photonics Technology Letters*, Vol. 8, pp.1522-1524, 1996.

[17] R. S. Weis, A. D. Kersey and T. A. Berkoff, “A four-element fiber grating sensor array with phase sensitive detection,” *IEEE Photonics Technology Letters*, Vol. 6, pp.1469-1472, 1994.

[18] D. J. F. Cooper, T. Coroy, and P. W. E. Smith, “Time-division multiplexing of large serial fiber-optic Bragg grating sensor arrays,” *Appl. Opt*., vol. 40, pp. 2643-2654, 2001.

[19] W. W. Morey, J. R. Dunphy, and G. Meltz, “Multiplexing fiber Bragg grating sensors,” in *Distributed and Multiplexed Fiber Optic Sensors*, A. Kersey and P. Dakin, eds., Proc. SPIE 1586, pp. 216–224, 1992.

[20] R.S. Weis, A.D. Kersey and T.A. Berkoff, “A four-element fiber grating sensor array with phase sensitive detection,” *IEEE Photonics Technology Letters*, Vol. 6, pp.1469-1472, 1994.

[21] A. B. L. Ribeiro, Y. J. Rao, L. Zhang, I. Bennion, and D. A. Jackson, “Time-and-spatial-multiplexing tree topology for fiber-optic Bragg-grating sensors with interferometric wavelength-shift detection,” *Appl. Opt*. 35, pp.2267-2273, 1996.

[22] C.C. Chan, Y.J. Gao, K.T. Lau, H.L. Ho, L.M. Zhou, W. Jin, “Characterization of crosstalk of a TDM FBG sensor array using a laser source,” *Optics & Laser Technology* 33, pp.299–304, 2001.

[23] A Wilson, S W James and R P Tatam, “Time-division-multiplexed interrogation of fibre Bragg grating sensors using laser diodes,” *Meas. Sci. Technol*. 12, pp.181–187, 2001.

[24] D. J. F. Cooper, T. Coroy, and P. W. E. Smith, “Simple high-performance method for large-scale time division multiplexing of fibre Bragg grating sensors,” *Meas. Sci. Technol*. 14, pp.965–974, 2003.

[25] K. P. Koo, A. B. Tveten and S. T. Vohra, “Dense wavelength division multiplexing of fibre Bragg grating sensors using CDMA,” *Electronics Letters*, Vol. 35, pp.165-167, 1999.

[26] M. A. Davis, D. G. Bellemore, M.A. Putnam and A. D. Kersey, “Interrogation of 60 fiber Bragg grating sensors with microstrain resolution capacity,” *Electronics Letters*, Vol.32, pp.177-178, 1996.

[27] P. K. C. Chan, W. Jin and M. S. Demonkan, “FMCW multiplexing of fiber Bragg grating sensors,” *Journal of Selected Topics in Quantum Electronics*, Vol. 6, pp.756-763, 2000.

[28] L. Zhang, Y. Liu, J. A. R. Wiliams, and I. Bennion, “Enhanced FBG strain sensing multiplexing capacity using combination of intensity and wavelength dual-coding technique,” *IEEE Photonics Technology Letters*, Vol.11, pp.1638–1641, 1999.

[29] P. C. Peng, J. H. Lin, H. Y. Tseng, and S. Chi, “Intensity and Wavelength-Division Multiplexing FBG Sensor System Using a Tunable Multiport Fiber Ring Laser,” *IEEE Photonics Technology Letters*, Vol.16, 2004.

[30] K. T. V. Grattan and B. T. Meggitt, “Optical Fiber Sensor Technology: Devices and Technology,” Volume Two, Chapman & Hall, 1998.

[31] M. A. Davis and A. D. Kersey, “All-fibre Bragg grating strain-sensor demodulation technique using a wavelength division coupler,” *Electronics Letters*, Vol. 30, pp.75-77, 1994.

[32] A. Locco, H. G. Limberger, R.P. Salathe, L.A. Everall, K.E. Chisholm, J.A.R. Williams and I. Bennion, “Bragg grating fast tunable filter for wavelength division multiplexing,” *Journal of Lightwave Technology*, Vol.17, pp.1217-1221, 1999.

[33] A. D. Kersey, T. A. Berkoff and W. W. Morey, “High-resolution fibre-grating based strain sensor with interferometric wavelength-shift detection,” *Electronics Letters*, Vol. 28, pp.236-238, 1992.

[34] Y. Hu, S. Chen, L. Zhang, I. Bennion, “Multiplexing Bragg gratings using combined wavelength and spatial division techniques with digital resolution enhancement,” *Electronics Letters*, Vol.33, pp.1973-1975, 1997.

[35] M. A. Davis and A. D. Kersey, “Application of a Fiber Fourier Transform Spectrometer to the Detection of Wavelength-Encoded Signals from Bragg Grating Sensors,” *Journal of Lightwave Technology*, Vol.13, pp.1289-1295, 1995.

[36] R. M. Measures, Fiber Optic Smart Structures, E. Udd, ed.Wiley, Toronto, 1995.

[37] D. J. F. Cooper, T. Coroy, and P. W. E. Smith, “Time-division multiplexing of large serial fiber-optic Bragg grating sensor arrays,” *Appl. Opt.*, vol. 40, pp. 2643-2654, 2001.

Bibliography

[38] David J. F. Cooper and Peter W. E. Smith, "Simple and highly sensitive method for wavelength Measurement of low-power time-multiplexed signals using optical amplifiers," *Journal of Lightwave Technology*, vol. 21, no. 7, pp. 1612-1620, 2003.

[39] Hyungdon Ryu, Hojoon Lee and Ki-Soo Kim, "An economical and multiple fibre grating sensor system with rapid response using code division multiple access," *Meas. Sci. Technol*., vol. 12, pp. 906-908, 2001.

[40] Hojoon Lee, "Multiple Fiber Bragg Grating Sensor System Using Code-Division Multiple Access," *Applied Optics*, Vol. 41, Issue 25, pp.5245-5248,2002.

[41] R. W. Fallon, L. Zhang, A. Gloag, and I. Bennion, "Identical broadband chirped grating interrogation technique for temperature and strain sensing," *Electron. Lett.* 33, pp.705–70, 1997.

[42] S. Abbenseth and S.I. Lochmann, "Distinct enlargement of network size or measurement speed for serial FBG sensor networks utilizing SIK-DS-CDMA," *J. Phys.: Conf.* Ser., vol. 15, no. 1, pp. 149-154, 2005.

[43] M. J. E. Golay, "Multi slit spectroscopy," *J. Opt. Soc. Amer*., vol.39, pp. 437-444, 1949.

Bibliography

[44] M. Nazarathy, S. A. Newton, R. P. Giffard, D. S. Moberly, F. Sischka, W. R. Trutna and S. Foster, "Real-Time Long Range Complementary Correlation Optical Time Domain Reflectometer," *Journal of Lightwave Technology*, vol. 7, no.1, pp. 23-38, 1989

[45] Yasuo Taki, Hiroshi Miyakawa, MitsutoshiHatori, Mand Seiichi Namba, "Even-Shift Orthogonal Sequences," *IEEE Trans. Information Theory*, Vol. 15, pp.295-300, 1969

[46] S. M. Melle, K. Liu, and R. M. Measures, "A passive wavelength demultiplexing system for guided wave Bragg grating sensors," *IEEE Photon. Technol. Lett*., vol. 4, pp. 516–518 , 1992

[47] A. D. Kersey, T. A. Berkoff, and W. W. Morey, "Multiplexed fiber Bragg grating strain-sensor system with a fiber Fabry–Perot wavelength filter," *Opt. Lett.* ,vol. 18, pp. 1370–1372 , 1993

[48] Qian Wang, Gerald Farrell, and Thomas Freir, "Study of transmission response of edge filters employed in wavelength measurements," *Applied Optics*, vol. 44, pp. 7789-7792, 2005

[49] Dennis Derickson, " Fiber Optic Test and Measurement," Prentice Hall PTR, pp.601-604, 1998

[50] M. Osinski et al, "Current Trends in Vertical Surface Emitting Lasers," 1995.

Bibliography

[51] Y. G. Zhao et al,"M. Osinski et al, "Transient temperature response of vertical-cavity surface-emitting semiconductor lasers," *IEEE J. Quantum Electron*, Vol. 31, p.1668, 1995.

[52] J.S. Gustavsson, J. Vukusic, J. Bengtsson, and A. Larsson, "A comprehensive model for the modal dynamics of vertical cavity surface emitting lasers," *IEEE J. Quantum Electron,* 38, pp.203, 2002.

[53] Herbert Li, Kenichi Iga (Eds.), Vertical-Cavity Surface-Emitting Laser Devices, Springer Press, 2002

[54] Joachim Piprek, Semiconductor Optoelectronic Devices: Introduction to Physics and Simulation, Academic Press, 2003

[55] T. Erdogan and J. E. Sipe, "Tilted fiber phase gratings," *J. Opt. Soc. Amer*. A, vol. 13, pp. 296–313, 1996.

[56] K. S. Lee and T. Erdogan, "Fiber mode coupling in transmissive and reflective tilted fiber gratings," *Appl. Opt*., vol. 39, pp. 1394–1404, 2000.

[57] T. Guo, A. Ivanov, C. Chen, and J. Albert, "Temperature-independent tilted fiber grating vibration sensor based on cladding-core recoupling," *Opt. Lett.*, vol. 33, pp. 1004–1007, 2008.

[58] T. Guo, L. Y. Shao, H. Y. Tam, P. A. Krug, and J. Albert, "Tilted fiber grating accelerometer incorporating an abrupt biconical taper for cladding to core recoupling," *Optics Express*, vol. 17, pp. 20651–20660,2009.

Bibliography

[59] Y. X. Jin, C. C. Chan, X. Y. Dong, and Y. F. Zhang, "Temperature independent bending sensor with tilted fiber Bragg grating interacting with multimode fiber," *Opt. Commun.*, vol. 282, pp. 3905–3907, 2009.

[60] C. J. Chang-Hasnain, "Tunable VCSEL," *IEEE J. Sel. Topics Quantum Electron.*, vol. 6, no. 6, pp. 978–987, Dec. 2000.

[61] B. S. Chen, F. Phil, and W. Ron, "Research and development of VCSEL-based optical sensors in industrial applications," Proc. SPIE, vol. 4286, pp. 210–218, 2001.

[62] F. Koyama, "Recent advances of VCSEL photonics," *Journal of Lightwave Technology*, vol. 24, no. 12, pp. 4502–4513, Dec. 2006.

[63] John Carson/AT&T, "Method and Means for Signaling with High Frequency Waves," US patent 1449382, filed on December 1, 1915

[64] R. Hui,B. Zhu, R. Huang, C. Allen, K. Demarest and D. Richards, "10-Gb/s SCM Fiber System Using Optical SSB Modulation," *IEEE Photonics Technology Letters*, Vol. 13, pp. 896-898, (2001)

[65] Tetsuya Kawanishi and Masayuki Izutsu, "Linear Single-Sideband Modulation for High-SNR Wavelength Conversion," *IEEE Photonics Technology Letters*, Vol. 16, pp. 1534-1536, (2004)

[66] Wangzhe Li and Jianping Yao, "Optical frequency comb generation based on repeated frequency shifting using two Mach-Zehnder modulators and an asymmetric Mach-Zehnder interferometer," *Optics Express*, Vol. 17, pp. 23712-23718 (2009)

[67] Jianping Li, Xiaoguang Zhang, Feng Tian, and Lixia Xi, "Theoretical and experimental study on generation of stable and high-quality multi-carrier source based on re-circulating frequency shifter used for Tb/s optical transmission," *Optics Express*, Vol. 19, pp. 848-860 (2011)